Science with Gaia: 2025

Essays on the scientific results from Gaia
michaelperryman.co.uk

Michael Perryman

Essays 210–241 (Jan – Dec 2025)

Preface

GAIA IS a mission of the European Space Agency dedicated to astrometry – the measurement of the positions of celestial bodies. The satellite was launched in 2013, and operated until January 2025. Gaia provides the distances and motions (and much other related data) of more than two billion stars in our Galaxy and beyond, with an unprecedented accuracy barely imaginable 25 years ago. It builds on the success of ESA's pioneering Hipparcos mission, which was operated in orbit between 1989–93. The Hipparcos Catalogue of nearly 120 000 stars was published in 1997.

Because of the enormous amount of data processing involved, improved Gaia catalogues are being released progressively, with Data Release 1 in 2016, Data Release 2 in 2018, Early Data Release 3 in 2020, and Data Release 3 in June 2022. Data Releases 4 and 5 are scheduled for the end of 2026, and 2030, respectively.

SINCE THE beginning of 2021, I have been writing a (mostly weekly) 2-page 'essay', picking out some scientific highlights of the mission as they are emerging, or as they caught my attention, and mixing them with occasional asides on related topics, including the history of astrometry, and some more technical, managerial, or developmental aspects of both Hipparcos and Gaia.

Who are they written for? Anyone who might have a general interest in science and astronomy, including amateur astronomers, young scientists starting out on their careers, mid-career scientists looking in on Gaia for the first time to get a feeling of what is possible, and even specialists looking in from different areas of astronomy, or physics more generally.

THE SCIENTIFIC TOPICS I select each week are not necessarily the most important. They do not follow any specific sequence. They are not a complete review of a given topic. Many will be quickly superseded by new results. But together, they are a look at what this long journey of space astrometry is achieving. They offer a snapshot of some of the discoveries that Gaia is making, and written in a form that I hope will be reasonably accessible to those not so deeply involved. I post these weekly essays on my own www site michaelperryman.co.uk.

In each, I have included a footer (DR1, DR2, EDR3, DR3) to indicate which of the (latest) data releases the essay refers to. I have used DR0 to signify technical or historical material not connected with any specific data release. This is intended to communicate how current (or out of date!) any particular essay is likely to be.

Only a few references are included, and these are (generally) 'discreetly' hyperlinked for those who want to read more. Where references appear in the form (Einstein 1908) or www.gaia.com, clicking on the text (even though not generally highlighted) should lead to the relevant (ADS) online article.

HERE, I gather all of my essays from one year in a single compilation, which can also be displayed on-screen in a 'flip book' format.

Michael Perryman

Contents

210. SETI, Game Theory, and Gaia

I LOOKED AT SOME aspects of SETI in essay 55, including Gaia's contribution to searching for an optical counterpart to the 'Wow!' radio signal of 15 August 1977. And I described two other examples of recently discovered celestial phenomena which probably have a purely physical explanation, but which have aroused interest as being possible alien techno-signatures, and where Gaia is contributing to a more complete picture: the 'interstellar travellers' (viz. Oumuamua and Borisov, essay 25), and the curious 'Boyajian-type' stars.

Here, I will look at a class of SETI search strategies which benefit substantially from the availability of high-accuracy astrometry.

LET ME FIRST recall some background. The search for extra-terrestrial intelligence, SETI, is motivated by the belief that intelligent life is likely to emerge under conditions similar to those on Earth. There is a substantial literature, amongst which are considerations by Cocconi & Morrison (1959), Drake (1961), von Hoerner (1961), von Hoerner (1973), Townes (1997), Leigh & Horowitz (1997), Bhathal (2000), Tarter (2001a), Drake (2008), Ćirković (2013), and Cabrol (2016).

Loosely connected but not implicit in such searches are various unproven and somewhat inconsistent postulates, amongst them the 'anthropic principle', which suggests that no assertion can be made about the probability of intelligent life based on a sample set of one (e.g. Barrow & Tipler, 1988); the 'mediocrity principle' which, given the existence of life on Earth, asserts that life typically exists on Earth-like planets throughout the Universe (e.g. von Hoerner, 1961); and the 'fine-tuning hypothesis', which asserts that the natural conditions for intelligent life elsewhere are implausibly rare.

SETI is generally not perceived as an activity which merits public funding, and is (with some exceptions) an aside to today's mainstream research. Nonetheless, many searches at radio, microwave, and optical wavelengths have been undertaken over the past 30–40 years. All have been unsuccessful, with some false alarms (essay 55), and I will not describe them further here.

THE CHALLENGES in searching for extraterrestrial intelligence are compounded by the multiple dimensions of potential search space. Accordingly, searches for (intentional or accidental) signals clearly benefit from insights as to what wavelengths and types of signal to search for, along with where (and when) to look (e.g., Tarter, 2001a; Tarter, 2001b; Shostak, 2011a; Shostak, 2011b; Fridman, 2011). And when transmitting a signal over large distances, it may well be more efficient to send a brief beamed signal than one which is continuous and omnidirectional, but this again requires that the receiver can figure out where and when to look.

The problem can be simplified if the signal transmission and reception are considered of mutual interest to both parties. In that case, appeal can be made to 'game theory' to formulate a cooperation in which, although the players cannot communicate, they can still establish strategies which are superior to purely random searches.

THE BACKGROUND has been nicely laid out by Wright (2018), and rests on concepts detailed in the book 'The Strategy of Conflict' by American economist Thomas Schelling (1960). The idea is to establish 'focal points' (aka 'Schelling points' or 'beacons') as preferred locations in space or time. Schelling's examples involved two people trying to find each other in a city (e.g. by considering prominent landmarks, or church bells), and the problem of choosing search frequencies for SETI.

Frequency choices range from the neutral hydrogen line at 1420 MHz (Cocconi & Morrison, 1959), to recent suggestions of the Planck energy multiplied by integer powers of the fine structure constant (Wright, 2020a).

The use of astronomical beacons as *temporal* markers has been considered by a number of authors, invoking synchronisation with supernovae (in particular SN 1987A) and novae (e.g. Dixon, 1973; Tang, 1976, 1981; McLaughlin, 1977; Makovetskii, 1977, 1980; Filippova et al., 1991; Lemarchand, 1994; Seto, 2021), binary stars (Pace & Walker, 1975; Pace, 1979), γ-ray bursts (Corbet, 1999; 2003), neutron star mergers (Nishino & Seto, 2018), and even Sgr A* at the Galactic centre (Seto, 2024).

THE IDEA underpinning these positionally-optimised search strategies is that a transmitting civilisation would transmit a signal at the moment that they register some chosen astronomical outburst. Then *their* transmission will be received on Earth with a delay (subsequent to the registration of the same astronomical event outburst on Earth) dictated by the path-length difference between the two routes (see figure below).

In the example given by Makovetskii (1977), using the outburst of Nova Cygni 1975, and a nova–Earth distance of 1600 pc (their 5200 light-years), the typical (pre-Hipparcos) star distance uncertainties at the time led to signal registration *uncertainties* on Earth, for 20 candidate transmitting stars, of the order of 10–100 d.

THE ACCURACY of the predicted delay, i.e. the duration of the required search window, clearly improves with better positional accuracies of event and transmitter. The availability of the Hipparcos astrometry in 1997 generated renewed interest in this possibility.

With his suggestion that γ-ray bursts provide excellent natural 'synchronisers' because of their luminosity, occurrence rate, isotropic distribution, large distance, and short duration, Corbet (1999) considered a transmitting civilisation propagating an 'announcement signal' downstream (i.e., ~ 180° away from the burst) immediately on receiving the burst signal. The searching civilisation (Earth) then monitors (angularly proximate) upstream targets star for a synchronised emitted signal at the time lag set by the additional path length.

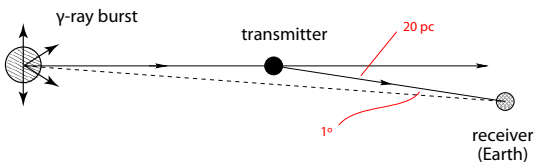

Corbet (1999) estimated that a planet-hosting star at 20 pc from Earth, and at an angle of 1° from the direction of a burst event seen from Earth, will transmit an event which would be detected on Earth 3.63 d later, and with an arrival time that can be predicted to ±1.8 h. Even 14 years before its launch, he pointed out that the timing uncertainty would drop to just 60 s in the case of 10 μas Gaia-level parallaxes. For a number of his hypothesised transmitting stars, the errors on these time delays remain modest, below 1 day, for offset angles up to 5°.

While there have been no definite SETI-type signals detected to date, an optimist might hypothesise that the few detections of non-repeating signals, such as the 'Wow!' event, which I considered in essay 55, could conceivably be genuine extraterrestrial signals that are transient simply because the transmission was intermittent… perhaps along these sorts of lines.

A GENERALISATION of this approach, introducing the concept of a 'SETI ellipsoid', had already been presented by Lemarchand (1994). Incidentally, it follows the same geometry adopted in the study of light echos around supernovae (Chevalier & Emmering, 1988).

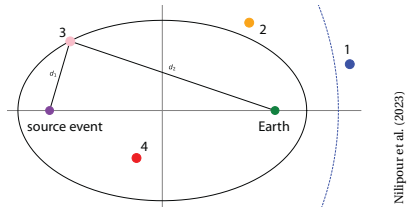

The foci of the ellipsoid (which expands with time) are the source event, and Earth. All stars then fall into four groups: (1) those that have not yet observed the event; (2) those that have observed it, but any transmitted signal has not yet reached Earth; (3) those, on the ellipsoid, whose possible signal would now be arriving at Earth; (4) those where a signal would have arrived in the past.

Davenport et al. (2022), who explain this more carefully through the geometric properties of the ellipse, used the EDR3 Gaia Catalogue of Nearby Stars to select targets on the SN 1987A 'SETI ellipsoid' (as well ellipsoids defined by 278 novae). Less than 8% of stars within the 100 pc sample are inside the ellipsoid, such that the majority are still viable targets for monitoring. Some 700 stars per year within 100 pc will intersect the ellipsoid.

Cabrales et al. (2024) identified 32 suitable SN 1987A 'SETI ellipsoid' targets in the TESS continuous viewing zone. Their TESS light curves showed no anomalous signatures during the ellipsoid crossings.

Nilipour et al. (2023) used four historical supernovae, including SN 1987A, and 10 million stars from the Gaia DR3-based variable star catalogue. Less than 0.01% of stars in the sample have ellipsoid crossing times within the range of the Gaia DR3 observations. They used these to search for 'technosignatures' as modulations in the variability parameters by splitting the stellar light curve at the crossing time.

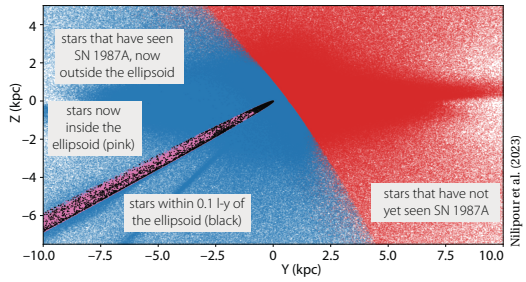

OTHER SEARCHES using Gaia data include consideration of the 'Earth's microlensing zone' from which Earth's photometric microlensing is most readily observable (Suphapolthaworn et al., 2022), and identifying targets for METI-like messaging (Seto & Kashiyama, 2020).

211. The end of Gaia operations

In just two days from today, on 15 January 2025, the Gaia satellite will cease its science operations. More than 10 years of spectacular astrometric (and related) observations of unprecedented accuracy, number, and magnitude range, will come to an end.

In an information note two months ago, ESA announced the planned end of observations. I quote:

"The Gaia spacecraft relies on a cold gas propellant to keep it spinning and scanning the sky. The amount of remaining cold gas decreases by about a dozen grams per day and is reaching its end in early 2025. The Gaia science observations will therefore end on 15 January 2025, meaning that no more nominal science data will be acquired by Gaia after that date. This is, however, far from being the end of this transformative mission.

"The Gaia scientific and engineering teams will continue to work full steam on the preparations for Gaia Data Release 4, which is not 'more of the same' but will make new groundbreaking science possible by including a much larger data volume, many more data products, and data of overall better quality compared to Gaia Data Release 3.

"In 2025, once all of Gaia's nominal science data have been downlinked to Earth, the processing for the final Gaia Data Release 5 will ramp up to full speed and run in parallel to the processing of Gaia Data Release 4. Gaia Data Release 4, covering 5.5 years of mission data, is expected in 2026 and Gaia Data Release 5, covering the full 10.5 years of mission data, around the end of the decade.

"After Gaia's science observations end on 15 January 2025, a period of technology tests will commence. These will allow us to study in more detail the behaviour of some spacecraft and instrument components, with the potential of further improving the Gaia calibrations and aiding the design of future space missions.

"After these tests, which will last several weeks, the Gaia spacecraft will leave its orbit around the Lagrange point L2 to be put into its final heliocentric orbit, away from Earth's sphere of influence. Eventually, the Gaia spacecraft will be passivated in March/April 2025 and reach its well-deserved retirement."

Let me recall the timeline of the Gaia data releases up to now, and the current plans for the future, as given in the above announcement.

Gaia DR1 was released on 14 September 2016, and the ESA Gaia www pages provide both an overview, and a description of the catalogue contents.

Gaia DR2 was released on 25 April 2018, and the ESA Gaia www pages provide both an overview, and a description of the catalogue contents.

Gaia EDR3 (Early Data Release 3) was made available on 3 December 2020, and the ESA Gaia www pages provide both an overview, and a description of the catalogue contents.

Gaia DR3 was released on 13 June 2022, and the ESA Gaia www pages provide both an overview, and a description of the catalogue contents.

Gaia FPR (Focused Product Release) was issued on 10 October 2023, and the ESA Gaia www pages provide both an overview, and a description of the contents.

In previous essays, I have given my own summaries of these various releases, covering DR1–EDR3 (essay 10), DR3 (essay 76), and the various topics covered by the Focused Product Release (essays 157–161).

For the future, the current plan is for Gaia DR4, based on 66 months of data, to be released not before mid-2026. This will consist of the full astrometric, photometric, and radial-velocity catalogues; all available variable-star and non-single-star solutions; source classifications plus astrophysical parameters (from BP/RP, RVS, and astrometry) for stars, unresolved binaries, galaxies, and quasars; an exoplanet list; and the epoch and transit data for all sources.

Gaia DR5, based on all 10.5 years of mission data, will not be available before the end of 2030, when it will consist of the complete Gaia Legacy Archive of all data.

Recalling that the latest full catalogue, DR3, covers just the first 34 months of mission data, those who have worked with the Gaia catalogues will have some appreciation for the harvest expected once the full mission data set, covering more than 10 years, becomes available.

FOR THOSE INVOLVED in the early ideas for Gaia, and in my own case as ESA's Project Scientist for the first 15 years of the mission, the acquisition of 10+ years of mission data is a wonderful achievement… but also one for which provisions were carefully made!

Our top-level specifications, presented in the 380-page Concept and Technology Study Report of July 2000, called for a 5-year design life, with an extended lifetime of a further 5 years. Specifying a 10-year *design* lifetime would have come with additional industrial costs, considered unnecessary for the basic mission objectives. But many scientific and technology studies underpinned arguments for an extended operation period. Let me quote our summary from the 2000 study report.

"Although the many advantages of the space environment permit significant measurements to be made in a relatively short time, some of the more complex motions cannot be properly explored on a time scale of 2–3 years. This concerns, in particular, binaries with periods up to several years. The instrument is also ideal for planetary detection, but measurements extending over a significant fraction of the orbital period are mandatory.

"Additional motivations for a longer temporal baseline are for the dynamical studies of asteroids, and for photometric variability studies. The design lifetime is used for the assessment of the astrometric and photometric accuracies, and for the evaluation of all instrument and system performances, including the reliability analysis. The design lifetime was subject to a major system trade-off, since a longer design lifetime could actually minimise the satellite complexity.

"An extended design lifetime of 5 further years has also been considered, during which the satellite's design features will permit additional measurements to be made. The extended lifetime has been used for the sizing of all consumables (propellant) as well as for the sizing of items which suffer from aging and radiation effects, including the solar cells and thermal surfaces."

THE TECHNOLOGY TESTS that are planned for the Gaia satellite, after 15 January, are detailed in the above referenced information note. I will summarise:

On 15 January 2025, the last of the remaining cold gas, estimated to be an equivalent of about 15 days of nominal operations, will be used for technology tests.

The goal of these technology tests is to learn more about the instruments. This could help to improve Gaia calibrations for future data releases, but also the design of future space missions. Some of the Gaia technologies have already been re-used, for example the mirror-drive electronics and cold-gas thrusters on EUCLID. Future science missions such as the gravitational wave observatory LISA or the potential next generation Gaia–NIR are going to be ever more sensitive and are good candidates that might profit from the Gaia experience.

Some specific payload calibrations are also planned. The special virtual object patterns on-board will be used for an extended period to map the straylight, CCD response, and wings of the point spread function. Additionally, high-rate pre-scan pixel sampling will be undertaken to probe some known issues, and to map the temperature variations across the focal plane.

To better understand the cause of the tiny variations in the 'basic angle' between the two fields of view (as measured by the 'basic angle monitor'), and so provide important information for the design of future space missions, tests will study how it varies following certain changes in the spacecraft configuration.

AS THE operations end, let me express my own deep appreciation to all the individuals and teams involved: scientists and engineers who worked since the early 1990s on the early designs, the ESA advisory groups responsible for Gaia's selection in 2000, the ESA and industrial teams, and the launch authorities. The ESOC satellite operations team merit special recognition for keeping Gaia operating efficiently throughout. As do all members of the Gaia Data Processing and Analysis Consortium, DPAC, who are working with intensity and dedication to create the remarkable mission products.

I ASKED JUST a few of those involved for their thoughts. 65 years after his first contributions to astrometry, and 35 years after his first designs of a Hipparcos successor, Erik Høg, now 92, said: *'It is like a dream to witness the mission's success'*. Lennart Lindegren, now 74 and a central scientific figure in both Hipparcos and Gaia, said: *'Coming to the end of the science data gathering is a bit sad, but also deeply satisfying, because we know that something truly extraordinary has been achieved'*.

Vincent Poinsignon, industrial project manager said: *'Gaia was one of our biggest satellite challenges, and probably our biggest scientific success. Airbus is proud to have contributed to this major advance'*.

David Milligan, the satellite operations manager at ESOC for most of the mission, said: *'Our operations team started work several years before launch, preparing for both routine operations and unexpected contingencies. It is wonderful to see its success'*.

Uwe Lammers, Gaia's mission manager, said: *'Ten and a half years of observing have given us a treasure trove of trillions of measurements which will be turned into a final legacy dataset (DR5) that is likely to remain a standard for astrophysical research in the coming decades. So, although satellite operations will, sadly, end soon, the best is yet to come!'*.

Anthony Brown, chair of the DPAC Consortium, said: *'Our 400-strong scientific consortium joins in celebrating over 10 years of surveying the Milky Way and beyond, and looks forward to delivering data releases DR4 and DR5'*.

212. Runaways stars in R136

I INTRODUCED THE SUBJECT of 'runaway stars' in essay 165, and made brief reference to the two known runaways in the young cluster R136 in the Large Magellanic Cloud. Recent results on runaways in this cluster merit a detailed discussion, but let me first summarise a few key points that I covered in that earlier essay.

Runaways are stars with such high space velocities, above an adopted threshold of 30 km s^{-1}, and sufficiently distinct from the overall stellar velocity distribution, that they must have been imparted by a particular formation process. Most are young massive O stars, or Wolf–Rayet stars (essay 105). [The even more extreme 'hypervelocity stars', hurled out from close encounters with the supermassive black hole in the centre of our Galaxy (essay 166), do not concern us here.]

The discovery of runaway stars followed from the realisation that many O stars (Blaauw, 1961; Gies & Bolton, 1986; Gies, 1987) and Wolf–Rayet stars (Moffat & Isserstedt, 1980; Moffat et al., 1998) lie well outside their likely birth places in open clusters and OB associations, with some motions 'pointing back' to their likely origin.

There are two main theories for the origin of runaway stars, and both appear to operate. In the *binary-supernova scenario*, BSS (detailed in essay 165), the disruption of massive binary systems due to one or other of the two successive supernova explosions can result in large recoil velocities of the companion. In the *dynamical ejection scenario*, DES, a star is ejected as a result of dynamical interactions in a young, compact cluster.

In essay 165, I summarised the pre-Hipparcos history of runaways (based largely on radial velocities), the modest advances made with the Hipparcos observations of ~1000 O–B5 stars (still limited by the 1 milli-arcsec level accuracies of distances and proper motions), and the identification and characterisation of many new candidates with Gaia. These include 25 new candidates 'escaping' from the Orion Nebula Cluster, others from the Small Magellanic Cloud, and some 200 new candidates from the Gaia DR3 astrometry of existing catalogues of Galactic O and Be stars. A very broad conclusion is that dynamical ejection appears to dominate.

OBJECTIVES in studying runaway stars include gaining insights into massive star formation; better understanding the two-step ejection processes involved in the binary supernova scenario; and modelling the end products of the BSS scenario (which include pairs of high-velocity single pulsars, as well as binary pulsars).

A better characterisation of the dynamical ejection scenario is also leading to an improved understanding of stellar kinematics in clusters and associations. Associated models employ increasingly detailed N-body simulations to study the effects of mass segregation, binary fraction, period distribution, binary mass ratios, and eccentricities (e.g. Oh & Kroupa, 2016).

As a result of one or other mechanism, it appears that at least 10 percent of OB stars are hurled out of their birth clusters before ending their lives as supernovae somewhere along their escape trajectory. Runaway stars often create spectacular 'bow shocks' as they plough through (and inform us about) the interstellar medium. Examples from HST–ACS imaging can be found here. A Spitzer image of the runaway ζ Oph can be found here.

AS HAS BECOME evident in the past few years, runaway stars also have an important role in the context of ΛCDM cosmology, where certain inconsistencies found in large-scale numerical simulations have been attributed to challenges in modelling the 'baryon cycle', i.e., how galaxies accrete and expel their gas (Naab & Ostriker, 2017). Stellar feedback (in which stars influence the surrounding environment through the injection of energy, momentum, and mass), is an important factor, involving contributions from protostellar jets, stellar winds, supernovae, and ionising radiation.

Runaway stars can travel hundreds of parsecs into the low-density interstellar medium, depositing momentum and energy, and affecting supernova rates and gas densities (e.g. Ceverino & Klypin, 2009; Andersson et al., 2020; Steinwandel et al., 2023; Andersson et al., 2023; 2024). For example, Andersson et al. (2020) found that including runaways leads to twice as many supernovae over a wide range of ISM densities.

GAIA IS PROVIDING some particularly interesting insights into runaway stars associated with the massive young cluster R136 in the Large Magellanic Cloud.

Named after the Radcliffe Observatory Magellanic Clouds Catalogue (Feast et al., 1960), R136 is the central concentration of stars in the NGC 2070 cluster, lies at the centre of (and illuminates) the Tarantula Nebula (aka 30 Doradus), and marks the nebula's most recent burst of star formation. Originally catalogued as the unresolved star HD 38268 (V = 7.25 mag), it comprises some 100 O and Wolf–Rayet stars within 5 pc/20 arcsec (Massey & Hunter, 1998; Doran et al., 2013).

With a cluster mass of $\sim 5 \times 10^5 M_\odot$, and a density far higher than typical OB associations, R136 hosts several extremely massive stars, including R136a1 ($200 M_\odot$, Crowther et al., 2010; Shenar et al., 2023). While these challenge the canonical stellar mass limit of around $150 M_\odot$ (e.g. Weidner & Kroupa, 2004), mergers of massive binaries may have produced a few single stars with such high masses (Banerjee et al., 2012). With an age of < 2 Myr, none of its members are significantly evolved, and none are thought to have exploded as supernovae.

THE FIRST runaways associated with R136 were provisionally identified using radial velocities from the VLT–FLAMES Tarantula Survey (Evans et al., 2011): VFTS 16 (Evans et al., 2010), and VFTS 682 (Banerjee et al., 2012) both of which were subsequently confirmed from their high proper motions in Gaia DR2 (Lennon et al., 2018, and Renzo et al., 2019, respectively).

N-body simulations of dynamical ejections met with some success in explaining their existence (Banerjee et al., 2012; Perets & Šubr, 2012; Oh & Kroupa, 2016). Another model invoked a single very massive wide binary (their 'bully binary') to scatters massive stars out of their host cluster (Fujii & Portegies Zwart, 2011).

Another 10 candidates, reaching out to around 35–400 arcsec (10–100 pc), were identified from two-epoch (2011–14) HST observations (Platais et al., 2018).

Proper motions from Gaia DR2/DR3 ($\lesssim 0.4$ mas yr^{-1}, corresponding to velocities 100 km s^{-1}) were later used to confirm some of these candidates through a comparison of their inferred flight times (dynamical ages) with their evolutionary ages (Gebrehiwot & Teklehaimanot, 2021; Teklehaimanot & Gebrehiwot, 2024).

NEW INSIGHTS came from the rotational velocities derived from the VLT–FLAMES Tarantula Survey. Sana et al. (2022) identified an overabundance of rapid rotators ($v \sin i > 200$ km s^{-1}) among the runaway stars, and suggestive of two distinct populations: one slower moving but rapidly rotating, and one faster moving but more slowly rotating.

They argued that the former result from binary ejections (and dominate the massive runaway population), while the latter result from dynamical ejections.

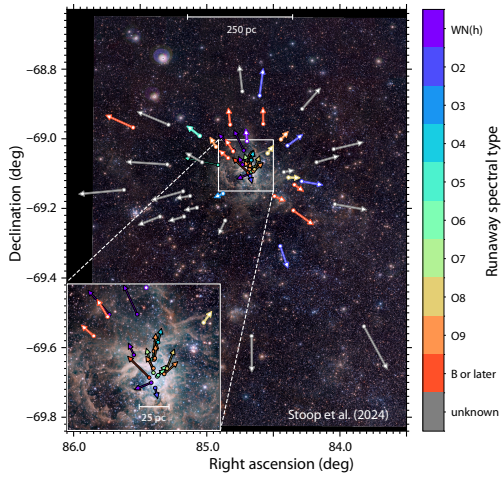

A MAJOR ADVANCE in characterising the runaway population from R136 came with Gaia DR3. Stoop et al. (2024), starting with 80 000 sources with $G < 18$ mag and within 1 degree of R136, identified 55 massive runaway stars, increasing the number of known runaways escaping from the cluster core by an order of magnitude.

They have reached (projected) distances of 3–460 pc from R136. This implies that half have already left the 30 Dor region, such that their ionising radiation and stellar winds (and eventually their powerful supernovae) affect relatively tenuous areas beyond the nebula itself.

They classified the runaways as dynamical ejections falling into two distinct groups (image above). The first comprises massive stars ejected isotropically (with kinematic ages peaking around 1.8 Myr) which, they show, are consistent with dynamical interactions during and after the birth of R136. They also provide an independent age estimate of the cluster. The second group comprises 16 stars with kinematic ages around 0.2 Myr, ejected preferentially in a northerly direction, which they attribute to the effects of a later cluster interaction.

They found that 23–33% of the most luminous stars in R136 are runaways, a dynamical escape fraction significantly higher than the model predictions noted previously. And this confirms the growing picture that their role in shaping and heating the interstellar and Galactic medium, along with their role in driving Galactic outflows, is more important than previously thought.

THEORISTS HAVE been quick to examine the implications. Polak et al. (2024) have recently proposed a third mechanism for the formation of runaway stars, in addition to binary supernova and dynamical ejection.

In their 'sub-cluster ejection scenario', a subset of stars from an infalling sub-cluster is ejected out of the cluster via tidal interactions with the contracting gravitational potential of the assembling cluster. And they propose that the group of runaways ejected to the north of R136 is a promising example of such a scenario.

213. Telescope calibration/pointing: 1

GAIA IS MAKING substantial contributions to the improved calibration and pointing of ground- and space-based telescopes. There are, however, few published descriptions of these sorts of applications.

Before detailing some of these developments with Gaia in my next essay, in part based on inputs from various observatories, I will look here at what is now largely consigned to history – how the first space astrometry positions from Hipparcos were applied to the calibration of photographic plates and meridian circles.

ASTROMETRIC MEASUREMENTS naturally divide into two broad categories. *Narrow-field* instruments, providing relative measurements over not more than a few degrees, include photography, CCD imaging, adaptive optics, speckle interferometry, and phase-referencing radio interferometry. *Wide-field* or semi-global techniques include meridian circles or transit instruments, astrolabes, optical phase interferometers, Michelson interferometry, radio interferometry including VLBI, and the satellites Hipparcos and Gaia.

Photographic and CCD instruments are further categorised, according to focal length, image scale, and field of view, into classical astrographs (as used for the early Carte du Ciel project), Schmidt telescopes which extended the field of view by compensating for spherical aberration, and long-focus instruments yielding a larger scale – originally based on refractors to provide better mechanical stability, but subsequently using reflectors. Later astrographs, e.g., those at Lick and Yale, had fields around $4-5°$, while the USNO Twin and Hamburg Zone Astrographs had fields of around $9°$.

The main challenge for wide-field or semi-global astrometry is the measurement of large angles, and in the provision of a fundamental system in the absence of any other reference frame. For several centuries, and until the end of the 20th century, the basic instrument was the meridian circle: a combination of a transit instrument and a vertical circle, from which the right ascension was deduced from the local sidereal time and the declination from the zenith distance at the time of meridian transit.

THE USE OF photography to determine star positions began around 1870, flourished with the immense international cooperation of the Carte du Ciel (e.g. Debarbat, 1988; Urban & Corbin, 1998; Jones, 2000), and remained a fundamenal astrometric technique almost until the end of the 20th century. Schmidt telescopes, from the 1930s onwards, also had astrometry as their main objective. Such surveys were only superseded, from the 1990s, by ground-based digital surveys. In parallel, fast and accurate measuring machines and associated reduction software were developed (e.g. Kovalevsky, 2002).

IN THE REDUCTION of photographic plates, the transformation between the celestial sphere, and the xy domain of a set of plate measurements, is generally a one-to-one vector transformation. But this must account for many factors: orientation of the plate axes, plate tilt and centre, scale factor, gnomonic projection, coma and field curvature, distortion, astigmatism, differential atmospheric refraction, chromatic aberrations, and magnitude equation, i.e. positional errors as a function of magnitude (e.g. Eichhorn & Williams, 1963; Kiselev, 1989; Brosche et al., 1989; Bienayme, 1993).

Before Hipparcos, an insuperable obstacle was the absence of a sufficiently accurate *and* dense stellar reference frame – both properties were necessary. A high-accuracy reference framework was required to exploit the intrinsic plate accuracy, of typically 0.1 arcsec or a little better, while a high reference star density was needed to model behaviour more complex than, say, a third-order polynomial in x and y.

This changed with the availability of the Hipparcos and Tycho Catalogues in 1997, with the accurate proper motions also ensuring that a high-accuracy reference frame could be propagated over half a century or more.

As a result, the subsequent decade saw a substantial effort from groups who re-reduced, and in many cases also re-measured, a wide variety of plate material obtained during the entire 20th century, as well as meridian circle observations, and data from other classical astrometric instruments (e.g. Vondrák et al., 2000).

I WILL GIVE just a few examples of these re-calibration efforts, referring the interested reader to Perryman (2009, Chapter 2) for further details.

Early application to the Bordeaux and La Palma automatic meridian circles replaced the previously used FK5 catalogue positions with those from Hipparcos (Requieme et al., 1995; Argyle et al., 1996). This resulted in *'a remarkable improvement in the post-fit residuals'*, with standard deviations falling from around 0.2–0.3 arcsec to around 0.02–0.05 arcsec in both coordinates.

Many such re-calibration efforts, and very extensive catalogues, were derived in this way. But the availability of the Hipparcos reference frame rapidly made classical visual meridian instruments obsolete, and several automatic circles were subsequently closed down. However it was demonstrated at Flagstaff (Stone et al., 1996) that, equipped with a CCD detector, and working in drift-scan mode, meridian circles could give internal errors of less than 50 mas to $V = 15 - 16$ mag, based on bright reference stars from the Hipparcos and Tycho Catalogues.

Plans to equip other meridian circles with CCDs were followed up at Bordeaux (Viateau et al., 1999), Mykolaiv (formerly Nikolayev) in Ukraine (Pinigin et al., 1997), Valinhos at São Paulo (Lopes et al., 1999), and the San Fernando (Cádiz) instrument at El Leoncito in Argentina (Muiños et al., 2002). The Carlsberg Meridian Telescope at La Palma (formerly the Carlsberg Automatic Meridian Circle) proved particularly productive in extending the magnitude limit to (Sloan) $r' = 17$ mag (Evans, 2001; Evans et al., 2002), although the instrument was also finally decommissioned in 2013.

In another example, the US Naval Observatory pole-to-pole catalogue $W2_{J00}$ (Rafferty & Holdenried, 2000) was constructed from observations between 1985–1996 using two transit circles, one located in Washington DC (the six-inch circle, operated there since 1897), and the other in Blenheim, New Zealand (a seven-inch circle, originally operated since 1948 from El Leoncito, Argentina). The authors commented: *'This project is the latest and largest of a long series of transit circle catalogues produced by the US Naval Observatory. It is also, because of advancing technologies, certainly the last'*.

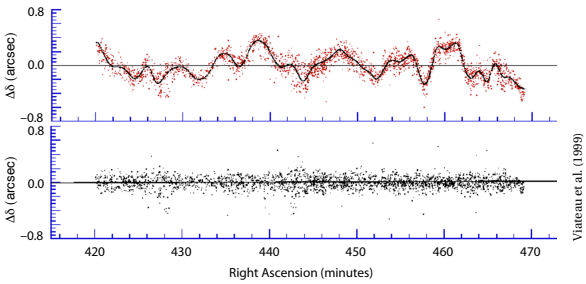

Top: residuals between a Bordeaux meridian circle strip and the mean catalogue positions from Hipparcos/Tycho, showing the best-fit B-spline. Bottom: after subtraction of the B-spline.

THE RE-CALIBRATION of photographic plates using Hipparcos positions was also pursued extensively, creating catalogues of positions and proper motions for large numbers of stars down to the plate limits.

Early re-reductions of Schmidt plates using the Hipparcos/Tycho data (Robichon et al., 1995) were followed by many plate digitisation and reduction efforts (e.g. exploiting the early Palomar POSS and later SERC plates) using the APM, APS, DSS, and SuperCOSMOS measuring machines, leading to (amongst others) the Digitised Sky Survey and the Guide Star Catalogue (GSC) for HST operations, with GSC II comprising 945 million stars (Robichon et al., 1995; Lasker et al., 2008).

Other substantial catalogues subsequently placed on the Hipparcos reference frame included the USNO A1 (Monet & Corbin, 1997), USNO A2 (Assafin et al., 2001), and USNO B1 (Monet et al., 2003) catalogues, and the early epoch AGK2 (Zacharias et al., 2004), CPC2 (Zacharias et al., 1999), and Lick NPM (Hanson et al., 2004) and SPM (Girard et al., 2004) catalogues.

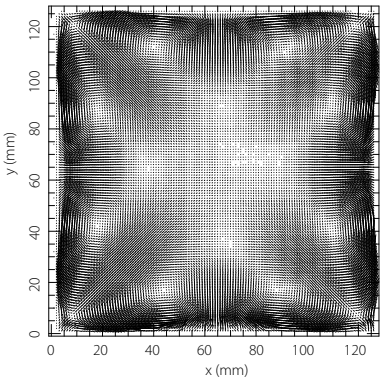

Fixed-pattern astrometric residuals for the first-epoch Palomar POSS O survey plate, reduced to the Hipparcos reference system, at 18 mag. The pattern is very different for bright stars (Monet et al., 2003).

A related and extensive topic, which I can only touch on here, is the use of Hipparcos in the re-calibration of the Astrographic Catalogue (to 11.5 mag, and completed in the first quarter of the 20th century), and the related but deeper (to 14 mag) Carte du Ciel plates, started in 1891 and finally completed only in 1950.

This huge undertaking started with a machine-readable version (Kuzmin et al., 1999), with 22 separate zones yielding the 4.6 million star Astrographic Catalogue at mean epoch 1907: AC2000 (Urban et al., 1998b; Urban et al., 2001). Two parallel efforts combined these first epoch measurements with the Tycho Catalogue: the TRC (Høg et al., 1998) and the ACT (Urban et al., 1998a), all eventually superseded by the Tycho 2 Catalogue of 2.5 million stars (Høg et al., 2000a; Høg et al., 2000b).

GAIA'S DEPTH and accuracy is such that re-analysis of old photographic and meridian circle observations provides little new astrometric information, and I am not aware of any such treatments. But as I will show in the next essay, Gaia does play a very important role in today's instrument calibrations and telescope pointing.

214. Telescope calibration/pointing: 2

In my previous essay, I looked at the use of the space-based Hipparcos and Tycho Catalogues in revisiting the calibration of (ground-based) photographic plate and meridian circle surveys carried out over the preceding decades. Here, I will continue this theme, and look at how the Gaia reference system, and its positions and proper motions, are being used in the pointing and calibration of ground- and space-based telescopes.

Both the Hubble Space Telescope and James Webb Space Telescope rely on the Space Telescope Science Institute's Guide Star Catalog (GSC) for telescope pointing and instrument calibration. But HST's astrometry has long been limited by uncertainties in the catalogue's celestial coordinates, with additional uncertainties arising in the alignment of the science instruments to the Fine Guidance Sensors (FGS).

GSC 1.1 (Aug 1992) had rms errors of at least 0.5–1 arcsec in each coordinate. GSC 2.4.0 (Oct 2017) used positions/proper motions from Gaia DR1 to reduce these errors to below 30 milli-arcsec. Further updates have been made with each Gaia data release, with the most recent GSC 3 using Gaia DR3 as its base catalogue.

Today, both HST and JWST use the Gaia DR3 catalogue for identifying reference stars, for their image calibration pipeline, and for updating the astrometric 'World Coordinate System' in their headers. The astrometry of *archival* HST observations has also been reprocessed using the improved Gaia reference frame.

More widely, GSC itself has been adopted for observation planning, preparing finding charts, and for the operation of ground-based telescopes. Amongst these, recalibration of the astrometry for Pan–STARRS1 has been carried out based on Gaia DR2 for the 1.7 billion objects in PS1/DR2 (Lubow et al., 2021) and later based on Gaia EDR3 (White et al., 2022).

The infrared Nancy Grace Roman Space Telescope (formerly WFIRST), due for launch in May 2027, makes use of the Gaia entries in GSC both for its guide stars, and for the pipeline image calibration. It is expected that GSC will have incorporated Gaia DR4 by that time.

For JWST, Gaia has also played a key role in the calibration of the optical distortion for all four instruments. These used a field of 180 000 bright stars in the Large Magellanic Cloud, lying within the telescope's 'continuous viewing zone', and with a star density sufficient for a very detailed distortion map. The field was first observed with HST–ACS/WFC in 2006, and again in 2017, both duly matched to the Gaia DR2 reference frame (Anderson et al., 2021). Other papers cover the astrometric calibrations for each instrument (Lützgendorf et al., 2022; Libralato et al., 2023; Patapis et al., 2024).

Gaia astrometry was also vital for knowing the positions of early science targets (e.g. high-z galaxy candidates previously found with HST) accurate enough that they could be observed using NIRSpec's Micro-Shutter Assembly: this consists of four separate 98×91 arcsec^2 quadrants each containing 365×171 individually addressable shutters whose open areas on the sky subtend 0.20×0.46 arcsec^2 (Ferruit et al., 2022). NIRSpec observations based on prior NIRCam exposures, which are placed on the Gaia reference frame, ensure that targets do fall within the 200 millli-arcsec wide MSA slitlets.

Continuing with the satellite theme, I described the principles of interplanetary spacecraft navigation in essay 52. As a prominent example, the New Horizons fly-by of Pluto and its moon Charon, in July 2015, was based on the JPL solar system ephemerides DE430, itself based on the celestial reference frame materialised by Hipparcos in the late 1990s. But the subsequent flyby of the trans-Neptunian object Arrokoth on 1 Jan 2019 made use of the Gaia DR2 star positions to adjust the spacecraft's pointing.

When the closest flyby images came back, Arrokoth was framed perfectly. *'None of that would have happened if we hadn't had the Gaia catalogue'*, Marc Buie, discoverer of Arrokoth, is quoted as saying. *'It's a fundamental rewriting of how we do positional astronomy'.*

At ESOC, ESA's satellite operations centre at Darmstadt, Germany, the Gaia catalogue is today used across all satellite operations and instrument pointing.

Autonomous Star Trackers are the primary sensors used for the 3-axis satellite attitude control of most satellites (e.g. Eisenman et al., 1997; Bürger et al., 2024). With their 20 deg full-cone field of view, magnitude limit of 5.5–6 mag (requiring some 3000 stars across the sky), and positional requirements of order 1 arcsec, the Hipparcos catalogue remains sufficient for many uses. The Gaia catalogue is now used in the 'very high-accuracy' star trackers which target an order of magnitude performance improvement. ESOC are using a design with full-cone field of 4 deg, requiring a much larger star catalogue with sub-arcsec positions and proper motions.

Space science observatories today also often require 'fine guidance sensors' to ensure stable long-duration pointing, and these are all making use of the Gaia catalogue. Amongst these, Euclid, launched in 2023 and operated at L2, uses stars down to 18 mag (Euclid Collaboration et al., 2025). Missions under development, and making use of Gaia for their fine guidance sensor control, include Plato (Grießbach et al., 2021), and Ariel (Mösenlechner et al., 2024).

Let me turn to a just a few examples in ground-based telescope operations. For the 11-m SALT, the South Africa Large Telescope, Gaia is used to select guide stars, and for pre-positioning the guiders during pointing, significantly increasing acquisition efficiency. Gaia's radial velocity information is also used to monitor the stability of their high-resolution spectrograph.

Elsewhere at the South African Astronomical Observatory, SAAO, their fully automated Lesedi 1-m telescope relies on the Gaia catalogue to generate suitable guide stars, operating as a background automated service and ensuring real-time targeting accuracy. For Meerlicht, the 'optical eye' of the radio MeerKAT telescope, Gaia provides absolute photometric calibration of every point source within the survey images. This has enabled rapid tagging and alerting of transient sources, integrating Gaia's precision into their alerting infrastructure.

Stephen Potter, SAAO's Head of Astronomy, summarised Gaia's contributions this way: *'Many of our new observatory operational and scientific developments have directly benefited from Gaia data releases in ways that were simply not possible before. Its high-precision astrometric and spectroscopic data has been transformative for both our operations and our science.'*

For SDSS, the Sloan Digital Sky Survey, Gaia *'has been transformative'*. It now provides a reliable dense set of guide stars for wide-field spectroscopy across the entire sky, especially for the southern hemisphere. Mike Blanton commented that *'Before Gaia, many many hours were spent cobbling together various sources of guide stars, ensuring they were on the same system, estimating magnitudes, etc. This instantly became a completely solved problem when Gaia data was available'*.

For SDSS–V, which provides multi-epoch optical and infrared spectroscopy, Gaia plays a key role. Targets come from many sources, including SDSS imaging, Pan–STARRS1, 2MASS, WISE, DECam, SkyMapper, and Gaia. The Gaia catalogue forms the base layer for the process of object cross-matching, as well as the most reliable source of coordinates (and, importantly, their proper motions) for the fibre placement.

Beyond the operational aspects, Gaia data is used in star selection for the 3 million star SDSS–V Milky Way Mapper program, using cuts on Gaia parallax, colour, and absolute magnitude (Almeida et al., 2023a).

At the 4.2-m William Herschel Telescope on La Palma, Gaia is one of the main reasons for building the new fibre-fed multi-object spectrograph, WEAVE, which will take spectra of up 1000 objects simultaneously. The instrument was built to provide spectroscopic follow-up for several large survey facilities, and in particular Gaia. Use is also made of the Gaia magnitudes of the guide stars to monitor the transparency of the sky while observing. This allows observations to be extended (or rescheduled) as required, again promoting more efficient use of the night.

More widely, use of Gaia's accurate coordinates, for both targets and guide stars, has made acquisition onto slits and fibres significantly more accurate than before, thereby improving instrument throughput, and the efficiency with which observing time can be used.

Similarly, LAMOST uses Gaia astrometry both as the Gaia identifier (GID, where 99% of targets have Gaia observations), and as the source catalogue for the proposed scientific targets, which is used to establish the accurate pointing of the telescope's 4000 optical fibres.

With first light in July 2025, the Vera C. Rubin Observatory presents various challenges for its astrometric calibration. With a 7 mag fainter limit than Gaia, it will embrace at least an order of magnitude more stars. And it uses the 3-colour Gaia photometry to transfer Gaia's rigid photometric system above the atmosphere to all objects observed (Ivezić et al., 2019).

Ivezić et al. (2019) continues: *'Astrometric calibration will be based [on Gaia], which will provide numerous high-accuracy astrometric standards in every [LSST] field'*. Wilson (2023) details the practical challenges involved in object matching, given that 90% of the sources are significantly fainter than the Gaia survey limit.

I am grateful to the following for the details used in this essay: Chris Benn (ING, La Palma), Mike Blanton (SDSS, New York University), Peter Jakobsen (JWST–NIRSPEC), Steeve Kowaltschek (ESOC), Ali Luo & Chenzhou Cui (LAMOST), Brian McLean (STScI/GSC), and Stephen Potter & Encarni Romero Colmenero (Head of Astronomy, SAAO, and Director of SALT, respectively).

215. Black holes and Gaia: an update

THERE IS OVERWHELMING evidence for the existence of black holes. Amongst them, supermassive black holes, with masses upwards of $10^5 M_\odot$, appear to exist at the centres of almost all large galaxies, growing over cosmological time by hierarchical galaxy mergers.

The existence of such objects so soon after the Big Bang, at redshifts $z > 7$ (e.g. Mortlock et al., 2011; Bañados et al., 2018; Wang et al., 2021) suggests that they originated by the seeding from massive star collapse in the early Universe, or perhaps more directly from the collapse of early supermassive stars, or even through the collapse of large gas clouds pre-dating the first stars.

Here, Gaia contributions include (a) the identification of dual active galactic nuclei as a result of galaxy mergers (essay 163), (b) the identification of hypervelocity stars originating from the supermassive black hole in the Galactic centre and elsewhere (essays 22 and 166), and (c) tidal disruption events, resulting from a star passing close to a supermassive black hole such that tidal forces overcome its self-gravity (essay 206).

Intermediate-mass black holes, $10^2 - 10^5 M_\odot$, are also inferred to exist in the centres of galaxies or globular clusters, and a few hundred candidates are known (e.g. Chilingarian et al., 2018). I described these, and Gaia's contribution to the evidence for such an object in the globular cluster M4 (Vitral et al., 2023), in essay 177.

STELLAR MASS black holes, with masses $5 - 50 M_\odot$ or higher, result from the gravitational collapse of massive stars at the end of their lives. Isolated stellar mass black holes are most directly discoverable from photometric microlensing, or less directly through their dynamical manifestations in open clusters (essay 175), or stellar streams (essay 176).

The only confirmed object is OGLE–2011–BLG–0462 ($7.1 M_\odot$, $d = 1.58$ kpc), characterised from astrometric measurements with HST (Sahu et al., 2022). A recent candidate, from the Gaia science alerts system (essay 202), is Gaia18ajz, at $4.9 M_\odot$ (Howil et al., 2025). Gaia constraints on Spitzer candidates are discussed by Rybicki et al. (2024), with prospects for detecting primordial black holes discussed by Verma & Rentala (2023).

THE DISCOVERY SPACE is much larger for stellar mass black holes in binaries. In compact systems, they may be identified from the X-ray emission arsing from mass transfer, divided (according to donor mass) into low-mass (LMXB) or high-mass (HMXB) X-ray binaries. There are more than 20 candidates, including Cyg X1 ($M_{\rm bh} \sim 21 M_\odot$ in a 5.6-d period binary) and V404 Cyg ($M_{\rm bh} \sim 12 M_\odot$ in a 6.5-d period binary) both at distances of 2–2.5 kpc. A recent Gaia result suggests that V404 Cyg is part of wide hierarchical triple (Burdge et al., 2024).

Black holes in binaries may also be manifest, photometrically, through the tidal distortion of the envelopes of their companion star, extreme examples of the class of ellipsoidal variables (essay 133). Rimoldini et al. (2023) identified 65 300 candidate ellipsoidal variables in Gaia DR3, and searches for black hole systems amongst them are ongoing (Gomel et al., 2023; Fu et al., 2022a; Rowan et al., 2024). Shahaf et al. (2023), for example, identified eight candidate black-hole systems with compact-object masses $\gtrsim 2.4 M_\odot$.

Among other discovery techniques are binary black hole mergers evidenced by gravitational waves, the first of which, GW150914, was detected by LIGO/Virgo in 2015. Efforts to extend Gaia's science alerts trigger limit to $G > 19$ mag, with the goal of detecting their electromagnetic counterparts, are ongoing (Kostrzewa-Rutkowska et al., 2020; Biswas et al., 2023; essay 202).

AN IMPORTANT discovery method, and a field now being opened up by Gaia, is the detection of black holes in wider, non-interacting binary systems, through the astrometric motion of their (visible) companion star.

I described the background, and the first of these discoveries, Gaia BH1 (Chakrabarti et al., 2023; El-Badry et al., 2023b), in essay 101. Gaia BH2 was discovered in a similar manner by El-Badry et al. (2023a). A third, Gaia BH3, was found by Panuzzo et al. (2024), with some illustrative animations here.

Other Gaia *candidates* include β Cyg (Albireo) (Bastian & Anton, 2018; Drimmel et al., 2021; Jack et al., 2022), and the Gaia DR3 objects G5870 (Tanikawa et al., 2023), and G3425 (Wang et al., 2024b).

System	G (mag)	$M_{\rm bh}$	M_2	$P_{\rm orb}$(d)	e	d (pc)
Gaia BH1	13.8	9.61	0.93	185	0.45	480
Gaia BH2	12.3	8.94	1.07	1280	0.52	1160
Gaia BH3	11.2	32.70	0.76	4250	0.73	590

PROPERTIES of these (bright) Gaia discoveries are summarised above. The published orbital solutions employ ground-based spectroscopy and radial velocities (of the visible component) to validate and refine the Gaia astrometric solution. For example, Gaia DR3 astrometry of Gaia BH1 defines a photocentric ellipse with a semi-major axis of only $a_0 = 3.00 \pm 0.22$ mas (El-Badry et al., 2023b). Their combined orbit solution used radial velocities from Magellan–E, Gemini–GMOS, VLT–X-Shooter, Keck–HIRES, ESO–FEROS, and Keck–ESI.

All three immediately entered the record books as the nearest known black holes, a distinction previously held by Cyg X1 (between 1975–86), and V616 Mon (from 1986 until the discovery of Gaia BH1 in 2023). And their proximity suggests that such wide black-hole binaries, while harder to detect than compact systems with ongoing accretion, must be significantly more common.

Also noteworthy are their large orbital periods, longer than any other black hole binaries. Follow-up searches have failed to detect radio or X-ray emission (El-Badry et al., 2023b, §7; El-Badry et al., 2023a, §3; Cappelluti et al., 2024; Gilfanov et al., 2024; Sjouwerman & Blanchard, 2024; Rodriguez et al., 2024), suggesting that the accretion rate at the event horizon is much lower than the Bondi–Hoyle–Lyttleton rate (El-Badry et al., 2023b, §3.12.2).

THE THIRD OBJECT, Gaia BH3, has attracted interest because of its high mass, $33M_\odot$, more than any other Galactic stellar-origin black hole. This ties in with the fact that gravitational waves from black-hole mergers have pointed to a population of extragalactic black holes in short-period binaries with masses $30-85M_\odot$ (Abbott et al., 2020; Abbott et al., 2021). These are more massive than predicted by most stellar evolution models, in which stars with an initial mass $M > 30M_\odot$ lose most of their mass due to strong winds, resulting in observed black hole masses below $\sim 20M_\odot$ (Vink, 2008; Belczynski et al., 2007; Sukhbold et al., 2016).

The suggestion that these more massive objects are the remnants of massive metal-poor stars (e.g. Belczynski et al., 2010) appears to be provisionally supported by the low metallicity of Gaia BH3's companion star, [Fe/H] $=-2.56 \pm 0.11$.

As shown by Panuzzo et al. (2024), its Galactic orbit is consistent with the halo structure of both the Sequoia and ED-2 streams (essay 71), while its metallicity is more consistent with ED-2 ([Fe/H] ~ -2.6) than with Sequoia ([Fe/H] ~ -1.7). The association with ED-2, which likely originated from a disrupted globular cluster, perhaps M92, has been confirmed by Balbinot et al. (2024).

THE FORMATION of these systems is a challenge for standard evolutionary models for isolated binaries (El-Badry et al., 2023b, §8.4; El-Badry et al., 2023b, §5). For example, starting with a $25M_\odot$ primary and a $1M_\odot$ secondary, mass transfer through Roche-lobe overflow of the primary, and starting at separations 10 au or less, would lead to an episode of common envelope evolution (which I have described further in essay 204), during which the orbital separation would be reduced by a factor 100 or more, leading to a present separation a factor of at least 50 smaller than observed.

Other formation channels were noted in the discovery papers. The systems may have originated as very massive primaries that never became a red supergiant, so avoiding mass transfer altogether. They may have formed dynamically through an exchange interaction in a dense cluster. Or they may have originated as a triple system, with the observed 'secondary' being the outer component of an inner close binary, composed of two massive stars (e.g. Hayashi et al., 2023). High-precision VLT–ESPRESSO observations of Gaia BH1 appear to exclude this latter possibility (Nagarajan et al., 2024).

Later models find support for two of these alternative formation channels. Iorio et al. (2024) found that systems such as Gaia BH3 can indeed form from low-metallicity ($Z < 0.01$) binaries initially composed of a massive star ($40-60M_\odot$) and a low-mass companion ($< 1M_\odot$) in a wide ($P > 10^3$ d) and eccentric ($e > 0.6$) orbit. Such systems never undergo Roche-lobe overflow, and the final orbital properties are largely determined at the core collapse of the primary. They suggested that some 4000 star–black hole systems in the Galactic halo have been formed in this way, of which ~100 are compatible with the properties of Gaia BH3, with only one at the distance of Gaia BH3.

Meanwhile, Marín Pina et al. (2024) used N-body simulations to show that such systems can be assembled dynamically in globular clusters. They estimate that the Galaxy halo contains of order 10^5 such systems, some of which may be detected in Gaia DR4 (see also Liu et al., 2022; Generozov & Perets, 2024; Li et al., 2024c). Other explanations have been given by Gilkis & Mazeh (2024).

FUTURE Gaia releases, DR4 and DR5, will likely identify dozens of similar systems (Yamaguchi et al., 2018; Shikauchi et al., 2020; 2022; Janssens et al., 2022; Chawla et al., 2022; El-Badry et al., 2023b, §10).

These will provide valuable tests of black hole formation, cluster dynamics, and their contribution to observable gravitational wave sources (Shikauchi et al., 2023).

They may also provide a direct test of whether black hole growth follows cosmological expansion (Andrae & El-Badry, 2023), motivated by the suggestion that stellar remnant black holes could be the astrophysical origin of dark energy, and the onset of accelerating expansion at $z \sim 0.7$ (Farrah et al., 2023a; Farrah et al., 2023b).

216. Star and exoplanet radii: an update

I DISCUSSED Gaia's early contributions to the determination of stellar and exoplanet radii in essay 21, where DR1 parallaxes were used to estimate the radii of 350 000 stars and 116 transiting exoplanets from the Kepler survey (Stassun et al., 2017; Stevens et al., 2017). I look here at more recent results on star and planet radii made possible with Gaia Data Releases DR2 and DR3.

THE MOST DIRECT method of determining stellar diameters involves measuring the star's *angular* diameter (using adaptive optics, lunar occultation, or interferometry; e.g. Baines et al., 2023), then converting the angular diameter to a *linear* diameter using knowledge of the star's distance. Angular diameters can also be determined using eclipse timings and radial velocities of detached eclipsing binaries, again requiring distances to convert them to linear measure (e.g. Torres et al., 2010).

Together, these methods have provided diameters for some 400–500 stars. These relatively few fundamental measures provide the most rigorous size constraints for models of stellar structure and evolution (e.g. Andersen, 1991; Torres et al., 2010; Stassun et al., 2014).

STELLAR RADII can also be estimated using spectroscopic indicators of surface temperature and luminosity to infer the radius using the Stefan–Boltzmann law: $L = 4\pi R^2 \sigma T_{\rm eff}^4$, where L is the bolometric luminosity, R the radius, and $T_{\rm eff}$ the effective temperature. This also requires distances to convert fluxes to luminosities.

Such estimates rest on various assumptions, different for different stellar types. For example, stars are not blackbodies and, for the hottest and coolest, much of the energy lies outside the optical region. Recent all-sky, broadband photometry from the far-UV (at 0.15 μm with GALEX) to the mid-IR (at 22 μm with WISE), has led to much improved estimates of bolometric luminosities.

But surface gravities, chemical abundances, the treatment of rotation and convection, and reddening, introduce further model dependencies. And the underlying assumptions of sphericity, and that the radius is well-defined, break down for the very largest, or for those stars that are heavily spotted.

TO PROVIDE the numerical context, I should mention that various estimates of stellar radii had been made based on Hipparcos distances, amongst them 32 early-type stars by Jerzykiewicz & Molenda-Zakowicz (2000), 1040 FGK stars by Valenti & Fischer (2005), 166 planet-hosting stars by van Belle & von Braun (2009), and 125 A–M dwarfs by Boyajian et al. (2012; 2013).

In contrast, Gaia is now providing the fundamental distances (and other data) needed for estimating stellar diameters for hundreds of millions of stars.

AS I NOTED above, the first application of Gaia distances gave estimated radii for more than 350 000 stars with DR1 parallaxes better than 10% (Stassun et al., 2017; Stevens et al., 2017). They derived bolometric luminosities, L, from fits to the spectral energy distributions (using a wide range of photometric data including Tycho, 2MASS, Galex and WISE), $T_{\rm eff}$ values from photometry and spectroscopy, and distances from Gaia DR1.

They estimated effective temperature, bolometric flux, and angular diameter uncertainties of order 1–2%, with final radius uncertainties of order 8%, slightly larger than some previous (model-dependent) estimates.

Yu et al. (2023) used the spectral energy distributions predicted by the MARCS and BOSZ models with 32 photometric bandpasses, and spectroscopic parameters from the APOGEE, GALAH, and RAVE surveys, along with distances from Gaia DR3, to estimate radii for 1.5 million stars, with an estimated accuracy of 7%.

AS EVIDENT from the additional photometric and spectroscopic data which is required for the better estimation of L and $T_{\rm eff}$, Gaia also contributes to the estimates of stellar radii by providing detailed and homogenous (albeit model-dependent) astrophysical information for each star, derived from Gaia's 3-colour photometry and its RVS (radial velocity spectrometer) spectra.

Results of the Gaia project's 'astrophysical parameters inference system' (Apsis, which I outlined in essay 89) were made available with Data Release 2 (Andrae et al., 2018), and Data Release 3 (Andrae et al., 2023a). Let me summarise the parts relevant to stellar radii.

Apsis employs two 'General Stellar Parameterizer' modules. The first, GSP–Spec, uses projection and optimisation methods to best match the mean RVS spectra with a large grid of *theoretical* spectra computed using MARCS models, with a range of atmospheric parameters ($T_{\rm eff}$, log(g), metallicity [M/H], [α/Fe]) and chemical abundances, [X/Fe], spanning the full space of Galactic stellar populations (Recio-Blanco et al., 2023).

The second, GSP–Phot, estimates $T_{\rm eff}$, log(g), [M/H], absolute magnitude, radius, distance, extinctions (A_0, A_G, A_{BP} and A_{RP}), as well as the reddening E(G_{BP}–G_{RP}), by forward-modelling the BP/RP spectra, apparent G magnitude, and parallax using a Markov Chain Monte Carlo (MCMC) method (Andrae et al., 2023a).

FLAME (Final Age and Mass Estimates) takes the output from GSP–Phot and GSP–Spec, along with astrometry and photometry, to derive the evolutionary parameters: radius, luminosity, mass, and age.

The bottom line is that, bundled with Gaia DR3, Apsis provides (model-dependent) stellar radii, along with $T_{\rm eff}$, log(g), and [M/H], for 470 million stars.

A further method used to estimate stellar radii and masses, at least for certain spectral types, is asteroseismology (essays 51 and 149). Here, Gaia distances allow for important tests of asteroseismic models.

Asteroseismic radii rely on the measured oscillation frequencies (notably the 'large frequency spacing' and the frequency of maximum oscillation power), along with more conventional stellar parameters, notably $T_{\rm eff}$, L, and [M/H] (e.g. Basu et al., 2010).

Early applications using Gaia DR2 have been described by Sahlholdt & Silva Aguirre (2018) and Bellinger et al. (2019). Other tests and comparisons based on Gaia DR3 have been described by Yu et al. (2023) and Valle et al. (2024). With due model calibration, and accurate metallicities, 'asteroseismic radii' for a few thousand stars accurate to a few percent have been derived.

One spin-off from the knowledge of stellar diameters is the ability to estimate the radii of transiting exoplanets, and in particular for the several thousand being discovered by NASA's Kepler and TESS missions. The radius of a transiting planet cannot be measured directly, but can be derived from the transit lightcurve, given the radius of its host star. Masses are constrained by radial velocity measures.

The planet's radius and mass yield its mean density, which in turn informs whether the planet is a gas giant (like Jupiter or Saturn), an ice giant (like Uranus or Neptune), or a rocky planet (like Earth or Mars). Combined with information about their periods and host star properties, the distribution of planetary radii is already yielding insights into the physics of planetary interiors and atmospheres, and of planet formation and evolution.

There are four main observables which characterise the profile of an exoplanet transit: the transit depth ΔF, the period, the interval between the first and fourth contacts, and between the second and third contacts.

The transit depth is determined by the planet/star radius ratio, $\Delta F = (R_{\rm p}/R_\star)^2$. But estimates of the *stellar* mass and radius require external constraints, such as its surface gravity, astroseismology, or an independent estimate of the stellar radius. Without going further into methodological details, let me summarise the results on exoplanet radii that have been obtained so far.

Using Gaia DR1 distances to derive the radii of the planet-hosting stars, Stassun et al. (2017) derived the radii of 116 exoplanets with uncertainties ~10–20%. Using DR2 parallaxes, Berger et al. (2018) gave revised radii for 177 911 Kepler stars. Their ~8% precision was a factor 4–5 improvement over previous estimates. From these stellar radii, they estimated the radius of 2123 Kepler planets (and 1922 candidates), confirming a gap in the radius distribution of close-in planets, those between Earth–Neptune size (see also Petigura, 2020).

This general picture was confirmed in a 1000 planet sample by Fulton & Petigura (2018). Their stellar radii improved from 11% to 3% precision (with good agreement with the Apsis results, their Figure 3), with planet radii improved to 5% precision. Improved stellar masses using DR2 was demonstrated by Stassun et al. (2018).

Further improvements in numbers and accuracies came with Gaia DR3. Berger et al. (2023) presented a homogeneous catalogue of 7993 planet-hosting stars (3248 from Kepler, 565 from K2, 4180 from TESS), and their total of 9324 transiting planets.

They used isochrone fitting and Gaia DR3 parallaxes, photometry, and metallicities to compute $T_{\rm eff}$, log(g), masses, radii, stellar densities, luminosities, ages, distances, and V-band extinctions, finding residual scatter (compared to interferometry and asteroseismology) of 2.8%, 5.6%, 5.0%, and 31% between their $T_{\rm eff}$, radii, masses, and ages and those in the literature.

They determined radii for 4281 Kepler, 676 K2, and 4367 TESS planets, with the 'planet radius gap' being less prominent in the K2 and TESS samples than in the Kepler sample alone. And they identified a clear radius inflation trend in their large sample of hot Jupiters.

In a loosely related study, Zink et al. (2023) used Gaia DR3 proper motions and radial velocities to identify a Galactic location trend: they found that stars making large vertical excursions from the Galactic plane host fewer super-Earths and sub-Neptunes.

I have focused here simply on the *numbers* of new stellar and exoplanet radii being enabled by Gaia. The above references go into more details of the consequences for planet formation and evolution models.

217. Zero-point of the Gaia parallaxes

GAIA HAS provided a breakthrough in positional astronomy by measuring the parallaxes (and related properties) of nearly 2 billion stars, galaxies, and quasars. The inverse of the parallax in arcsec gives the distance to the source in parsec. For nearby stars with large parallaxes, this simple prescription serves us well.

For more distant sources, parallax errors complicate things considerably. Even for a normal error distribution – which, incidentally, leads to the appearance of (non-physical) negative parallaxes – the distribution of the (reciprocal) distance errors is non-Gaussian, and associated distance estimates are inevitably biased. Bailer-Jones (2015) provides a didactic introduction to this problem, with later papers in the same series going into greater detail (Astraatmadja & Bailer-Jones, 2016a; 2016b; Bailer-Jones et al., 2018; 2021; 2023).

Any *systematic* parallax errors add further complications. Even small systematics affect estimates of the mean properties of distant populations. Examples include determining the cosmological distance scale using Cepheids (e.g. Riess et al., 2021) or the tip of the red giant branch (e.g. Li et al., 2023e), or understanding the dynamics of the Large Magellanic Cloud and halo streams.

THE DESIGN of Gaia, with its two widely-spaced fields of view, and whole-sky revolving scanning, in principle allows the measurement of *absolute* parallax distances (Perryman et al., 2001; essay 172). However, even small variations of the 'basic angle' between the two fields, and in particular periodic variations caused by heating of the rotating satellite by solar radiation, can lead to variations that are degenerate with the astrometry, so leading to a *global* shift of the parallaxes.

Identified as a concern for Hipparcos by Lindegren (1977), its effect on the Hipparcos parallaxes was estimated to be negligible (Arenou et al., 1995), implying good short-term stability of its basic angle. For the much higher accuracies targetted by Gaia, the near-degeneracy between a possible basic-angle variation induced by solar heating, and a global parallax offset, is particularly problematic (Butkevich et al., 2017).

THESE CONSIDERATIONS led to the inclusion of a dedicated laser-metrology system on board Gaia (the basic angle monitor, BAM) to measure short-term variations. But due to the above degeneracies, a variation that evades measurement by the on-board metrology can only be identified by comparison with external data.

While the many quasars in Gaia's grasp offer the prospects of calibrating any global shift, higher-order effects such as magnitude or chromatic terms, a dependency on ecliptic latitude, or even temporal changes in quasar structure, demand due consideration of other external tests. I might recall that 1 μas corresponds to a Bohr radius at a distance of 10 m!

Measurements during the first year of nominal operations suggested an amplitude of the relevant Sun-aspect term ($\cos\Omega$, where Ω is the spin-phase relative to the barycentre) of amplitude 848 μas, corresponding to a parallax bias of some 700 μas (Lindegren et al., 2016). For Gaia DR1 (Gaia Collaboration et al., 2016), observations were corrected for the basic angle variations based on a simple harmonic fit to the BAM measurements.

THE SECOND data release, DR2, allowed for a more detailed analysis. From 500 000 quasars, which also define Gaia's celestial reference frame, Lindegren et al. (2018, §5.2) estimated a global parallax offset of -29 μas. But plots versus magnitude and colour (below) reveal systematic trends of $\sim$20 μas over the relevant data ranges. The plot against ecliptic latitude furthermore shows a roughly quadratic variation, with parallaxes $\sim$10 μas smaller towards the ecliptic poles.

It is in this context that the various zero-point estimations for DR2 (see table over), dependent on population, direction, and magnitude, can be interpreted.

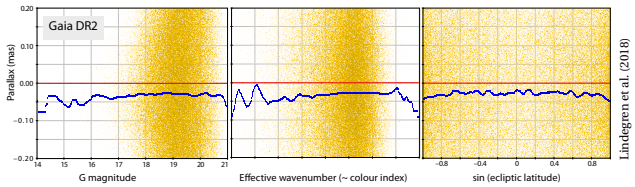

STUDIES BASED on EDR3 also showed systematic offsets of a few tens of microarcseconds (Lindegren et al., 2021a). From their sample of just over 1 million quasars in the range $G = 13.4 - 21$ (although only 541 with $G < 16$), they found a weighted mean parallax of –21 μas. They also extended their analysis to brighter sources, and a broader range of colours, using Large Magellanic Cloud stars (their §4.2), as well as the individual components of physical binaries (their §4.3).

For EDR3, the parallax bias again depends, in a non-trivial way, on magnitude, colour, and ecliptic latitude, and with different dependences for the 5- and 6-parameter solutions (their §5). They provided provisional bias functions Z_5 and Z_6 (see their Figs 21–22), to be subtracted from the catalogue value, as Python implementations at the Gaia web pages (which in turn points to the gitlab-hosted `gaiadr3_zeropoint`).

More detailed dependencies, including as a function of angular scales, are given in the description of the EDR3 astrometric solution by Lindegren et al. (2021b), while verification of the biases through comparisons with open clusters is given by Fabricius et al. (2021).

An independent treatment of the parallax bias in Gaia EDR3, also using quasars and physical binaries, and also revealing both spatial and magnitude dependences, but less so on colour, was given by Groenewegen (2021). More on the possible underestimation of the parallax errors of orbital and acceleration binary solutions is given by Nagarajan & El-Badry (2024).

DATA RELEASE 3, DR3, contains the same source list, positions, proper motions, parallaxes, and broadband photometry as EDR3 (Gaia Collaboration et al., 2023b), such that *'the systematic errors present in the astrometry published in Gaia EDR3 carry over to Gaia DR3'* (their §3.3). Accordingly, the parallax bias functions Z_5 and Z_6 (and the Python implementations) noted above, apply equally to Gaia DR3 as well as EDR3.

These bias functions have since been widely used in detailed studies (e.g. Eastman et al., 2023; Fouesneau et al., 2023; Li et al., 2023e; Sanders, 2023; Wang et al., 2023; Elliott et al., 2024; Naik & Widmark, 2024; Valle et al., 2024; Stoop et al., 2024, amongst many others).

I HAVE LISTED in the table opposite some of the other community-led investigations into the parallax systematics, divided into studies based on EDR3 or DR3 (even though their *astrometric* content is the same).

Investigations include binary stars (El-Badry et al., 2021); eclipsing binaries (Ren et al., 2021a; Stassun & Torres, 2021); seismology (Zinn, 2021; Khan et al., 2023); and globular clusters (Vasiliev & Baumgardt, 2021; Maíz Apellániz et al., 2021). Some studies are particularly detailed, some are with respect to the EDR3 prescriptions, and so not easy to characterise with a single offset value.

Data Release/Reference	Source sample	$\Delta\varpi$ (μas)
Gaia DR1 (Sep 2016):		
Arenou et al. (2017)	DR1 validation	–40
Gaia DR2 (Apr 2018):		
Lindegren et al. (2018)	DR2 astrometry	–29
Arenou et al. (2018)	DR2 validation	–70/–20
Brown et al. (2018a)	quasars	–29
Groenewegen (2018)	Cepheids	–49
Riess et al. (2018)	Cepheids	–46
Ripepi et al. (2019)	Cepheids	–70
Muraveva et al. (2018)	RR Lyrae	–57
Layden et al. (2019)	RR Lyrae	–42
Shao & Li (2019)	globular clusters	–28
Stassun & Torres (2018)	eclipsing binaries	–82
Graczyk et al. (2019)	eclipsing binaries	–31
Sahlholdt et al. (2018)	seismology (dwarfs)	–35
Hall et al. (2019)	seismology (red clump)	–41
Khan et al. (2019)	seismology (giants)	–50
Zinn et al. (2019)	seismology (giants)	–53
Leung & Bovy (2019)	distances (APOGEE)	–52
Chan & Bovy (2020)	red clump (APOGEE)	–48
Schönrich et al. (2019)	radial velocity kinematics	–54
Xu et al. (2019)	VLBI (astrometry)	–75
Lindegren (2020)	VLBI (radio stars)	–76
Xu et al. (2021)	VLBI (radio stars)	–75
Gaia EDR3 (Dec 2020):		
Lindegren et al. (2021a)	EDR3 parallax study	–94/+36
Fabricius et al. (2021)	EDR3 verification	–
Groenewegen (2021)	quasars/binaries	–
Riess et al. (2021)	Cepheids	–24
Molinaro et al. (2023)	Cepheids	–22
Molnar et al. (2022)	Cepheids/RR Lyrae	–
Kovacs et al. (2021)	RR Lyrae	–20
Maíz Apellániz et al. (2021)	globular clusters	–
Maíz Apellániz (2022)	clusters/LMC/SMC	–
Huang et al. (2021b)	red clump (LAMOST)	–26
Ren et al. (2021a)	eclipsing binaries	–29
Stassun & Torres (2021)	eclipsing binaries	–37
Zinn (2021)	seismology: giants	–
Flynn et al. (2022)	open clusters	–
Wang et al. (2022a)	giants (LAMOST)	–28
Ding et al. (2021)	X-ray bursters	–
Bobylev (2022)	radio stars (VLBI)	–22
Khan et al. (2023)	seismology: red clump	–
Gaia DR3 (Jun 2022):		
Groenewegen (2023)	orbital parallaxes	–
Ding et al. (2024)	Galactic plane sources	–
Andriantsaralaza et al. (2022)	AGB/maser (VLBI)	–77

Studies without a simple numerical value for $\Delta\varpi$ are shown '–'.

In a study of 200 nearby AGB stars, Andriantsaralaza et al. (2022) found a large offset of -77 μas, and suggest that the DR3 parallax errors are underestimated by a factor 5.4 for the brightest (G <8 mag), and 2.7 at $G = 8 - 12$.

Several studies (of course) identify individual parallaxes that are particularly suspect, often related to their unmodelled multiplicity. One of many examples is the nearby 19.5-yr binary system GJ 67AB (Torres, 2022).

I WILL FINISH with the application of Benford's law (see essay 146) to the specific case of Gaia DR2 by de Jong et al. (2020). They showed that the 1.3 billion observed parallaxes in Gaia DR2 closely follow Benford's law: those with a parallax starting with digit 1 are five times more numerous than those starting with digit 9. The agreement is marginally affected, albeit adversely, by the inclusion of any plausible zero-point correction.

218. Red supergiants: the biggest stars

THE BIGGEST stars have radii $\sim 1500 R_\odot$, far larger than the naked-eye monsters Antares ($680 R_\odot$) or Betelgeuse ($640 R_\odot$). Scaled to the solar system, their photospheres would extend beyond the orbit of Jupiter. The largest of those reliably known is WOH G64 in the LMC, $R \sim 1540 \pm 77 R_\odot$, discovered by Westerlund et al. (1981).

Stars larger than a few hundred solar radii are mostly red supergiants, or the still rarer hypergiants, occupying the upper-right region of the HR diagram.

Observationally, the former are 'cool' ($T_{\rm eff} \lesssim 4200$ K), luminous ($L/L_\odot \geq 10^4$) objects, highly evolved descendants of main-sequence stars of initial mass $10-40 M_\odot$ (Iben, 1974; Messineo & Brown, 2019, §3), with their high masses distinguishing them from the lower mass ($0.5-8 M_\odot$) AGB stars. They are amongst the brightest stars in the infrared, detectable out to Mpc distances.

Early catalogues of red supergiants include those of Humphreys (1978), Elias et al. (1985), and Jura & Kleinmann (1990), the latter reporting just 21 (20 M-type, one L-type) within 2.5 kpc of the Sun. Skiff (2014) provided the most recent compilation of about 1400 Galactic candidates. But this census remains highly incomplete, given our location within the disk and the associated dust obscuration, distance uncertainties, and the overlapping luminosities of red supergiants and subgiants.

DURING the M supergiant phase, lasting 200 000–400 000 yr, a star of initial mass $20 M_\odot$ returns some $3-10 M_\odot$ into the interstellar medium (Jura & Kleinmann, 1990). Their late-stages of nucleosynthesis, stellar winds, and eventual explosions as supernovae represent key processes in a galaxy's chemical enrichment.

Nonetheless they remain a poorly characterised evolutionary phase, with models failing to match some cool or luminous objects (Massey & Olsen, 2003; Levesque et al., 2009; Wing, 2009). Challenges include their molecular opacities, extended atmospheres, sonic velocities of the convective layers, and supersonic velocities in their atmospheres, resulting in shocks, photospheric asymmetries, and imprecise radii, as evident in the case of Betelgeuse (Young et al., 2000; Freytag et al., 2002).

TECHNIQUES FOR MEASURING stellar radii include the use of spectroscopic indicators of surface temperature and luminosity, angular size measurements using interferometry, or, in a few cases, from eclipsing binaries (e.g., VV Cep), all requiring distance estimates.

The former method rests on the Stefan–Boltzmann law, $L = 4\pi R^2 \sigma T_{\rm eff}^4$, where L is the bolometric luminosity, R the radius, and the use of an 'effective temperature', $T_{\rm eff}$, sidesteps the assumption of blackbody radiation. Noteworthy is the fact that since L is a steep function of temperature, a cool star must be huge to be as luminous as a hotter star. But the underlying assumptions that the star is spherical, and that the radius is well-defined, break down for the very largest. More on the challenges of spectral (and luminosity class) classification, and measurement of their diameters and distances, is given by Levesque et al. (2005), and Wing (2009).

The supergiant nature of the prototypes Betelgeuse (α Ori), Antares (α Sco), and Herschel's Garnet Star (μ Cep), was known since the early 20th century from their insignificant parallaxes and proper motions. Hipparcos gave $\varpi = 6.55 \pm 0.83$ mas (152 pc), 5.89 ± 1.00 mas (170 pc), and 0.55 ± 0.20 mas (1800 pc), respectively.

THE COOLEST and most luminous stars in the study by Levesque et al. (2005), viz. KW Sgr, Case 75, KY Cyg, and μ Cep, have $R \sim 1500 R_\odot$ (7 au), in agreement with the largest radii predicted from their MARCS models using improved molecular opacities inspired by the anticipation of the Gaia data (Gustafsson et al., 2003; Plez, 2003). *'It is believed'*, they state, *'that stars above this radius would be too unstable and simply do not form'*.

Stars seemingly unaware of the MARCS models include the interacting binary VV Cep, with a radius variously estimated as $1200-1600 R_\odot$, and the 'humongous' VY CMa for which Keck interferometry found a photospheric radius of $3020 R_\odot$ (Monnier et al., 2004), implying an extremely cool star, 2225 K, or some 'unique evolutionary state' (Humphreys et al., 2005). More recently it is considered to be linked to episodic mass-loss clumps (Kamiński, 2019; Humphreys et al., 2024).

AVAILABILITY of the Gaia astrometry has brought the possibility of significantly improving both the census of red supergiants and, perhaps more importantly, the knowledge of the distances to individual objects.

Messineo & Brown (2019) started with the 1400 candidate Galactic red supergiants compiled by Skiff (2014), and presented a catalogue of those with a Gaia DR2 entry. They included a revised spectral type for each object, and a unified $T_{\rm eff}$ based on the temperature scale of Levesque et al. (2005). Parallaxes were found for 1342 stars, with a high-quality subset of 889. Most are located along the Galaxy's spiral arms (their Fig. 6), although generally in isolation, with only some 13% known to be associated with open clusters, reinforcing questions about their Galactic distribution, as well as how and where they formed (Messineo et al., 2016).

Healy et al. (2024) used distances from Gaia DR3, infrared photometry from 2MASS, and a Galactic dust map, to select a distinct sample of luminous bright late-type stars. Bolometric luminosities and effective temperatures were compared to Geneva stellar evolution tracks to determine likely candidates, and to identify contamination using a catalogue of Galactic AGB stars of similar L and $T_{\rm eff}$. This resulted in a quality sample of 578 probable (and 62 likely) Galactic red supergiants, along with multiplicity, variability, and classification as a runaway as given by the proper motions.

I HAVE ALREADY referred to the very short evolutionary lifetimes of these red supergiants, the consequence being that they are particularly important as potential future core-collapse supernova progenitors.

Healy et al. (2024) assessed their catalogue's use for the Supernova Early Warning System (SNEWS, Molla, 2021), and showed that exploiting neutrino fluxes and their 3D positions as an early warning trigger, the number of candidates can be reduced significantly, improving prospects of observing the progenitor pre-explosion and the early phases of core-collapse supernovae.

WHILE MANY occur in isolation, some open clusters do host concentrations of red supergiants, amongst them χ Per, NGC 7419, and Westerlund 1 (essay 106), all now with well-determined distances from their mean Gaia DR2 parallaxes (Davies & Beasor, 2019).

They put it eloquently in their abstract: *'Galactic, young massive star clusters are approximately coeval aggregates of stars, close enough to resolve the individual stars, massive enough to have produced large numbers of massive stars, and young enough for these stars to be in a pre-supernova state. As such these objects represent powerful natural laboratories in which to study the evolution of massive stars. To be used in this way, it is crucial that accurate and precise distances are known, since this affects both the inferred luminosities of the cluster members and the age estimate for the cluster itself.'*

THERE HAVE also been a number of recent discoveries of remarkably massive clusters of red supergiants at the near-end of the Galactic bar, at distances of around 6–7 kpc, seen only in the infrared (Messineo et al., 2016), with several designated as Red Supergiant Clusters: RSGC1 (Figer et al., 2006); RSGC2, aka Stephenson 2 (Stephenson, 1990; Davies et al., 2007); RSGC3 (Alexander et al., 2009; Clark et al., 2009); RSGC4, aka Alicante 8 (Negueruela et al., 2010; Asa'd et al., 2023); RSGC5, aka Alicante 7 (Negueruela et al., 2011); and RSGC6, aka Alicante 10 (González-Fernández & Negueruela, 2012).

The evolutionary and mass-loss histories of three of these clusters, RSGC1–3, along with NGC 7419, have been assessed by Humphreys et al. (2020).

BEYOND OUR own Galaxy, red supergiants have been identified in the Magellanic Clouds, and in M31 and M33, all making use of the Gaia parallax and proper motion as membership discriminants. The 1098 identified in the LMC are being used to place constraints on their lower mass limit (Yang et al., 2024a). Reasonably complete samples of 5498 and 3055 objects have been identified in M31 and M33 (Ren et al., 2021b).

MANY OF the largest objects have their own literature detailing classification, mass-loss, etc., although with limited insights yet from Gaia. They include:

WOH G64, with $R \sim 1540 \pm 77 R_\odot$ (Levesque et al., 2005; Beasor & Smith, 2022). The DR3 parallax, $\varpi = -0.2477 \pm 0.0430$ mas, is consistent with its LMC membership.

Stephenson 2–18, aka St2–18, Stephenson 2 DFK1, and RSGC2–01, located close to RSGC2 (Fok et al., 2012). A radius of $2150 R_\odot$ is given in its wiki entry, presumably with large uncertainties, although I was not able to trace the reference. It is not included in Gaia DR3.

UY Scuti, with $R \sim 1708 \pm 192 R_\odot$ derived from VLTI–AMBER observations and PHOENIX model atmospheres (Arroyo-Torres et al., 2013). This is based on their assumed distance of 2.9 kpc, while Gaia DR3 yields the significantly smaller $\varpi = 0.5166 \pm 0.0494$ mas, or 1.94 kpc.

Others include **RSGC1–F01** (in RSGC1), with $1530 R_\odot$ (Humphreys et al., 2020); **AH Sco**, with $1411 \pm 124 R_\odot$, also from VLI–AMBER and PHOENIX models (Arroyo-Torres et al., 2013); and **RW Cep**, with $900 - 1760 R_\odot$ making use of the Gaia parallax (Anugu et al., 2023).

WE ARE in the early stages of what Gaia will inform us about the biggest stars, and in particular their place in the evolution of red supergiants.

And having noted their non-sphericity, I'll add that, at the other extreme, KIC–11145123, with $P_{\rm rot} \sim 100$ d, has been claimed as the 'roundest' object in Nature, with asteroseismology-based $\Delta R/R = (1.8 \pm 0.6) \times 10^{-6}$ which, for $R_\star = 2.3 R_\odot \sim 1.5$ Mkm, implies $\Delta = 3 \pm 1$ km between its polar and equatorial radii (Gizon et al., 2016).

219. Open clusters: numbers

I HAVE CONSIDERED the substantial topic of open clusters with Gaia in two previous essays, detailing some of the early results from EDR3 (essay 74), and the numbers of open clusters identified in DR3 (essay 144).

In these next four essays, I will give an update of some of Gaia's latest advances, drawing on a recent review by Cantat-Gaudin & Casamiquela (2024). Here, in the first of these, I will look at their overall properties and Galactic distribution.

AROUND A THIRD of the open clusters known before Gaia were catalogued by Charles Messier, and William and John Herschel, and subsequently compiled into the New General Catalogue (NGC; Dreyer, 1888).

Clusters found in photographic surveys were added in the 20th century, with more recent discoveries from proper-motion surveys. Before Gaia DR2, in April 2018, the two largest catalogues were by Dias et al. (2002), with about 2000 objects, and by Kharchenko et al. (2013) listing over 3000. But a significant fraction of these were apparent 'overdensities', while the compilations were also highly incomplete (Cantat-Gaudin et al., 2019b, §1).

THE EARLY Tycho–Gaia Astrometric Solution (TGAS; Michalik et al., 2015) provided improved proper motions and, for the first time, parallaxes, for the two million stars of the Tycho-2 catalogue. This allowed the astrometric characterisation of a hundred clusters within 1 kpc (Cantat-Gaudin et al., 2018b).

Gaia DR2 provided proper motions improved by a factor of 100, and a full astrometric solution for over one billion stars to ~20 mag. Attempting to identify all ~3000 known clusters in the Milky Way disk, Cantat-Gaudin et al. (2018a) confirmed just 1169, implying that a large number in the literature were *apparent* groupings with no physical reality, many created by extinction patterns in the inner Milky Way (Cantat-Gaudin & Anders, 2020).

The presence of this fictitious old, inner-disk population had been difficult to explain (Martinez-Medina et al., 2016). Based on the Gaia revisions, Anders et al. (2021) showed that the cluster-age function of the Milky Way is indeed in line with empirical expectations.

AT LEAST 30 STUDIES have since identified some 25 000 open clusters out to 15 kpc, exploiting the DR3 parallaxes and proper motions, and using clustering algorithms such as DBSCAN (Castro-Ginard et al., 2022), HDBSCAN (Hunt & Reffert, 2023), and various others. The *Unified Cluster Catalogue* of Perren et al. (2023), online at https://ucc.ar, has compiled these into a list of almost 14 000 unique Milky Way clusters, with more than a million probable members in total (essay 144).

Typical clusters have around 50 members, but many of the most populated have several hundred up to several thousand. Most have half-number radii in the range 2–6 pc, somewhat independent of numerical size (Tarricq et al., 2022; Zhong et al., 2022; Hunt & Reffert, 2023).

These advances allow better studies of membership, Galactic distribution, age, chemistry, and dynamics.

CLUSTER AGES are most commonly obtained by comparing colour–magnitude diagrams to theoretical isochrones. Bayesian analysis (von Hippel et al., 2006) using Gaia photometry to derive ages, distances, and reddening, was applied to 269 clusters by Bossini et al. (2019), and to 1743 clusters by Dias et al. (2021).

Recent age determinations (e.g. Li & Shao, 2022) aim to better account for unresolved binaries, field stars, and reddening (see figures over). Stellar rotation, and the presence of blue stragglers, are further complications (e.g. Kounkel & Covey, 2019; Cantat-Gaudin et al., 2020; Hunt & Reffert, 2023; Cavallo et al., 2024). I say more on this topic in essay 220.

OPEN CLUSTERS ARE found to be concentrated in the Galactic plane, confirming the pre-Gaia picture but with much greater precision and clarity. The youngest are typically located less than 100 pc from the mid-plane, where the cold gas densities are highest, while the oldest have reached heights of more than 1 kpc (Soubiran et al., 2018; Tarricq et al., 2021). The inner disk hosts relatively few old clusters, the denser environment presumably leading to higher disruption rates, although the inner population remains poorly constrained as a result of extinction and reddening (Minniti, 2024).

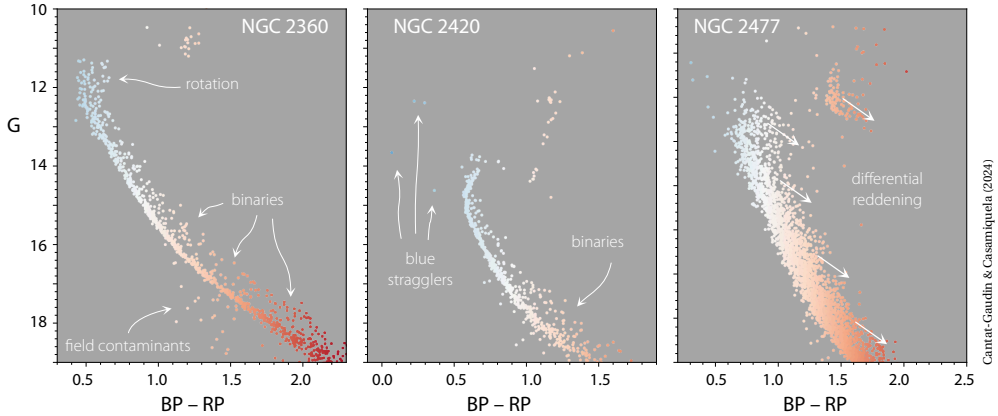

SOME ASPECTS of their Galactic distribution remain uncertain. For example, the dearth of young clusters in the outer disk may be a result of star formation, which is clearly still ongoing at large distances, but which occurs at densities too low to form gravitationally bound clusters (Pflamm-Altenburg & Kroupa, 2008).

Old clusters beyond ~12 kpc may have formed in the inner Milky Way before migrating outwards. And the fact that the orbits of clusters older than 3 Gyr have larger eccentricities and inclinations than field stars of the same age, suggests that clusters are more likely to survive if their orbits take them beyond the plane for most of the time (Viscasillas Vázquez et al., 2023). In the outermost regions of the disk, distant clusters tend to be found *below* the Galactic plane (Cantat-Gaudin et al., 2020), following the disk's known warp (e.g. He, 2023).

THE DISTRIBUTION OF young clusters has long been considered to broadly follow the expected trace of the spiral arms, although pre-Gaia, distances uncertainties were too large to allow for an accurate characterisation of the spiral structure in the solar neighbourhood. The greatly enlarged Gaia census, along with improved distances and photometry, has brought significant insights into their distribution within 2 kpc.

But challenging the picture of a grand-design Milky Way with continuous and well-defined structures, these studies find a fragmented pattern (Cantat-Gaudin et al., 2018a; 2019b; Molina Lera et al., 2019; Cantat-Gaudin et al., 2020; Kuhn et al., 2021; Pantaleoni González et al., 2021; Hunt & Reffert, 2023).

Their distribution and dynamics is also contributing to the long-standing question of whether the spiral perturbations are global and stationary, or local and transient (e.g. Shen & Zheng, 2020). Using young clusters, Castro-Ginard et al. (2021) showed that the Galaxy's four classical spiral arms have distinct pattern speeds, all of them close to the corotation of the disk. This supports the idea that they are short-lived structures, rather than long-standing Galaxy-scale density waves.

IN A FUTURE ESSAY, essay 223, I will go further into the connection between open clusters and the more loosely bound 'stellar associations' and 'moving groups'. Let me only mention here that some young coeval and co-moving superstructures can now be traced with Gaia over hundreds of parsecs.

The Vela OB2 association, for example, has grown from 200 Hipparcos members to more than 14 000 today (Armstrong et al., 2018; Franciosini et al., 2018; Beccari et al., 2018; 2020; Cantat-Gaudin et al., 2019c; Pang et al., 2021). And the clusters NGC 2547, NGC 2451B, Collinder 140, Collinder 135, and UBC 7 are now known, from Gaia, to be part of a continuous co-moving alignment of coeval (~35 Myr) stars extending over 200 pc (Cantat-Gaudin et al., 2019a; Beccari et al., 2020).

Nor will I say more here on the very massive star clusters ($> 10^4\,M_\odot$) found in the inner regions of the Galaxy. These are expected to form from hierarchical merging of smaller clusters, and include systems such as Westerlund 1 (essay 106) and Westerlund 2.

BUT I WILL CONCLUDE with a mention of 'binary clusters'. Rozhavskii et al. (1976) was perhaps the first to comment that open clusters are sometimes found in pairs. More recent simulations and observations indeed suggest that such pairs may form together, orbiting each other before gradual mass loss leads to them eventually separating and evolving as two independent clusters (Camargo et al., 2016; Casado, 2021).

Such discoveries and detailed kinematic studies with Gaia include three open clusters near the Aquila Rift cloud: UPK 39, UPK 41, and PHOC 39. Here, Ye et al. (2022) used Gaia DR3 to conclude that UPK 39 and UPK 41 are a primordial open cluster binary pair, which are likely to have been formed at the same time, with PHOC 39 possibly capturing both in the future.

Ishchenko et al. (2024) showed that Collinder 135 and UBC 7 perhaps formed together 50 Myr ago. And Qin et al. (2025) used Gaia DR3 proper motions to discover that NGC 2323 is, in reality, a compact binary.

220. Open clusters: ages

THIS IS THE SECOND in a series of four essays on Gaia's ongoing advances in the studies of open clusters. In essay 219 I looked at the *number* of clusters that have been confirmed or discovered with Gaia, and at their Galactic distribution. Here, I will go further into the subject of age determination, again drawing on the recent review by Cantat-Gaudin & Casamiquela (2024).

CLUSTER AGES are most straightforwardly obtained by comparing colour–magnitude diagrams to theoretical isochrones. Accurate ages nonetheless require knowledge of the cluster's metallicity and extinction, as well as sufficient members in key evolutionary phases.

In some of the first Gaia studies, using DR2 astrometry and photometry, Bayesian analysis (von Hippel et al., 2006) was used to derive their ages, distances, and reddenings. This technique was applied to 269 clusters by Bossini et al. (2019), to 45 clusters by Monteiro et al. (2020), to 150 clusters by Monteiro & Dias (2019), and to 1743 clusters by Dias et al. (2021).

Studies using EDR3/DR3 aimed to better account for unresolved binaries, field stars, differential reddening, stellar rotation, and even the presence of blue stragglers.

In this spirit, Li & Shao (2022) treated an open cluster as a mix of single and binary stars, with some field stars. Applied to 10 clusters using EDR3, they found binary fractions of 30–50%, and best-fit isochrones generally consistent with previous measurements, but with more precise ages. The inferred slope of the mass function is in the range −2.7 to −1.6 for clusters younger than 2 Gyr, while older clusters are significantly flatter.

Machine-learning (see reviews by Baron, 2019; Fluke & Jacobs, 2020) has led to more robust estimates of ages (and other parameters): for 1900 clusters and co-moving groups (comprising 300 000 sources) within 1 kpc by Kounkel & Covey (2019), for about 2000 clusters by Cantat-Gaudin et al. (2020), for some 4000 by Hunt & Reffert (2023), and some 5400 by Cavallo et al. (2024). The latter authors, for example, argue that their algorithm effectively traces sequences in colour–magnitude diagrams despite photometric errors and outliers.

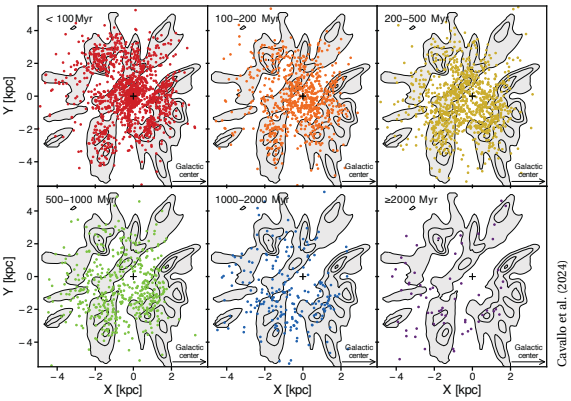

THE RESULTS provide greater details of the local Galactic structure, but also inform about cloud collapse and star formation on larger scales. Kounkel & Covey (2019) found filamentary structures, oriented parallel to the Galactic plane, and some hundreds of parsecs in length. Most lack a central cluster, indicating that the filamentary structure is primordial. Their velocity dispersion increases with age, suggesting a timescale for dynamical heating and disruption of 300 Myr, leaving only individual clusters to be identified at the oldest ages.

The figure shows the results from Cavallo et al. (2024) in Galactic XY coordinates, divided into age groups, and with an over-density map shown in grey. Their results reproduce the Galactic metallicity gradient found in high-resolution spectroscopic surveys, while finding systematically older ages compared to previous analyses.

LET ME TURN to other methods used for estimating cluster ages, all being advanced by Gaia.

For ages in the range 20–200 Myr, the 'lithium depletion boundary' provides an independent spectroscopic age estimate. Since stars burn lithium in their cores but not in their outermost layers, ages can be inferred from equivalent width of the Li I 670.8 nm absorption line in low-mass stars, since its strength depends both on mass (and hence on the importance of convection) and age (e.g. Rebolo et al., 1992; Burke et al., 2004).

Gaia is providing the opportunity to re-assess the consistency between ages determined from the lithium depletion test, based on improved cluster membership, bolometric luminosities, and effective temperatures (e.g. Lodieu et al., 2019; Miret-Roig et al., 2024).

While agreement is often found, other studies (using Gaia DR2 or DR3) point to the effects of 'radius inflation', attributed to enhanced contributions of star spots and magnetic activity in the youngest stars (Galindo-Guil et al., 2022; Franciosini et al., 2022), as well as rotational dependencies, with fast rotators generally preserving Li over longer times (Jeffries et al., 2021; Binks et al., 2022; Sun et al., 2023; Tsantaki et al., 2023). Jeffries et al. (2023), for example, used Gaia DR3 to provide empirical models of the Li equivalent width, calibrated on 6200 stars in 52 open clusters with ages from 2–6 Gyr.

A SECOND INDEPENDENT method of age estimation uses gyrochronology. This exploits the decrease of stellar rotation with time, due to magnetic braking, which enables the use of rotation periods as a proxy for age. One goal is to provide ages of main sequence stars, as well as clusters too young or too sparse to host the evolved stars more robustly used as age markers (e.g. Barnes, 2003; Meibom et al., 2015; Douglas et al., 2024).

The field *'…has benefited from a tremendous boost enabled by Gaia'* (Cantat-Gaudin & Casamiquela, 2024), with its astrometry providing improved membership, and its photometry already providing rotation periods for 3 million stars (Frémat et al., 2023, essay 103).

Gaia (DR2/DR3) is providing such age estimates for Hyades and Praesepe (Douglas et al., 2019), α Per (Boyle & Bouma, 2023), M 67 (Gruner et al., 2023), NGC 2281 (Fritzewski et al., 2023), NGC 2477 (Palakkatharappil & Creevey, 2023), NGC 2516 (Fritzewski et al., 2020; Bouma et al., 2021), NGC 3532 (Fritzewski et al., 2021b; 2021a), NGC 6709 (Cole-Kodikara et al., 2023), NGC 6811 (Curtis et al., 2019a), Ruprecht 147 (Gruner & Barnes, 2020; Curtis et al., 2020), ASCC 123 (Frasca et al., 2023), the Pisces–Eridanus stream (Curtis et al., 2019b), as well as the Gaia discoveries UBC 1 (Fritzewski et al., 2024), and the moving group X (Messina et al., 2022; Newton et al., 2022). Various software tools are also available (Angus et al., 2019; Bouma et al., 2023; Van-Lane et al., 2023).

While a full theoretical interpretation remains challenging, it is useful to emphasise that an important contribution of Gaia is to challenge and advance existing models of star formation and evolution. A broad conclusion offered by Bouma et al. (2023) is that *'the uncertainty floor varies still strongly with both stellar mass and age'*. Gruner & Barnes (2020) conclude that *'models describing the rotational evolution of solar metallicity cool main sequence stars need to include three distinct physical processes if they are to account for the fast, slow, and low mass rotators observed in open clusters to date'*.

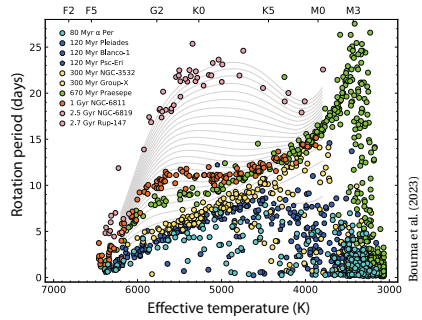

ANOTHER age estimate, especially relevant for young or sparse clusters and associations, uses Gaia's high-accuracy proper motions to yield age estimates from the 'dynamic traceback' of their members. I have covered Gaia's contributions to this topic in essay 186, and will mention only a couple of key poins here.

For the β Pic cluster, where literature age estimates ranged from 10–40 Myr, Miret-Roig et al. (2020) found a traceback age of 18.5 Myr (see also Couture et al., 2023). Galli et al. (2023) found the dynamical age of Tucana–Horologium (~40 Myr) to be consistent with both isochronal and Li ages. And Miret-Roig et al. (2022) found that the dynamical age of Upper Scorpius is younger than that from its colour–magnitude diagram.

For six young associations, Miret-Roig et al. (2024) found traceback ages consistently younger than those from isochrones by 5.5 ± 1.1 Myr. They concluded that the two have different time origins: if the cluster is gravitationally bound before dispersion of the parent gas cloud, the zero-point of the expansion time scale is a few Myr after that probed by the colour–magnitude diagram.

In other words, the dynamical traceback 'clock' starts when the system begins to expand after expelling most of the gas, whereas the isochrone 'clock' starts earlier when most stars form. Pelkonen et al. (2024) showed that the oldest age (corresponding to the first star to leave the cluster) generally provides a better match to the isochronal age than the traceback method.

FINALLY, I should mention ages inferred from asteroseismology, although they are determined somewhat indirectly: the detection of solar-like oscillations (in Kepler, as well as in Gaia photometry) provide global seismic parameters such as the 'large separation' and the frequency of maximum oscillation power which, combined with the effective temperature, can be used to derive stellar masses through so-called 'scaling relations'. In turn, the mass can be used to provide an indirect estimate of age through evolutionary models.

Bossini et al. (2019) used this approach for red giant stars with asteroseismic parameters derived by Kepler for NGC 6791, NGC 6811, and NGC 6819, and found ages broadly compatible with their (log) isochronal ages, of 9.972, 8.94, and 9.30 Gyr respectively.

221. Open clusters: kinematics

OPEN CLUSTERS were formed from the collapse of giant molecular clouds, and they travel on roughly circular orbits through the Galactic disk. They are progressively disrupted over time as a result of internal dynamical processes, and gravitational encounters with other molecular clouds and the wider Galactic potential. It was the dearth of clusters older than 500 Myr that led Spitzer (1958) to suggest that clusters are 'dissolved' by the very clouds from which they formed.

Gaia's distances and proper motions are allowing the identification of many more clusters (essay 219), along with rigorous members and age estimation (essay 220). The motions of *individual* stars allows measurement of their Galactic orbits (e.g. Soubiran et al., 2018), as well as details of their dissolution, bulk rotation, and internal dynamics (Cantat-Gaudin & Casamiquela, 2024).

AS A RESULT of two- or three-body encounters within the cluster, stars can reach the escape velocity, slowly diffusing into the field population. Preferential escape through the cluster's Lagrange points leads to the creation of 'tidal tails' in both the leading and trailing directions along their orbit (Fukushige & Heggie, 2000; Gieles & Baumgardt, 2008; Portegies Zwart et al., 2010).

Tidal tails were first discovered around *globular* clusters (Grillmair et al., 1995), and examples include Pal 5 (Odenkirchen et al., 2001, essay 109) and NGC 5466 (Belokurov et al., 2006a). The low-density tidal tails of *open* clusters only became evident with Gaia.

Elongation of the Hyades was found in Gaia DR1 by Reino et al. (2018). The tidal tails were later revealed in detail with DR2 (Lodieu et al., 2019; Röser et al., 2019; Meingast & Alves, 2019; Oh & Evans, 2020; essay 20).

Studies with EDR3 extended these tails to ±400 pc (Jerabkova et al., 2021). Their models shows that their orientation relative to the cluster's bulk motion constrain its initial rotation. Interestingly, they also identified spatial concentrations in both tails consistent with epicyclic overdensities (Just et al., 2009; Küpper et al., 2010; 2012). These, in turn, provide constraints on both the cluster properties, and also on the Galactic potential.

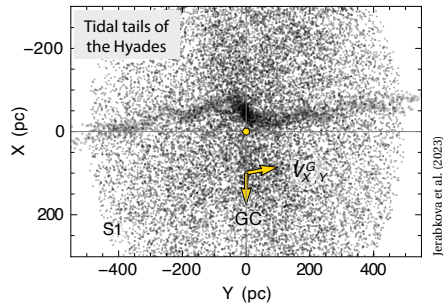

There is a growing literature on the numbers of clusters with known tidal tails as a result of the improved Gaia astrometry and photometry, along with their numerical modelling, and the interpretation of properties such as their asymmetries and mass-loss rates.

Such clusters include Praesepe/NGC 2632 (Röser & Schilbach, 2019; Alfonso & García-Varela, 2023); the Pleiades (Alfonso & García-Varela, 2023); the rapidly dissolving Ruprecht 147 (Yeh et al., 2019); the disk-shocked M 67 (Carrera et al., 2019); Coma Ber (Tang et al., 2019); NGC 752 (Bhattacharya et al., 2021; Boffin et al., 2022); UBC 274 (Casamiquela et al., 2022); and the Gaia discovery COIN–Gaia 13 (Bai et al., 2022).

In the case of Blanco 1 (Zhang et al., 2020; Alfonso & García-Varela, 2023) association of the tails with the cluster has also been confirmed via their TESS-based gyrochronological ages (Sha et al., 2024).

More than a hundred other nearby open clusters now have either known tidal tails, or an elongated morphology consistent with their tidal disruption (e.g. Hu et al., 2021a; 2021b; Meingast et al., 2021; Bhattacharya et al., 2022; Coronado et al., 2022; Moranta et al., 2022; Tarricq et al., 2022; Fürnkranz et al., 2024; Kos, 2024; Noormohammadi et al., 2024).

Various studies have been specifically targeted at a better understanding of their tidal-arm asymmetries (Pflamm-Altenburg et al., 2023; Kroupa et al., 2024); with some considering the asymmetric structures in the framework of MOdified Newtonian Dynamics (MOND; Thomas et al., 2018; Kroupa et al., 2022).

SOME OPEN CLUSTERS are also expected to experience bulk rotation, whether inherited from their parent molecular cloud, provided by impulsive interactions with massive structures, or resulting from the long-term action of tidal forces, each likely to result in distinct patterns, perhaps with a dependency on cluster age.

Indeed an open question in star formation concerns the amount of angular momentum that newly formed clusters possess after emerging from their parent cloud. For example, Corsaro et al. (2017) found an alignment of stellar spins and binary orbital spins in star clusters. While this would support a scenario in which clusters are born with net angular momentum, propagating down to stellar scales, and with the imprint surviving over several Gyr, other studies suggest that turbulent scrambling dominates (e.g. Healy et al., 2023).

Evidence for rotation based on the proper motions from DR2 was reported for the ancient (8 Gyr) NGC 6791 by Kamann et al. (2019). Their estimate of the inclination angle was broadly consistent with the mean inclination determined for its constituent stars.

For Praesepe/NGC 2632, Loktin & Popov (2020) found a rotation velocity of 0.4 km s^{-1} at the cluster's periphery. With improved proper motions from EDR3, Hao et al. (2022a) found a mean rotation velocity, within its tidal radius, of 0.2 ± 0.05 km s^{-1}, with the rotation axis tilted by $41 \pm 12°$ to the Galactic plane.

Also using EDR3, Guilherme-Garcia et al. (2023) found rotational signatures in eight open clusters (nine others displaying a possible rotation), and identified 14 expanding clusters, with contraction evident in two.

Hao et al. (2024) used the astrometry and radial velocities from Gaia DR3 to determine the mean 3D rotation velocities of the Pleiades, α Per, and Hyades clusters, within their tidal radii, of 0.24 ± 0.04, 0.43 ± 0.08, and 0.09 ± 0.03 km s^{-1} respectively.

From a study of 1379 open clusters with Gaia DR3, Jadhav et al. (2024) identified spin signatures in 10 clusters and 16 candidates, with expansion found in 18 and contraction in three. The expansion rate was compatible with theoretical estimates based on the expulsion of residual gas, while the orientation of the spin axis is independent of the cluster's orbital angular momentum. They concluded that at least 1% of clusters are born rotating, or have undergone strong interactions since.

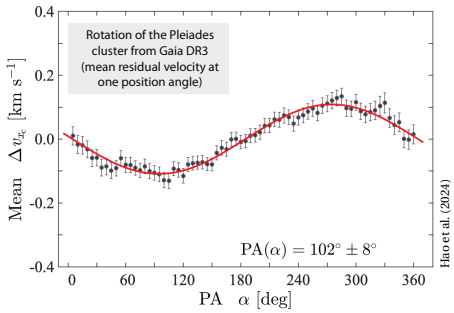

THE STRUCTURE of an initially spherically symmetric star system evolves through small changes of velocity during 2-body encounters ('relaxation'). And this is accompanied by 'mass segregation': high-mass stars and binaries sinking to the centre, and low-mass stars being elevated to the cluster halo where they more easily evaporate (e.g. Spitzer, 1969; Kroupa, 1995; Khalisi et al., 2007; Binney & Tremaine, 2008 §7.5).

Pre-Gaia evidence for mass segregation includes Praesepe and NGC 6231 (Raboud & Mermilliod, 1998; Khalaj & Baumgardt, 2013), and the Hyades (Röser et al., 2011), although it has not always been clear whether this is a result of relaxation, or due to the preferential formation of more massive stars towards the cluster centres.

With the Gaia data, mass segregation has been observed in Coma Ber (Tang et al., 2018), in Ruprecht 147 (Yeh et al., 2019, Fig. 10), in Czernik 3, where simulations indicate that the observed mass segregation is indeed a consequence of relaxation (Sharma et al., 2020, §4.1), in ASCC 92 (Piatti, 2023), and in several of the 15 clusters using EDR3 data by Ebrahimi et al. (2022).

In a study of 773 clusters using Gaia EDR3, Almeida et al. (2023b) found '… *no significant evidence that clusters lose and segregate mass with age*'. But in a study of 60 clusters using Gaia DR3, Angelo et al. (2023) found that the core radii do appear to decrease with age. Other studies are underlining the inherent complexity of disentangling the many effects at work (Viscasillas Vázquez et al., 2023; Alvarez-Baena et al., 2024; Hu et al., 2024).

THE EVOLUTION of open clusters is also influenced by its binary population, and their own disruption by passing perturbers. Various studies have used Gaia DR3 to probe their influence. For 78 clusters, Cordoni et al. (2023b) found a binary fraction ranging from 15–60%, hints of a correlation between the total fraction of binary stars and the central density, and with a radial distribution depending on cluster age. Comparable ranges of binary fractions were found for 202 clusters by Donada et al. (2023), and for 16 clusters by Long et al. (2023).

Pang et al. (2023) found a decreasing binary fraction with increasing cluster age (depending strongly on stellar density), only limited evidence for mass segregation, but clear evidence for the early disruptions of binary stars, with the binary fraction depending strongly on radial distance. Several other studies along these lines have been reported (Childs et al., 2024; Chulkov, 2024; Jiang et al., 2024; Alexander & Albrow, 2025).

FINALLY, I SHOULD mention the search for the likely presence of stellar-mass black holes in open clusters, which I considered in some detail in essay 175. I will only mention here that in their study of the Hyades, Torniamenti et al. (2023) found that their Gaia DR3 observations are best reproduced by models with 2–3 black holes still in the cluster today.

222. Open clusters: chemistry & models

THE SCIENTIFIC importance of open clusters is underpinned by the *assumption* that their stars started life at the same time, formed from the same giant molecular cloud, so are of similar age, and with similar initial composition. These two boundary conditions provide strong constraints on models of stellar structure and evolution. Gaia's rigorous membership lists, and accurate distances and photometry, allow for the construction of clean and accurate colour–magnitude diagrams for main-sequence fitting, the identification and characterisation of stars in specific evolutionary phases, and deviations from existing state-of-the-art models.

THE NEAREST open cluster, the Hyades, has revealed remarkable tidal tails extending more than 100° across the sky. But of specific interest here is the Gaia DR3-based colour–magnitude diagram by Brandner et al. (2023), which I have considered in some detail in essay 151. Shown below is their colour–magnitude diagram for 600 single stars, and their best-fitting PARSEC isochrones (Nguyen et al., 2022). While this gave an improved fit compared with MESA 1.2 (Jermyn et al., 2023), they found that, over the colour range $B_P - R_P$ = 2.4−3.2 mag (0.22−0.40$M_\odot$), stars are still systematically brighter (or redder) than the isochrone predictions.

Even for this nearby cluster, a wide range of ages is still found. As examples, their PARSEC isochrones gave an age 775 ± 20 Myr. My own work using the Hipparcos data gave 625±50 Myr (Perryman et al., 1998), while from the cooling ages of the 9 known Hyades white dwarfs, Lodieu et al. (2019) derived 640^{+67}_{-49} Myr.

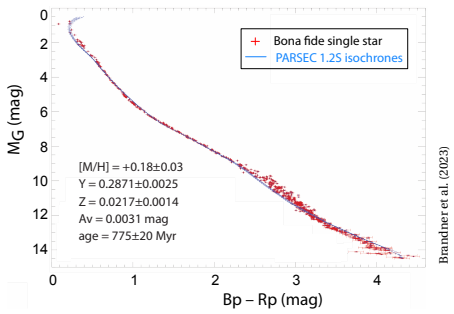

DISCREPANCIES BETWEEN stellar models and observations for sub-solar mass stars were partly attributed, by Castellani et al. (2001), to limitations in the description of superadiabatic convection in the outer layers of partially convective stars. Improvements in the definition of the Hyades main sequence, as the nearest open cluster, have led to improvements in stellar models, for example in the incorporation of updated input physics, including opacities (Kopytova et al., 2016).

Recently, Wang et al. (2025) derived empirical colour corrections based on the latest MIST and PARSEC models, and the Gaia $B_P - R_P$ and $G - R_P$ colours of the Hyades, Pleiades, and Praesepe. Applying these empirical corrections to 31 other clusters and three moving groups gave significantly better agreement between the isochrones and observed colour–magnitude diagrams, and isochrone ages consistent with the 'lithium depletion boundary' method (essay 220).

Clearly, some physics is missing. What we will see advanced in the coming years are the different estimates of the cluster's mean metallicity, and the problem of the degeneracy between metallicity ([Fe/H]), the He-to-metal enrichment ($\Delta Y/\Delta Z$), and the convective mixing length parameter (α_{ML}), with the latter also dependent on the part of the main sequence being modelled. For example, using the PISA evolution models, and estimates of [Fe/H] = 0.14–0.18, and the Gaia DR2 photometry and parallaxes, Tognelli et al. (2021) obtained mean values of $\alpha_{ML} = 2.01 \pm 0.05$ and $\Delta Y/\Delta Z = 2.03 \pm 0.33$.

I HAVE GONE into more details of convection in essay 150: why it is important (and uncertain), how it is modelled, and where Gaia is contributing; e.g. in understanding the so-called 'kissing instability' (van Saders & Pinsonneault, 2012). But we will also see progress in understanding the effects of rotation, more secure estimates of the He abundance (where the primordial abundance is imprinted in the lowest mass stars), eliminating still unidentified (more extreme) brightness- and mass-ratio binary systems, the effects of stellar activity and variability, and the possibility of 'radius inflation' identified in some of the Hyades stars (Jaehnig et al., 2019).

THE 'TURNOFF' region of the Hertzsprung–Russell diagram, the region where stars begin to leave the main sequence and evolve into giants, presents various puzzles, all being advanced by Gaia. One is the 'extended main sequence turnoff' (eMSTO), a broadening of the turnoff seen in many clusters (e.g. Cordoni et al., 2018). Once tentatively attributed to an age spread, Gaia studies have shown that the redder stars often corresponds to fast rotators, whereas bluer stars rotate more slowly (Bastian et al., 2018; Cordoni et al., 2018; Marino et al., 2018; Lim et al., 2019; He et al., 2022; Griggio et al., 2023). For the Galactic cluster Stock 2, the effect is attributed to differential reddening (Alonso-Santiago et al., 2021).

The extended turnoffs in the Magellanic Clouds also appear to involve stellar rotation, but combined with significant age spreads (e.g. Goudfrooij et al., 2014), and effects of stellar variability (Salinas et al., 2016).

'Isochrone clouds' have been invoked to describe a coeval population of various masses, and fractional core masses, due to different internal mixing profiles (Johnston et al., 2019b). But Johnston et al. (2019a) concluded that a *'global theoretical interpretation is still lacking'*.

BLUE STRAGGLERS are more luminous, and have a higher $T_{\rm eff}$ (hence bluer), than the cluster's main sequence turnoff. First identified in M3 by Sandage (1953), they are inconsistent with standard evolutionary theory – they should have consumed their nuclear fuel, and evolved to become white dwarfs, long ago. Rather, they are considered to result from collisions, from binary stars in the process of merging (or recently merged), or a result of mass-transfer in a binary (Mapelli et al., 2006; Boffin et al., 2015). Ahumada & Lapasset (2007) listed 1887 candidates in 427 open clusters.

Gaia is providing the improved location and fidelity of candidates in the colour–magnitude diagram. From Gaia DR2, Rain et al. (2021a) confirmed just 897 (and 77 yellow stragglers) in 408 open clusters. At the same time, also from DR2, Jadhav & Subramaniam (2021) found 868 blue stragglers in 228 clusters. And they established that their numbers *increase* with cluster age and mass. Using Gaia DR3, Li et al. (2023a) found a further 138.

Their radial distribution provides an important dynamical probe for globular clusters, and Gaia has enabled similar studies for open clusters. I will simply refer here to DR2-based studies of seven such clusters by Vaidya et al. (2020), and three more by Rain et al. (2021b).

Based on sixteen old nearby ($d < 3500$ pc) open clusters, Leiner & Geller (2021) found that their fractional number increases with age. They also found that population synthesis models in which blue stragglers form by mass transfer, dramatically under-produce the numbers in old clusters, as well as overproducing high-mass relative to lower-mass stragglers. Again, additional physics seems to be required to explain these findings.

Ultraviolet observations combined with astrometry and photometry from Gaia DR2/EDR3 now accurately locates blue stragglers in various other clusters (Vaidya et al., 2022; Panthi et al., 2022; Rani et al., 2023; Jadhav et al., 2023), confirming many as post-mass-transfer binaries as inferred from their high ultraviolet flux.

An important Gaia discovery is a double blue straggler sequence in the ancient (8.5–10 Gyr) Galactic cluster Berkeley 17 (Rao et al., 2023). Parallel sequences have been seen previously in four *globular* clusters (the first of which was M30, Ferraro et al., 2009), the bluer attributed to stellar collisions, and the redder to the results of binary mass transfer. However, the lower densities of open clusters makes formation via collisions unlikely, suggesting a mass-transfer formation channel for both, but with an unexplained offset between them.

I HAVE COVERED various aspects of white dwarfs in several previous essays. Of relevant here is that those in clusters come with a known age. This helps constrain the 'initial-to-final mass relation' (IFMR) which provides a mapping (through evolutionary mass-loss models) between the zero-age main sequence mass and its end-of-life white dwarf mass (essays 134 and 178).

Various Gaia studies have searched for other white dwarfs specifically associated with clusters (e.g. Gentile Fusillo et al., 2019; Prišegen et al., 2021; Richer et al., 2021). Others have used these to study the IFMR (e.g. Si et al., 2018; Canton et al., 2021; Heyl et al., 2022). As an example, Prišegen & Faltová (2023) found 63 such 'cluster' white dwarfs, 36 of which were new, with six falling in relatively unconstrained regions of the IFMR where the relation seems to exhibit non-linear behaviour.

THE STUDY OF chemical abundances in open clusters is a huge topic, and I will give only a couple of 'pointers' most directly related to Gaia. Gaia DR3 itself included stellar parameters and chemical abundances for 5.6 million stars derived from its Radial Velocity Spectrometer (Recio-Blanco et al., 2023), and applied to 503 open clusters by Gaia Collaboration et al. (2023f).

Gaia-based memberships are assisting recent or planned large-scale spectroscopic surveys focused on Galactic chemo-dynamics, including the Gaia–ESO survey, APOGEE, GALAH, LAMOST–LEGUE, RAVE, 4MOST, and WEAVE, and several other smaller programmes.

Goals include understanding their chemical homogeneity and the relationship to 'strings' (Liu et al., 2016a; 2016b; Manea et al., 2022; Zucker et al., 2022), the idea of chemical tagging (Freeman & Bland-Hawthorn, 2002; Casamiquela et al., 2022; Bhattarai et al., 2024), and stellar nucleosynthesis processes and the radial metallicity gradient in the Galaxy (e.g. Casamiquela et al., 2019; Jofré et al., 2019; Donor et al., 2020; Spina et al., 2022; Zhang et al., 2022; Magrini et al., 2023; Palla et al., 2024).

223. Associations – an update

WHAT ARE 'associations', and how do they differ from open clusters? What was the state of knowledge pre-Gaia, and what has Gaia contributed to the census of nearby associations? And what do we now know about their formation, dynamics, and dispersal?

I presented some early results on associations based on Gaia DR2 in essay 18 (in early 2021). Let me recall that, in contrast to the higher stellar density and gravitationally bound open clusters, *associations* were originally defined by Lada & Lada (1991) as looser groups of some 10 or more physically related stars, often of large spatial extent. In the case of OB associations, they are characterised by their overdensity of O and B stars (there are also, for example, T-associations comprising T Tauri stars). High masses and luminosities imply that the stars are young and short lived, and so implicitly associated with sites of recent star formation. They are unbound, and survive as recognisable groups only for a short time, 25–50 Myr… although somewhat longer with Gaia!

A number of OB associations within 150 pc of the Sun have long been known (with early work by Kapteyn, 1914; Rasmuson, 1921; Pannekoek, 1929; Blaauw, 1946), including Scorpius–Centaurus (with subgroups including Lower Centaurus Crux and Upper Scorpius), Taurus–Auriga, Hercules–Lyra, and Tucana–Horologium. Their large extent on the sky has traditionally prevented accurate kinematic membership determination for any but the brightest stars. Many studies were already made with the Hipparcos data, which provided a major improvement in their kinematic detection.

EARLY IDEAS OF 'monolithic formation' posited that associations were expanding from their origins as gravitationally bound clusters. Gaia DR1/DR2 results showed that, instead, many probably formed in a highly sub-structured state with multiple small-scale star formation events rather than a single, monolithic burst.

Such a conclusion was suggested based on the Gaia DR1 data for the Sco–Cen OB association by Wright & Mamajek (2018), and in a much larger (12 000 OB stars) Gaia DR2-based study by Ward et al. (2020).

MY STARTING POINT in this essay is the general picture already reached in 2021: that the Gaia results are far more consistent with a scale-free, hierarchical picture of star formation, in which stars are formed across a continuous density distribution throughout molecular clouds, rather than exclusively within clusters, and in which OB associations are formed *in situ* as relatively large-scale and gravitationally-unbound structures (e.g. Ward & Kruijssen, 2018).

Before continuing with the subsequent studies, let me stress that the subject of associations, the advances being made by Gaia, and the inferences being made in more theoretical studies of star formation, is a very substantial field, for which I refer to some recent reviews for the broader context and many more details (Krumholz et al., 2019; Wright, 2020b; Cantat-Gaudin, 2022; Wright et al., 2023; Zucker et al., 2023; Quintana, 2024).

THE GAIA DATA, using parallaxes, proper motions, radial velocities and photometry, has enabled the improved membership and characterisation of all known associations, and the discovery of many others.

Studies extended out to around 150 pc with DR1 (Gagné et al., 2018a; 2018b; 2019), to several hundreds of parsecs with DR2, including associations in Orion, Perseus, Taurus, and Sco–Cen (Zari et al., 2018; Kounkel & Covey, 2019; Dickson-Vandervelde et al., 2021; Kerr et al., 2021; McBride et al., 2021; Teixeira et al., 2021), and to beyond 1 kpc with EDR3/DR3 (Zari et al., 2021; Moranta et al., 2022; Pang et al., 2022; Prisinzano et al., 2022; Kerr et al., 2023; Luhman, 2023).

One recurring theme that emerges from these studies is their spatial complexity. For example, the massive star-forming regions within 600–700 pc, such as Orion, Sco–Cen, and Vela, trace a complex three-dimensional pattern (Prisinzano et al., 2022). Most young stars are not organised into distinct spiral arms (Zari et al., 2021). And cluster analyses points to structural connections between often-separated populations, such as between the Orion Complex and Perseus OB2, and between the subregions of Vela (Kerr et al., 2023).

THE NEAREST and most well-studied association is Scorpius–Centaurus (Sco–Cen, aka Sco OB2), and subgroups including Lower Centaurus Crux and Upper Scorpius. At 130 pc, and extending over 2000 sq. deg., Hipparcos identified over 400 members (de Zeeuw et al., 1999). Gaia allows a more rigorous membership, and the detection of lower-mass stars, and has brought the latest census to around 15 000 (Goldman et al., 2018; Luhman et al., 2018; Röser et al., 2018; Wright & Mamajek, 2018; Damiani et al., 2019; Luhman & Esplin, 2020; Squicciarini et al., 2021; Luhman, 2022; Briceño-Morales & Chanamé, 2023; Ratzenböck et al., 2023a; 2023b; Zerjal et al., 2023; Bobylev & Bajkova, 2024).

Amongst these, within Lower Centaurus Crux, Goldman et al. (2018) reported *'… the revelation of a large moving group containing more than 1800 intermediate- and low-mass young stellar objects and brown dwarfs that escaped identification until Gaia DR2'*.

Also from Gaia DR2, Damiani et al. (2019) identified 11 000 pre-main-sequence members, while Zerjal et al. (2023) identified eight kinematically distinct components consisting of 8185 stars distributed in dense and diffuse groups, each with an independently fit kinematic age. From EDR3, Luhman (2022) estimated that the complex contains 10 000 members with masses $\gtrsim 0.01 M_\odot$. With DR3, Ratzenböck et al. (2023b) found more than 13 000 young co-moving objects (19% of substellar mass), organised into 37 co-moving groupings.

Squicciarini et al. (2021) concluded that star formation in Sco–Cen lasted more than 10 Myr, proceeding in small groups that, after a few Myr, dissolve in the field of the older population but continue to retain memory of their initial structure. A detailed star-formation chronology is given by Ratzenböck et al. (2023a).

Of more general applicability, Buckner et al. (2024) ran simulations of the detectability and reliability of these associations based on Gaia DR3.

Melnik & Dambis (2021) estimated the contribution of binary systems to the velocity dispersion inside OB-associations derived from the Gaia DR2 proper motions. The maximum contribution to the velocity dispersion is given by binaries with orbital period around 5.9 yr.

WHETHER ASSOCIATIONS are expanding or not is linked to the underlying star-formation processes. During the early phases, radiation from hot stars and supernovae can rapidly strip residual gas, although not necessarily resulting in the association's rapid dispersal (e.g. Kruijssen, 2012; Kruijssen et al., 2012).

Equipped with the individual space motions from Gaia, it appears that many associations *are* expanding, some albeit only slowly (Melnik & Dambis, 2017; Ward & Kruijssen, 2018; Kuhn et al., 2019; Melnik & Dambis, 2020; Ward et al., 2020), although others are not (Kounkel et al., 2018; Wright & Mamajek, 2018).

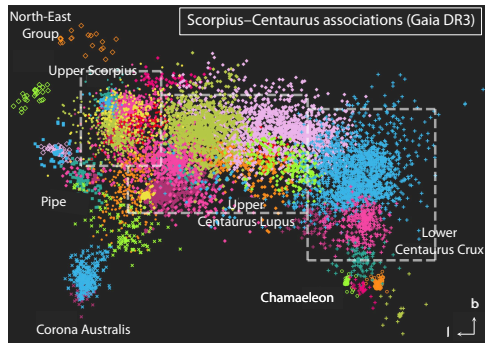

IN THEIR wide-ranging review, Krumholz et al. (2019) opened their abstract as follows: *'Star clusters stand at the intersection of much of modern astrophysics: the interstellar medium, gravitational dynamics, stellar evolution, and cosmology'*. They summarise the present understanding of the formation, evolution, and eventual disruption of star clusters so authoritatively and lucidly, that I will quote verbatim from their abstract.

"The current literature suggests a picture of this life cycle with several phases:
• clusters form in hierarchically-structured, accreting molecular clouds that convert gas into stars at a low rate per dynamical time until feedback disperses the gas;
• the densest parts of the hierarchy resist gas removal long enough to reach high star formation efficiency, becoming dynamically-relaxed and well-mixed. These remain bound after gas removal;
• in the 100 Myr after gas removal, clusters disperse moderately fast, through a combination of mass loss and tidal shocks by dense molecular structures in the star-forming environment;
• after ~100 Myr, clusters lose mass via two-body relaxation and shocks by giant molecular clouds, processes that preferentially affect low-mass clusters and cause a turnover in the cluster mass function to appear on 1–10 Gyr timescales;
• after dispersal, some clusters remain coherent and detectable in chemical or action space for multiple Galactic orbits."

FOR THOSE STILL struggling to understand the big picture, Krumholz et al. (2019) perhaps provide some comfort. For despite this broad and broadly satisfying picture, star clusters, which cover a huge range of mass, size, and density scales, *'remain mysterious'*. *'Conceivably'*, they continue, *'all stars formed in groups, clusters, or hierarchies, although, for this to be true, most clusters must have dissolved into the Galactic background soon after formation. However, our understanding of when, how, and why stars cluster remains primitive'*.

Gaia is contributing significantly to their understanding, and I will finish with a quote from Wright (2020b): *'It is clear now that OB associations have considerably more substructure than once envisioned, both spatially, kinematically and temporally. These changes have implications for the star formation process, the formation and evolution of planetary systems, and the build-up of stellar populations across galaxies.'*

224. Strings, snakes and pearls

I WILL START this essay with the opening words of the review by Zucker et al. (2023): *'Most of what we know about the formation of stars, and essentially everything we know about the formation of planets, comes from observations of our solar neighbourhood within 2 kpc of the Sun. Before 2018, accurate distance measurements… were few and far between. Since 2018, data from the Gaia mission are revealing previously unseen and often unexpected 3D distributions of gas, dust, and young stars in the solar neighbourhood.'*

In my previous five essays, I summarised our latest knowledge of the structure and evolution of nearby open clusters and associations as revealed by Gaia's astrometry and photometry. Here, I will look at some new – and unexpected – structures associated with star formation in the solar neighbourhood, including those described in the discovery papers as 'strings', 'snakes', and 'pearls'.

IT IS PERHAPS useful to recall the definition of open clusters and associations by Lada & Lada (1991): groups of stars of the same physical type whose surface density significantly exceeds that of similar field stars.

They then considered *clusters* to be physically related groups of 10 or more stars whose stellar density, of around $1\,M_\odot\,\mathrm{pc}^{-3}$, would render it stable against tidal disruption by the Galaxy, as well as by passing interstellar clouds. *Associations* are loose groups of 10 or more physically related stars whose space density is considerably below the tidal stability limit. At least some 'moving groups' are the remnants of such structures. Today, we might be less strict on membership numbers, and we know that clusters progressively 'dissolve' as a result of gas dispersal, as well as internal and external disruptive processes. But these definitions serve as a guide.

KNOWLEDGE OF THE 3D distribution of young stars, as well as the gas and dust from which they form, is essential for modelling the many processes that determine star formation, such as gravity, turbulence and magnetic fields (e.g. Hartmann et al., 2001; Kennicutt & Evans, 2012; Evans et al., 2014; Heyer & Dame, 2015).

MAPPING OF THE local distribution of gas and dust has been greatly advanced using Gaia astrometry to derive the distances and 3D structures of molecular clouds and local star-forming regions, a topic which I detailed in essay 192. In the present context, I will only emphasise the point that the gas in giant molecular clouds, such as Orion, is often found in the form of extended filaments (e.g. Bally et al., 1987; Hacar et al., 2018; Kounkel et al., 2018; Zucker et al., 2021).

Of Gaia's new open cluster discoveries, a particular curiosity is Meingast–1 (Meingast et al., 2019), aka the Pisces–Eridanus stream (Röser & Schilbach, 2020; Ratzenböck et al., 2020), a massive elongated co-moving population at a distance of only 100 pc. This extends 120° on the sky, viz. several hundred pc in length. Identified in velocity space, it was 'hiding' amongst hundreds of thousands of unrelated field stars. It is held to be a dissolving open cluster, with an age similar to that of the Pleiades, around 120 Myr (Curtis et al., 2019b; Arancibia et al., 2020; Hawkins et al., 2020), and with at least one planetary system so far identified (Newton et al., 2021).

EVEN MORE CURIOUS are the nearby discoveries reported by Kounkel & Covey (2019). From Gaia DR2, they identified 1901 distinct groups within 1 kpc, together comprising 288 370 stars. Many of these groups appear to be filamentary structures that they refer to as 'strings', oriented parallel to the Galactic plane, and with some spanning hundreds of pc in length. One of the largest, α Per, seen here in light blue, extends over 120°.

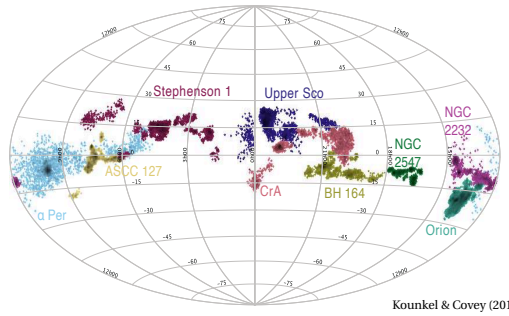

Kounkel & Covey (2019)

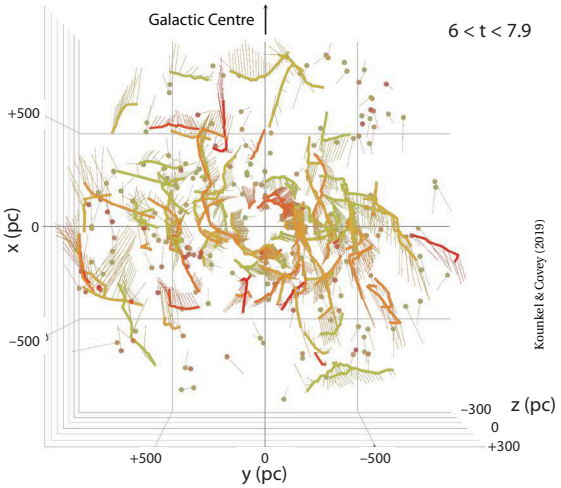

THE ANALYSIS by Kounkel & Covey (2019) found that these nearby 'strings', shown above, appear to be coherent both spatially and kinematically, and roughly parallel to the Galactic plane. Each can be characterised with a single isochrone, spanning ages of $10^7 - 10^9$ yr, albeit with a possible scatter of few Myr. The youngest strings (< 100 Myr) are the most prominent, and are orthogonal to the Local Arm. The older features appear to be remnants of other arm-like structures that cannot be presently traced by dust and gas.

Most lack a central cluster, implying that their filamentary nature is primordial, rather than the result of, say, tidal stripping. The velocity dispersion increases with age, and suggests a timescale for dynamical heating of ~300 Myr. This timescale is also consistent with the age at which the string population begins to decline, while the population in more compact groups continues to rise. This all suggests that various dynamical processes are disrupting the more weakly bound string populations, leaving only individual clusters to be identified at later times.

Kounkel et al. (2020) extended this search to a distance of 3 kpc, and compiled a catalogue (referred to as Theia; Kounkel et al., 2022) of 8292 separate low-density filamentary or streams, comprised of hundreds to thousands of stars and spanning hundreds of pc.

OTHER YOUNG and highly elongated stellar structures in the solar neighbourhood have been reported. In the area of the Vela OB2 association, stellar bridges extending over a few hundred parsecs and connecting several known clusters suggest a star-formation episode in a filamentary giant molecular cloud about 35 Myr ago (Beccari et al., 2018; Tian, 2020; Wang et al., 2022b).

Jerabkova et al. (2019) identified a 17 Myr old and 90 pc long stellar relic filament in the Orion star-forming region, too young to have been entirely shaped by tidal forces, and also attributed to a filamentary remnant.

Beccari et al. (2020) detected a 260 pc-long structure linking two previously known clusters, BBJ 1 and NGC 2547. Tian (2020) identified a young (30–40 Myr) stream, 200 pc long and 80 pc wide, comprising several thousand stars, which they referred to as a 'snake'.

Somewhat distinct from these filaments are the stellar 'pearls': distinct clusters that follow similar Galactic orbits, and identified as overdensities in action-angle space (Coronado et al., 2022). While these are not, it seems, coeval systems originating from the same molecular gas cloud, their existence points to recent star formation which is strongly clustered along an orbit.

AN UNAMBIGUOUS picture of how these filamentary structures arise and evolve remains unclear. GALAH-based studies of the chemical abundances of five of the large stellar strings do suggest that they are, in general, chemically homogeneous (Manea et al., 2022).

In a follow-up study of Theia 456, a low-density thin-disk stream extending nearly 200 pc and 20° across the sky, Andrews et al. (2022) supplemented Gaia astrometry with spectroscopic metallicities from LAMOST, and rotation periods from ZTF and TESS photometry. They reported strong evidence that the members have a common age (175 Myr), a common dynamical origin, and were formed from chemically homogeneous pre-stellar material, with [Fe/H] = –0.07 dex.

However, Zucker et al. (2022) suggest that the large radial velocity dispersions of some filaments, averaging ~16 km s^{-1} as found with Gaia DR3, would imply that their reported ages are significantly larger than the inferred dispersal times. The chemical homogeneity may also not be conclusive, together perhaps calling into question their true physical association.

GAIA IS REVEALING considerable and largely unexpected complexity in the various physical and kinematical structures in these young star-forming regions. While they can be roughly broken down into smaller components of varying densities that may evolve separately over time, many appear to be formed from the same parental cloud complex.

And while Kounkel & Covey (2019) used the term 'group' to embrace gravitationally bound clusters, associations, and co-moving groups, they emphasised that the question of nomenclature, and whether there is indeed a conceptual difference between them, needs to be revisited in the future.

I WILL FINISH with another quote from Zucker et al. (2023), to which I refer for a more substantial review: *'This new 3D view of our solar neighbourhood in the age of Gaia shows that star-forming regions once thought to be isolated are often connected on kpc scales, causing us to reconsider models for the arrangement of gas and young stars in galaxies.'*

225. Rotational parallaxes

TRIGONOMETRIC PARALLAXES provide the fundamental geometric distance measurement principle at the heart of Gaia, and of Hipparcos before it. Distances are derived, essentially by straightforward trigonometry, from the difference in the angular position of a source, compared to background sources, along different lines-of-sight as the Earth (and Gaia) orbit the Sun.

THERE ARE other geometric distance methods, which only apply to specific source types, and which rest on radial velocities combined with angular measures. If there is a physical relation between the two, then the angular measures from astrometry (in $\mathrm{mas\,yr^{-1}}$) are related to the radial velocities (in $\mathrm{km\,s^{-1}}$) through the object's distance. Some examples will make this clearer:

(a) if the expanding shells of a supernova remnant are spherically symmetric, the maximum transverse motion (in the plane of the sky) is equal to the maximum radial velocity (on the line-of-sight). This 'expansion parallax' was applied to the Crab pulsar by Lundmark (1926) and Trimble (1973). Most recently, Lin et al. (2023) used radio VLBI to determine $\varpi = 0.53 \pm 0.06$ mas ($d = 1.90 \pm 0.20$ kpc), remarkably consistent with the parallax from Gaia DR3, $\varpi = 0.51 \pm 0.08$ mas (Antoniadis, 2020). It has also been used for planetary nebulae (e.g. Li et al., 2002).

(b) for pulsating Cepheids, the 'geometric' Baade–Wesselink method, or 'parallax-of-pulsation' method, relates the diameter changes during a pulsation cycle (using interferometry) to the radial velocity of its photosphere, yielding both its size and its distance (e.g. Lane et al., 2002; Breitfelder et al., 2016).

(c) orbital parallaxes provide distances for double-lined spectroscopic binaries with an astrometric orbit, again exploiting dual constraints from astrometry and radial velocities (e.g. Torres et al., 1997).

(d) kinematic distances to globular clusters can be obtained from a combination of proper motions and line-of-sight velocity measurements by appeal to simple spherical dynamical models, as first applied to M3 (Cudworth, 1979), and more recently ω Cen (van de Ven et al., 2006), 47 Tuc (McLaughlin et al., 2006), and others.

THE 'rotational parallax' method of distance determination is in principle applicable to Local Group disk galaxies, such as M31 and M33, and it could provide an independent check of other extragalactic distance techniques (e.g. using Cepheids, RR Lyrae, tip of the red giant branch, red clump, Tully–Fisher, planetary nebulae, and eclipsing binaries).

As applied to M31 and M33, it was included as part of the extensive scientific case for Gaia in the Concept and Technology Study Report, ESA–SCI(2000)4. The Gaia data are not yet at the point that meaningful rotational parallaxes can be derived, but I will explain the principles, and describe the present status.

CONSIDER a disk galaxy with known centre-of-mass space motion, flat rotation curve, i.e. independent of radial distance, and at some unknown inclination to the line-of-sight. Then for a target star on a circular orbit, three observables – its two proper motion components and its radial velocity – are, in principle, sufficient to determine the three unknowns: the orbit inclination, the rotational velocity, and the distance (Olling & Peterson, 2000; Olling, 2007). The method again makes use of the fact that since proper motions are distance-dependent, and radial velocities are distance-independent, determination of a rotation curve using both methods can provide the distance.

There are various complications in practice: the galaxy has some bulk space motion; stars are not on strictly circular orbits (e.g. due to spiral-arm streaming motions), they might have large z-heights or non-equilibrium velocities (e.g. runaway stars), and lie at significantly different distances (e.g. the near side of M31 is 5% closer than the far side). On the other hand, the galaxy's inclination can be estimated from the axis ratio of the image, or from the H I or Hα radial velocity fields.

Olling (2007) estimated that an accuracy of a few per cent in the distances to M31, M33 and the Large Magellanic Cloud requires radial velocities at the $10\,\mathrm{km\,s^{-1}}$ level, and proper motions which should be attainable by Gaia, or perhaps through VLBI observations of water masers in high-mass star-forming regions.

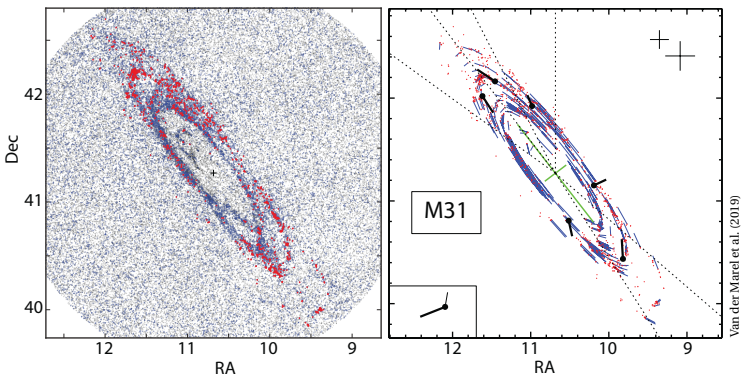

Left: the Gaia DR2 sources selected for M31, with blue and red points showing sources passing progressively stricter quality criteria. Right: the red points show the same sources, while the blue lines are the proper motions predicted by the best-fit rotating disk model. The inset shows the centre-of-mass proper motion (thick line), and the average proper motion of surrounding quasars (thin line). From van der Marel et al. (2019).

ANOTHER IMPORTANT reason for determining the rotational parallaxes of M31, M33, and others, is that the Local Group is the best and most proximate example of cosmological large-scale structure. Their orbits provide important tests of the predictions of hierarchical structure formation in the ΛCDM paradigm.

Such lofty goals are hampered by the small proper motions. As a result, their relative motions with respect to the Milky Way, central to understanding the past, present, and future evolution of the Local Group, have been subject to considerable debate (e.g. van der Marel et al., 2012; Banik et al., 2018; Patel et al., 2018; Semczuk et al., 2018; Salomon et al., 2021; Wempe et al., 2024).

For example, Patel et al. (2017) concluded that M33 is either on its first infall into the halo of M31, or that it is on a long-period (6 Gyr) orbit with a past pericentric approach at ~100 kpc. This would be consistent with first infall orbits expected for satellites in this mass range at the present epoch (Boylan-Kolchin et al., 2011).

MAPPING of a galaxy's large-scale rotation based on 3D velocity measurements was first reported for the Large Magellanic Cloud by van der Marel & Kallivayalil (2014). They used HST proper motions in 22 fields (2–3 epochs over 2–7 yr), combined with line-of-sight velocities for 6790 stars. They applied the rotational parallax method by requiring that the rotation amplitude from the proper motions and radial velocities matched.

Complications included defining the galaxy's dynamical centre and the proper motion of its centre of mass, the inclination of its disk, and its rotation curve amplitude. They nonetheless derived a kinematic distance modulus for the LMC of 18.48 ± 0.40 mag, consistent but not competitive with other methods at the time.

USE OF Gaia DR2 to study the proper motion fields of M31 and M33, providing many more stars than HST, and the next steps in determining their rotational parallaxes, was made by van der Marel et al. (2019). For the selection of member stars, they imposed cuts in parallax and proper motion, and in the relevant colour–magnitude diagrams.

The Gaia DR2 data do not meaningfully constrain the shape of the rotation curve, which they assumed to be flat (see Fig. 6 of Zhang et al., 2024b). Nor do they yet reach the accuracy to significantly constrain the viewing angle, or the position, distance, and line-of-sight velocity to the centre-of-mass, for which they adopted existing values from photometric and radial velocity studies (with $D = 770$ kpc for M31, and 794 kpc for M33). The proper motion field is then determined by three free parameters, the two proper motion components of the centre of mass, and the rotation velocity of the disk.

Under various assumptions, they derived the proper motion of the centre-of-mass of both relative to background quasars in DR2, and the outward radial component in the proper motion field due to their approaching velocities. They detected the rotation of both galaxies (in the proper motion field), consistent with the known line-of-sight rotation curves: $V_{\rm rot} = -206 \pm 86\,{\rm km\,s^{-1}}$ (counter-clockwise) for M31, and $V_{\rm rot} = 80 \pm 52\,{\rm km\,s^{-1}}$ (clockwise) for M33. With future Gaia data releases, it should be possible to better quantify the outward radial component in the proper motion field, and obtain a kinematic distance estimate by comparison with the line-of-sight velocity of the centre-of-mass.

A SIMILAR ANALYSIS using Gaia DR3 was carried out by Rusterucci et al. (2024). They improved the connection to the quasar reference frame, and attributed variations in the inferred proper motions across different regions of M31 to systematics. They derived the bulk proper motion of M31 as $46.9 \pm 11.7 \pm 50.6\,\mu{\rm as\,yr^{-1}}$ in RA, and $-29.1 \pm 9.4 \pm 35.6\,\mu{\rm as\,yr^{-1}}$ in dec (statistical/systematics). They argued that the systematics remain the dominant source of uncertainty, being comparable to the proper motion of M31 itself. They provide equivalent results for M33.

They found that a significant reduction in the systematic uncertainties occurred between DR2 and DR3. They concluded that if similar progress is made with Gaia DR4, future Gaia-based estimates would match the level of uncertainties of HST, and could be used to refine the dynamics and history of both M31 and M33.

226. Heartbeat stars

HEARTBEAT STARS are a class of detached binary with eccentric orbits, ($e \gtrsim 0.3$), and short periods, typically in the range 1–100 d. They generally display very small amplitude variations, 1–2 mmag, which are driven by tidal distortion, reflection and Doppler beaming.

These effects are most prominent near periastron, where they combine to generate the characteristic electrocardiogram-like 'heartbeat' signature which gives them their name (Thompson et al., 2012). Many continue to oscillate after periastron and throughout the entire orbit, behaviour attributed to the tidal excitation of oscillation modes within one or both stars.

They are attracting considerable theoretical interest, as probes of tidal dissipation, internal stellar structure, orbit circularisation, and short-period binary formation (e.g. Shporer et al., 2016; Moe & Kratter, 2018; Toonen et al., 2020). Gaia is starting to contribute to their understanding. I will start with a pre-Gaia synopsis.

EARLY DISCOVERIES, some tentatively attributed to the effects of tidal distortion but without a full picture, included the well-studied but enigmatic ϵ Per (Frost & Adams, 1904; Tarasov et al., 1995; De Cat et al., 2000b), the eccentric binary HD 209295 (Handler et al., 2002), the SPB (slowly-pulsating B) star HD 177863 (De Cat et al., 2000a; Willems & Aerts, 2002), the eccentric CoRoT discovery HD 174884 (Maceroni et al., 2009), and the δ Scu variable HD 51844 (Hareter et al., 2014).

More than 100 with asymmetric light curves, attributed to large eccentricities and tidal distortions, were identified in the OGLE catalogue of ellipsoidal variables (Soszyński et al., 2004), of which they are a subset.

As a result of their small amplitude variations and characteristic time scales of order days, they were only found in larger numbers, and with better light curve characterisation, with Kepler (Welsh et al., 2011; Thompson et al., 2012; Hambleton et al., 2013; Beck et al., 2014; Kirk et al., 2016); and more recently with TESS (Murphy et al., 2020; Jayasinghe et al., 2021; Kołaczek-Szymański et al., 2021; Li et al., 2024a; Solanki et al., 2025; Uronen et al., 2024). Many others have since been found in the OGLE data (Wrona et al., 2022a; Wrona et al., 2022b).

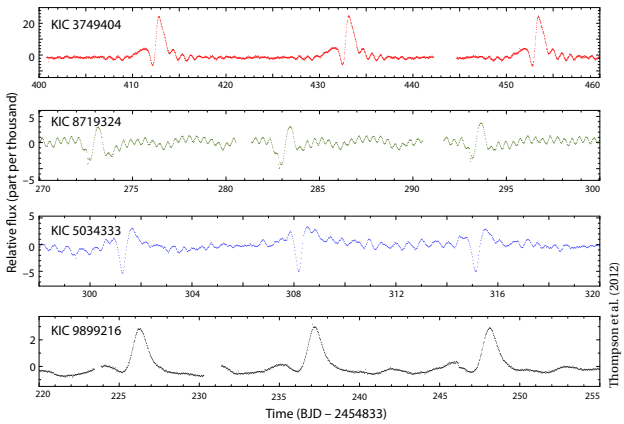

OF SOME 300 known today, four example light curves from the Kepler mission, are shown here. The ellipsoidal distortion, increasing towards periastron, results in part of the observed brightness changes (in common with other ellipsoidal variables, essay 133). But the strong tidal forces cause more rapid changes, resulting in the heartbeat-like fluctuations. Under certain conditions, tidal oscillations are also resonantly excited.

Orbital parameters are derived from the light curves, accounting for ellipsoidal variability, Doppler beaming, reflection effects, and eclipses (Kumar et al., 1995). Available codes for this include `eBEER` (Engel et al., 2020), and `PHOEBE` (Horvat et al., 2018).

Out of 180 heartbeat stars identified from 240 short-period ($P < 10$ d) binaries from TESS, Solanki et al. (2025) found 133 with eclipses. Some 30 with both primary and secondary eclipses show a secular change in inter-eclipse timing and relative eclipse depth over a multi-year baseline, attributable to orbital precession.

THE PHYSICS GETS more interesting in systems in which 'tidally excited oscillations' have been seen in their light curves, a phenomenon predicted by Kumar et al. (1995). One of the most-studied exemplars is the fourth heartbeat system discovered, the high eccentricity ($e = 0.83$, $P = 41.8$ d) Kepler discovery, KOI–54 (Welsh et al., 2011).

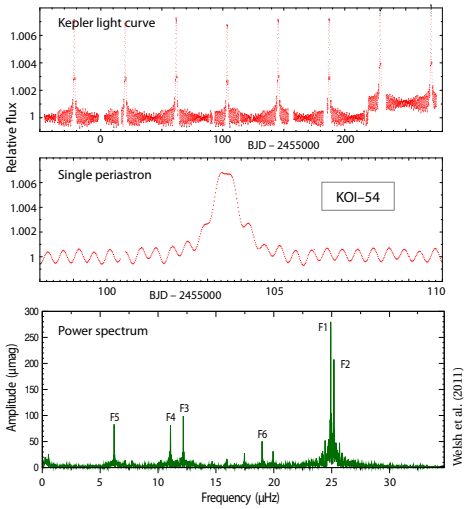

This, in turn, provides valuable constraints on the theories of dynamic tidal forces on stellar binaries (e.g. Willems, 2003; Burkart et al., 2012; Fuller & Lai, 2012; Cheng et al., 2020; Guo et al., 2020).

A key signature of tidally excited oscillations is their occurrence at integer multiples of the orbit frequency (Fuller, 2017), the largest corresponding to resonances between harmonics of the orbit frequency and the star's normal modes. For KOI–54, two dominant oscillations, responsible for the beating pattern, are at the 90th and 91st harmonic of the orbit frequency (Welsh et al., 2011).

The response comprises two components (Fuller, 2017): the equilibrium tide (the steady-state hydrostatic deformation due to the companion in the absence of orbital motion), and the dynamical tide (the oscillation due to the time-varying nature of the tidal forcing). The former contributes to the 'heartbeat' signature near periastron, while the dynamical tide results in tidally excited oscillations visible at all orbital phases.

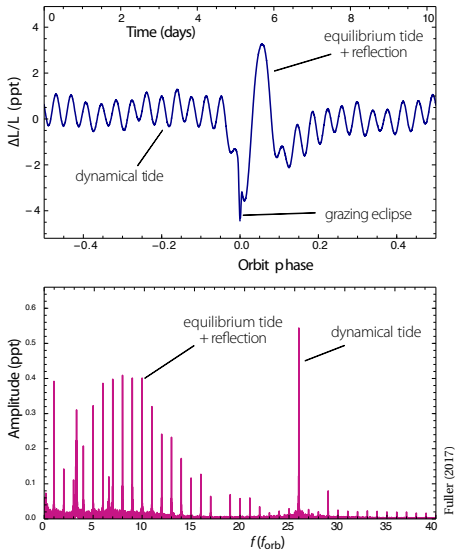

I HAVE MENTIONED that typical oscillation amplitudes of heartbeat stars are of order 1–2 mmag. In this context, particularly noteworthy is the system with the 'loudest' heartbeat: the 13 mag MACHO 80.7443.1718 in the Large Magellanic Cloud. This shows peak-to-peak variability of 40% near periastron (Jayasinghe et al., 2021). Its high-mass components, a $35M_\odot$ supergiant and a $16M_\odot$ O9.5 secondary, are in a 32.8 d, $e = 0.51$ orbit, and the system shows tidally excited oscillations at the 25th and 41st orbital harmonics.

Another peculiarity is the 'single-sided pulsator' HD 74423, discovered in the TESS data (Handler et al., 2020). It is inferred to have a 'teardrop' shape, with the star pulsating on only one side. More formally, it is interpreted as an obliquely pulsating distorted dipole, with a pulsation axis aligned with the tidal axis.

THE FIRST study of heartbeat stars that makes substantive use of Gaia data is for the 180 TESS systems identified by Solanki et al. (2025). Their fits to the phase curves, using `eBEER`, revealed that there is a potential degeneracy in constraining the stellar masses, radii, and temperatures using photometry alone. These were improved using the Gaia magnitudes and distances to estimate the absolute magnitudes, and improved (blackbody) estimates of $T_{\rm eff}$ and $R_\star$. Gaia strongly constrains upper limits on the masses, radii, and temperatures, and yields masses in good agreement with main-sequence predictions based on the Gaia temperatures.

They also found good agreement between their estimates of eccentricity, e, and argument of periastron, ω, compared with those derived on the basis of supplementary radial velocity data (Shporer et al., 2016).

Finally, by examining the Gaia 'renormalised unit weight error' (RUWE, where large values might suggest the presence of a tertiary), they confirmed that the orbital precession measured for a number of systems (which reaches 9°/yr in the case of TIC 451708707) is indeed most likely driven by tides and not, for example, by Kozai–Lidov oscillations from a tertiary companion.

STUDIES OF THE rich complexities of heartbeat stars is still in its infancy. Searches to date suggest that many more systems will be discovered even in the TESS data alone (Solanki et al., 2025). And the use of the Gaia data to assist determination of improved orbits and stellar properties will surely be picked up in future studies.

Given their high eccentricities, short-period heartbeat systems represent a particular subset of all close binaries. The formation of close binaries with orbital periods $P \lesssim 10$ d ($a \lesssim 0.1$ au) is a subject of ongoing study (e.g. Moe & Kratter, 2018; Meyer et al., 2018; Hwang & Zakamska, 2020). Whether heartbeat binaries originate from the same formation channels as other circularised short-period binaries is, today, still an open question.

227. Essays, podcasts and NotebookLM

I LISTEN TO quite a few podcasts. And given more time, knowledge, and certain skills that I almost certainly don't have, I have considered turning my own essays on Gaia science into audio/podcast form. The goal would be to make them more accessible, and a little less formal. And I have experimented on a couple of occasions: reading them aloud, or doing so after re-writing them in a different style. My attempts were rather disappointing!

NOTHING PREPARED me for the remarkable results of converting the pdf documents to audio format using AI. Specifically, I have converted the essays into a discussion-type dialogue between two avatars.

I will explain below what I have done, and the tools that I used, but let me first urge anyone curious to listen to one, perhaps taking a look at the corresponding pdf source first. So far, I have put essays 1–51 on a dedicated YouTube channel @GaiaEssays. Here are a few representative examples, linked directly:

- Essay 005: An Input Catalogue, or … (16:22)
- Essay 013: The distance to the Pleiades (12:04)
- Essay 024: Occultations of Europa and Triton (14:02)
- Essay 033: Nearby stars (19:42)
- Essay 035: Stellar flybys (16:03)
- Essay 037: Ultra-wide binaries (19:07)
- Essay 047: Iterative solution: implementation (15:28)
- Essay 050: The DIVA project (13:38)

THE SPEECH is rather fast, and the accent is American, so the resulting audio may not be so easy for non-native English speakers to follow. For the prototype software that I used, Google NotebookLM, it is not possible to change the delivery speed, the voices, or the accents. One of the reasons for using YouTube as host medium is that the listener can request (Google-generated) subtitles, and a slower playback speed (e.g. at 75%).[1]

LET ME SAY a little about the principles of AI underlying the creation of these audio files before being more specific on NotebookLM, and then commenting on the resulting accuracy and fidelity in my trials.

First, some background. The generative AI chatbot ChatGPT burst onto the scene at the end of 2022. Developed by OpenAI, it is a chatbot based on 'large language models' (LLM), such as GPT-4o. Considered to represent a significant breakthrough in the field of artificial intelligence, ChatGPT is a *'pre-trained AI model designed to engage in natural language conversations, utilising sophisticated techniques from Natural Language Processing, Supervised Learning, and Reinforcement Learning to comprehend and generate text comparable to human-generated text'* (Roumeliotis & Tselikas, 2023).

In turn, Large Language Models are a type of machine-learning designed for natural language processing tasks such as language generation. These models acquire predictive power regarding grammar, syntax, semantics, and ontologies (definitions and relations) inherent in human language.

An accessible introduction to LLMs, and ChatGPT (GPT refers to 'generative pre-trained transformer'), is given in this YouTube video by Stephen Wolfram

Basically, LLMs model how text is generated. They extend text in a statistically meaningful way, essentially one word (or 'token') at a time. They are based on neural nets, and with their many parameters trained with self-supervised learning on a vast amount of text; Wolfram refers to 175 billion *training* parameters for ChatGPT.

In this 2023 video, he also refers to ChatGPT as making use of the results of `CommonCrawl`, which *'maintains a free, open repository of web crawl data that can be used by anyone'*. This www repository comprises the billions of web pages and millions of books and other documents that have been indexed.[2]

[1] Anyone wanting to take these concepts further could change the voices (even using one's own voice!) using other AI software which first transcribes the audio file into a (voice-labelled) text stream (e.g. `Descript`), then re-records the text using a library of available avatar voices (e.g. `ElevenLabs`).

[2] The 'indexed web' refers to the portion of the internet that search engines like Google have discovered, crawled, and stored in their databases, making it searchable. The number of such pages is updated daily at www.worldwidewebsize.com, and was estimated at around 50 billion at the start of 2025.

THE IMPACT of ChatGPT led to the development of several other LLMs, including Gemini developed by Google DeepMind (released in May 2023, and as Gemini 2.5 Pro Experimental in March 2025), and the Chinese DeepSeek (in early 2025). In contrast to previous LLMs, Gemini is 'multimodal', viz. not trained on text alone, but making use of multiple date types simultaneously, including text, images, audio, video, and computer code.

THIS BRINGS ME to Google's NotebookLM (where the LM refers to 'language model'). It was launched in 2023, with its 'audio overview' feature of interest here added in September 2024 (using Gemini 2.0). Google describes it as *'a virtual research assistant that can summarise facts, explain complex ideas, and brainstorm new connections–all based on the sources you select'*.

To create the audio version, I go to Google NotebookLM, upload an essay in its original pdf form, then in the right-hand panel, under 'Audio Interview/Deep Dive Conversation', click on 'Generate'. The two-host format conversation is generated within a couple of minutes.

Reaction to these products is generally along the lines of 'amazing', 'unnerving', and 'scary'. Even Stephen Wolfram, in the video I referred to above, described the results of these Large Language Models as being *'remarkable that it works as well as it does'*.

The fact that the output is generated from my self-contained essays is particularly relevant when aiming to create a factually reliable audio version. Indeed, I have found the results to be essentially 100% accurate, and remarkably well constructed. They include 'back-and-forth' banter, and sufficient informalities of the spoken language (interjections, hesitations, etc.) to be almost indistinguishable from human speech. They do not contain what AI/LLM jargon refers to as 'hallucinations'.

CURRENTLY, NotebookLM provides just two voices: one male, one female (named Jaimie and Jamie by Google). So until a wider choice becomes available, there will probably be a lot of similar-sounding audios appearing on YouTube, Spotify, and beyond.[3]

To be super-critical, some spoken mannerisms (including a liberal sprinkling of surprised reactions) can be a little repetitive. Also, the voices alternate between one being the expert and the other the interrogator. And the generator seems to have been program-loaded with a fair degree of 'wow'- and 'amazing'-type sentiment, which nevertheless works quite well in this context.

[3] For anyone wanting to experiment further (and in addition to the voice options that I mentioned in footnote 1), there are even the prospects of using the resulting audio file to create a *video* podcast, with self-chosen avatars. Here, generative AI web apps like Hedra allow for uploading audio and imagery, then mixing them to create a *video* that animates the image with the audio.

I AM HUGELY IMPRESSED with the audio files generated by NotebookLM from the essays that I've processed so far. They are comprehensive, accurate, didactic, and engaging, and they seem to fill in bits of background information to give the whole thing meaning. They even pick out key information from a table or figure.

If you are one of the Gaia 'insiders', and already know something of the history of astrometry (essay 3), the objects that are so important as Galactic tracers (essay 6), about on-board detection (essay 7), or the Pleiades distance controversy (essay 13), do listen – and prepare to be astonished! They far exceed anything that I could contemplate doing myself.

Multiple source documents can be loaded and processed. In the case where I have written something on one topic, then provided an update a year or two later, NotebookLM can create a useful merging of the two, taking into account some repeated preamble. I have tried this on my two essays on OB associations, #18 and #223, but I will probably not use this sort of merging.

THERE ARE OTHER FEATURES of NotebookLM, perhaps slightly less relevant in this context, but which seem quite powerful as general tools when assessing other complex source material. The first is the immediate creation of a short summary of the source. Here is the summary created from essay #5 (on source selection), retaining NotebookLM's use of capitalisation:

> *The provided text contrasts the approaches of the Hipparcos and Gaia space missions for observing stars.* **Hipparcos** *required a meticulously prepared input catalogue of around 100 000 pre-selected stars due to technological limitations that allowed only one star to be observed at a time.* **Constructing this catalogue** *in the 1980s was a complex, international effort involving significant coordination and debate over which stars were most important to observe.* **Gaia**, *on the other hand, observes every object brighter than a specific magnitude as it scans the sky,* **eliminating the need for a pre-defined observing program** *and enabling the detection of transient events and a much larger number of stars.* **This shift** *in methodology was driven by technological advances and the lessons learned from the challenges faced during the Hipparcos mission.*

Other options in NotebookLM include creating FAQ sheets, briefing notes, and timelines from the material provided (all these are accessible from below the Audio Overview panel). For example, the 'timeline' option generates a chronological listing of the cited references, with their main results, and a list of the authors referenced.

In the central panel, below the chat summary, is another button labelled 'Mind Map'. This results in an interactive visual representation of the source content, with nodes that can be further expanded where relevant.

I PLAN to convert the rest of my essays, more than 200, to this audio discussion format, with the goal of publicising the achievements of Gaia more widely. I would appreciate wider feedback, via the YouTube channel.

228. Cepheid variables: an update

I DESCRIBED Gaia's early contributions to the study of Cepheid variables in essay 43, where I gave a broad introduction, and essay 44, where I focussed on their part in determining the Hubble constant. These were written at the end of 2021, before Gaia Data Release 3. Before bringing the topic up-to-date, let me recall the state of knowledge at that time, about three years ago.

Cepheids are bright pulsationally unstable stars, located in a narrow region of the Hertzsprung–Russell diagram, with typical periods of 1–30 days, but extending towards 100 days. There are two sub-classes. Classical Cepheids (or δ Cephei stars) are high-mass core He-burning supergiants, young Population I objects found in the Galactic plane, notably in spiral arms and in open clusters. Type II Cepheids are low-mass metal-poor Population II objects found at high Galactic latitudes, in the Galactic bulge, and in globular clusters, and sub-divided by period into BL Her, W Vir, and RV Tau-type variables.

THEIR IMPORTANCE as distance indicators is due to their strong period–luminosity correlation, discovered empirically by Henrietta Leavitt (1908), and subsequently explained theoretically. A historical review is given by Fernie (1969). The relationship nevertheless shows a significant scatter about the mean line, even when corrected for reddening, due to the finite (temperature) width of the instability strip. If a colour-term is introduced, the scatter is significantly reduced.

While the Cepheid period–luminosity relation has traditionally provided the most accurate method to derive distances to nearby galaxies, various complications are encountered in practice. A key goal of Cepheid studies is to establish the slope and zero-point of the period–luminosity relation, such that an observed period yields the object's luminosity, and hence its distance.

An important and related question is whether the period–colour and period–luminosity relations for classical Cepheids in the Large and Small Magellanic Clouds have the same slopes and zero-points as the Galactic Cepheids; differences would greatly complicate their use for the extragalactic distance scale.

AS WELL AS their use as distance indicators, the fact that Cepheids can be seen to very large distances, and the fact that they reflect the young population of the Galaxy, means that they also provide an important tracer of spiral arms. For similar reasons, their proper motions also provide a powerful measure of Galactic rotation. Important information is also encoded in their vertical distribution above and below the Galactic plane, and its age dependence. In a simplified picture, Cepheids with very young ages are found preferentially close to the Galactic plane, their assumed birth sites.

THE GAIA RESULTS, pre-DR3, that I outlined in essay 43, already made major contributions. For Gaia DR2 (using the first 22 months of mission data), a 'Specific Object Study' pipeline was used to validate and characterise Cepheids and RR Lyrae stars, originally using the period–amplitude and period–luminosity relations in the G band, and subsequently extended to $G_{\rm BP}$ and $G_{\rm RP}$ (Clementini et al., 2019; Rimoldini et al., 2019).

Accordingly, Gaia DR2 provided results, with mean magnitudes and pulsation characteristics, for 9575 Cepheids, of which 3767 are in the LMC, 3692 in the SMC, and 2116 are elsewhere. The majority of those in the Magellanic Clouds were already known from OGLE, although Gaia DR2 identified 118 new objects. The all-sky sample includes Cepheids in 87 globular clusters and 14 dwarf galaxies, of which 350 were new discoveries. Other analyses of the DR2 Cepheid selection were made by Ripepi et al. (2019), and Molnár et al. (2018).

Kervella et al. (2019) combined the Hipparcos and Gaia DR2 positions to determine the mean proper motion of a sample of classical Cepheids, searching for proper motion anomalies caused by close-in orbiting companions. They concluded that their binary fraction is likely to be above 80%. Other pre-DR3 studies were used to characterise Galaxy rotation (Mróz et al., 2019; Kawata et al., 2019; Ablimit et al., 2020), the component of their velocities perpendicular to the Galactic plane (Skowron et al., 2019b), and as probes of our Galaxy's structure more generally (Skowron et al., 2019a).

CONCERNING THEIR USE in determining the Hubble constant (essay 44), the latest pre-DR3 studies by Riess et al. (2021) used 75 Milky Way Cepheids with HST photometry and the greatly improved Gaia EDR3 parallaxes. Applied to the calibration of Type Ia supernovae, it gave $H_0 = 73.0 \pm 1.4\,\mathrm{km\,s^{-1}\,Mpc^{-1}}$. Combined with the best complementary sources of Cepheid calibration, they found $H_0 = 73.2 \pm 1.3\,\mathrm{km\,s^{-1}\,Mpc^{-1}}$, reaching 1.8% precision, but still a 4.2σ difference with the estimate from the Planck microwave background observations.

WITH GAIA DR3, came new radial velocities, and a wealth of astrophysical data derived from Gaia's BP/RP photometry and RVS spectroscopy. These allowed further unprecedented identification of variability across the HR diagram more generally (Gaia Collaboration et al., 2023d; Maíz Apellániz et al., 2023).

Dedicated processing of the Cepheids, again using the 'Specific Object Study' Cepheid/RR Lyrae pipeline, is detailed by Ripepi et al. (2023). It resulted in 15 006 Cepheids of all types: 4663 in the LMC, 4616 in the SMC, 321 in M31, 185 in M33, with the other 5221 objects elsewhere over the sky. The sample includes Cepheids in the Galactic field, in open clusters, and in a number of small satellite galaxies. Among them, 327 objects were previously known as variable stars but with a different classification, while 474 were new Gaia discoveries.

Studies of the period–luminosity relation continue (e.g. Trentin et al., 2024; Bras et al., 2024; Das et al., 2024; Musella et al., 2024). I will not attempt a synthesis here!

AN IMPORTANT FOCUS of these more recent DR3-based Cepheid studies has been to better establish their membership of open clusters and associations (and to identify new open clusters associated with known or newly discovered Cepheids), to aid in distance estimation (e.g. Majaess & Turner, 2024; Majaess et al., 2024). Amongst these studies, Hao et al. (2022b) associated 50 classical Cepheids with 45 open clusters, while Wang et al. (2024a) found 43 Cepheid–cluster memberships.

The high-quality sample of Cruz Reyes & Anderson (2023) identified 34 Cepheids in 28 open clusters, of which 27 are pulsating in the fundamental mode, and 7 in overtones. They found three new cluster Cepheids (V0378 Cen, ST Tau, and GH Lup), and corrected the host cluster for three others. They found the fraction of Cepheids occurring in open clusters within 2 kpc to be about 9%. Cluster parallaxes could be determined to around 7 micro-arcsec in the range $G = 12.5 - 17$ mag.

Their combined cluster and field Cepheids yield a calibration of the period–luminosity relation for several photometric passbands, providing excellent (0.3σ) agreement with the latest Hubble Space Telescope (SHOES) distance ladder (Riess et al., 2022), confirming the continuing early/late Universe 'Hubble tension'.

THE GAIA DR3 CEPHEIDS have been applied to several important studies of Galactic structure. As part of a much bigger mapping of the Galactic disk, Gaia Collaboration et al. (2023e) used 2800 classical Cepheids younger than 200 Myr to show that its spiral features extend outwards as far as 10 kpc from the Sun.

High-resolution ground-based spectroscopy by da Silva et al. (2023) gave metal abundances for 70 of the Gaia Cepheids, covering a wide range of Galactocentric distances, pulsation modes, and pulsation periods. This allowed them to trace the elemental O, S, and Fe abundance gradients across the disk. They presented detailed conclusions about their radial gradients, which are in turn used as inputs to models of Galactic kinematics and chemical enrichment history of the thin disk.

A detailed programme of ground-based all-sky radial velocity observations (from CORALIE and HERMES, between 2010–22), comprising 18 225 measurements of 258 classical Cepheids, is providing detailed insight into their pulsation properties, spectroscopic variability, and offsets with respected to Gaia's own RVS radial velocity estimates (Anderson et al., 2024).

Bobylev (2023) used 200 Gaia Cepheids to estimate the Sun's distance from the Galactic centre, $R_0 = 8.24 \pm 0.20$ kpc, and the rotation velocity at the solar circle, $V_0 = 268 \pm 8\,\mathrm{km\,s^{-1}}$. Further details of the rotation curve, based on 1705 Cepheids amongst 700 000 young disk stars out to 19 kpc, were given by Beordo et al. (2024).

FOR THE LARGE AND SMALL Magellanic Clouds, the improved Gaia Cepheid samples have been used to verify neural network classifiers of SMC membership (Jiménez-Arranz et al., 2023), to investigate the so-called 'flux-weighted gravity' versus luminosity relation (Groenewegen & Lub, 2023), and as structural diagnostics of the LMC (Bhuyan et al., 2024).

THERE ARE various outstanding questions about the detailed physics of Cepheid variables. Amongst these, ultralow amplitude (ULA) Cepheids are a poorly understood class, near the edges of the classical instability strip. For six CoroT candidates in the Galactic plane, Tarczay-Nehéz et al. (2023) used Gaia distances and magnitudes to rule out their pulsating nature, instead attributing their variability to rotation.

An interesting case of Gaia's mis-classification is the ultra-long period (ULP) Cepheid OGLE–GD–CEP–1884, classified as a Cepheid from 10 years of OGLE monitoring (Soszyński et al., 2024), but as a long-period variable in Gaia DR3. With a pulsation period of 78.14 days, nearly 10 d longer than the previous record holder, S Vulpeculae, it is perhaps the most luminous, youngest, and most massive Cepheid known in our Galaxy. Possible implications for understanding the Hubble tension are detailed by Musella et al. (2024).

229. RR Lyrae variables: an update

I DESCRIBED Gaia's early contributions to the study of RR Lyrae variables in essay 45, where I included an introduction to their nature and importance. Essay 43 was written at the end of 2021, before Data Release 3. Before bringing the topic up-to-date, let me recall the state of knowledge at that time, about three years ago.

GIVEN THEIR long lifetimes, stars of approximately solar mass are still present in old Population II systems, including globular clusters. After ascending the giant branch, terminating in the helium flash, they evolve rapidly onto the 'zero-age horizontal branch' with masses around $0.6 - 0.8\,M_\odot$, where they basically comprise a static He-burning core and a H-burning shell.

RR Lyrae are a subset of the horizontal branch giants, occurring where the horizontal branch intersects the instability strip (e.g. Catelan, 2009). They have pulsation periods around 1 day or less. Like Cepheids, although less luminous, their distinctive light curves allows detection to large distances, as far as the Galactic centre in the low-absorption Baade Windows, and in crowded fields.

The RRab subgroup, most relevant to the distance scale, are metal-poor spheroidal component stars, with asymmetric light curves, longer periods (above 0.4 day), larger amplitudes (around 0.5–1.5 mag), and pulsating in the fundamental mode. The less numerous RRc type are old disk component stars, with more symmetric almost sinusoidal light curves, shorter periods (below 0.4 day), smaller variability amplitudes, and pulsating in the first overtone. There are also double-mode pulsators, denoted RRd, which pulsate simultaneously in the fundamental mode and in the first overtone. I say more on the origin of this nomenclature in essay 230.

An underlying period–luminosity relation has long given RR Lyrae stars a role as standard candles for relatively nearby targets, especially within the Milky Way and Local Group. Although more common than Cepheids, there are greater difficulties in accounting for the effects of metallicity, faintness, and blending. As for the Cepheids, they also provide tests of evolutionary and pulsation models, and are important kinematic tracers.

THEIR TYPICALLY large distances means that trigonometric parallaxes have largely been unavailable in the past, and various other less-direct methods have been used for luminosity calibration. Pre-Gaia, several thousand Galactic RR Lyrae stars were known. But because of their magnitudes, only 179 were observed by Hipparcos. And it eventually gave useful parallaxes for only a few, with only the class's prototype, RR Lyrae itself at $\pi = 4.38 \pm 0.59$ milli-arcsec, being reasonably accurate.

THE HIGH-ACCURACY parallaxes from Gaia, combined with its multi-colour multi-epoch precision photometry, makes the mission extremely powerful for identifying and characterising variability across the entire HR diagram. The first Gaia data release, DR1, included 2595 RR Lyrae stars in the Large Magellanic Cloud region, which was observed at high cadence during the first 28 days in the 'ecliptic poles scanning configuration' (Clementini et al., 2016).

For Gaia DR2, covering the first 22 months of mission data, a 'Specific Object Study' pipeline was used to validate and characterise both Cepheids and RR Lyrae stars, originally using the period–amplitude and period–luminosity relations only in the G band, and subsequently extended to G_{BP} and G_{RP} (Clementini et al., 2019; Rimoldini et al., 2019). Gaia DR2 accordingly provided astrometric and photometric results, including mean magnitudes and pulsation characteristics, for 140 784 RR Lyrae stars as faint as $G = 20.7$ mag, of which some 50 000 were new discoveries.

This huge sample includes objects in the Milky Way disk, bulge, and halo; in the Large and Small Magellanic Clouds; 1569 distributed over 87 globular clusters; and 417 distributed over 12 dwarf spheroidal galaxies (including seven ultra-faint dwarf galaxies). The largest numbers are in M3 (159), NGC 3201 (83), Sculptor (176) and Draco (176).

The accurate multi-epoch photometry resulted in 121 234 objects whose light curves could be modelled with at least two harmonics, and 67 681 modelled with at least three harmonics.

For the 83 097 stars with both G_{BP} and G_{RP} photometry, the colour–magnitude diagram shows the different regions occupied by the RRab, RRc, and RRd classes, along with clumps associated with the Large and Small Magellanic Clouds, as well as the Draco and Sculptor dwarf spheroidals (Clementini et al., 2019, Figure 15).

As detailed in essay 45, the DR2 sample was used for improved period–luminosity–metallicity relations (e.g. Neeley et al., 2017; Neeley et al., 2019; Muraveva et al., 2018), and to probe the triaxial structure, kinematics, and accretion history of the Galaxy halo (e.g. Utkin et al., 2018; Iorio et al., 2018; Iorio & Belokurov, 2019).

RR Lyrae stars found well beyond a system's tidal radius provide evidence for tidal disruption, both for Galactic globular clusters (Kundu et al., 2019), and ultra-faint dwarf satellite galaxies (Vivas et al., 2020a). Some 6000–11 000 have been associated with the Sagittarius tidal stream (Ramos et al., 2020), others with the Gaia–Enceladus stream (Prudil et al., 2020), and some 15 000 with the Milky Way's central bulge (Du et al., 2020).

Gaia DR3 brought a wealth of new astrometric and photometric information. As for the Cepheids (essay 228), specific processing of the RR Lyrae again used the (updated) 'Specific Object Study' Cepheid/RR Lyrae pipeline (Clementini et al., 2023). This included analysis of the Gaia three-colour (G, BP, RP) time-series photometry, along with the epoch radial velocities (available for 1096). From 271 779 initial candidates, a high-quality sample of 270 905 RR Lyrae stars was constructed (of which 70 611 are new discoveries), comprising 174 947 fundamental-mode (RRab), 93 952 first-overtone (RRc), and 2006 double-mode (RRd) pulsators.

The sample includes RR Lyrae in 95 globular clusters and 25 Milky Way companions (the Magellanic Clouds, seven dwarf spheroidal galaxies, and 16 ultra-faint dwarf satellites). The catalogue includes an estimate of the interstellar absorption for 142 660 fundamental-mode pulsators (based on the G-band amplitude, the $G-G_{RP}$ colour, and the pulsation period). Metallicities, derived from the Fourier parameters of the light curves, are included for 133 559 objects. Further analyses include independent metallicity estimates (Jurcsik & Hajdu, 2023), leading to individual metallicities and distances for 134 000, as well as mean metallicities and distances to the LMC/SMC, and to 38 Milky Way globular clusters (Muraveva et al., 2025).

Further studies of the period–luminosity–metallicity relations have followed (Bhardwaj et al., 2023; Mullen et al., 2023; Zgirski et al., 2023), which I will not attempt to synthesise. The Gaia DR3 samples have also been used for new calibrations of the Baade–Wesselink (or parallax-of-pulsation) technique, based on a comparison of the variation of the star's linear radius and its angular diameter (Bras et al., 2024; Zgirski et al., 2024).

Application of the enlarged DR3 sample to studies of Galactic structure have also continued. These include determination of the distance and dynamics of the bulge region (Prudil et al., 2024a; Prudil et al., 2024b; Kunder et al., 2024; Prudil et al., 2025), and the structure and rotation of the inner and outer halo (Culpan et al., 2024; Cabrera Garcia et al., 2024; Tkachenko et al., 2024). The possible accretion origin for some of them provides support to the idea that the accretion of subhaloes largely contributes to the outer halo stellar populations (Medina et al., 2023).

The DR3 RR Lyrae sample also provides an important probe of the recently-identified (and various unidentified) Galactic phase-space sub-structures (Sun et al., 2025). From 46 575 of the halo stars (and using a Gaussian prior for the radial velocities), their friends-of-friends algorithm successfully identifies groups moving along similar orbits, amongst which are the Sagittarius stream, the Hercules–Aquila Cloud (HAC), the Virgo Overdensity (VOD), the Gaia Enceladus–Sausage (GES), various other halo streams (Orphan–Chenab, Cetus–Palca, Helmi, Sequoia, and Wukong), as well as the LMC leading arm, and another 18 unknown groups.

An independent catalogue of 2824 RR Lyrae stars in 115 Galactic globular clusters (including 1594 fundamental-mode, 824 first-overtone, and 28 double-mode pulsators) has been given by Cruz Reyes et al. (2024). They found that 77% of the known RR Lyrae stars in globular clusters are included in the Gaia DR3 Specific Object Study, with 82% being correctly classified. The majority of the missing sources are located in the crowded cluster centres.

Although they found that 80% of RRab, 84% of RRc, and 100% of the RRd pulsators are located within theoretical instability strip boundaries predicted using MESA models (with metallicity Z = 0.0003, mass $M = 0.7 M_{\odot}$, and helium Y = 0.290), they also found that 25% of cluster member stars located within the empirical instability strip are not RR Lyrae stars, and appear to be non-variable. They concluded that a *higher* He content, Y = 0.357, is required to fully match the location of the RRc pulsators, but that a *lower* content, Y = 0.220, is needed to match the location of the RRab stars.

Cruz Reyes et al. (2024) also drew attention to the fact that their catalogue does not exhibit the 'Oosterhoff dichotomy', viz. the division of Galactic globular clusters into two groups based on their average RRab periods. This is a long-standing problem in Galactic astrophysics which has been explicitly advanced by Gaia, and which I will look at further in essay 230.

Other studies have used the DR3 RR Lyrae sample to focus on specific globular clusters, including NGC 7006 (Arellano Ferro et al., 2023b), Palomar 2 (Arellano Ferro et al., 2023a), and NGC 1851 (Arellano Ferro et al., 2024).

230. The Oosterhoff dichotomy

THE OOSTERHOFF dichotomy is a long-standing problem in the understanding of Galactic globular clusters. It refers to the observational fact that they divide into two distinct groups according to the average period of their RR Lyrae stars pulsating in the fundamental mode (RR ab), $<P_{ab}>$. There is a gap between the two mean periods, of about 0.55 days and 0.65 days, referred to as the Oosterhoff gap, which divides systems into the classes Oosterhoff I and II (Oo I and Oo II) respectively.

Oosterhoff (1939) offered no explanation, although he concluded that *'Globular clusters seem to hide many secrets, which probably may be at least partly uncovered when more accurate data about the variable stars will be obtained.'* More than a century later, this particular secret has at last been 'partly uncovered' by Gaia.

IT IS USEFUL to start this story a decade or two before Oosterhoff's work, with Solon Bailey of the Harvard College Observatory. His extensive studies of variable stars in globular clusters are at the origin of the nomenclature used to classify RR Lyrae variables (Bailey, 1902; Bailey et al., 1919). He divided these so-called 'cluster variables' into four classes (a–d), of which classes a and b are usually grouped together as RR Lyrae ab. These are the most common, comprising 90% of all RR Lyrae, pulsating in the fundamental mode, and displaying the characteristic steeply rising asymmetric light curve.

And, today, his widely-used period–amplitude diagrams are referred to as 'Bailey diagrams'. Two examples, from Smith et al. (2011), are shown over: the first illustrates the separation between the RR Lyrae ab and RR Lyrae c variables in M15 (this is *not* the Oosterhoff gap!). The second shows the Oosterhoff gap, evident in the plot of the mean period of RR ab stars versus [Fe/H] for Galactic globular clusters (two unusual clusters, NGC 6388 and NGC 6441, are labeled as Oo III).

Numerous studies since have tried to explain the Oosterhoff gap. While there is now a consensus that it is correlated with the cluster's metallicity, with the more metal-poor (Oo II) having larger mean periods (Castellani et al., 2003), an explanation remains elusive.

WITH REFERENCE to some recent overviews of its historical development (e.g., Fabrizio et al., 2021; Luongo et al., 2024), I will pick out just a few milestones.

In an early study, van Albada & Baker (1973) suggested that the dichotomy was related to the transition between pulsation modes: between the blue edge of the fundamental mode and the red edge of the first overtone mode, RR Lyrae stars can pulsate in both modes, sometimes simultaneously as double pulsators (and confirmed theoretically by Bono et al., 1997). In this case, the Oo I pulsators would extend to higher temperature, and hence with a shorter average pulsation period.

Sandage (1981) proposed that it stemmed from a higher luminosity of Oo II RR Lyrae ab stars at a fixed temperature (and assuming similar mass), resulting in longer pulsation periods. Since a significant He enrichment is needed to justify the assumed Oo II overluminosity, this explanation would imply an anticorrelation between metallicity and helium, since Oo II clusters are generally more metal-poor. Later evidence has argued against a strong dependence of the RR Lyrae luminosity on metal content (Castellani et al., 2003).

Pre-Gaia studies of the Oosterhoff dichotomy have also been focussed on specific populations, for example in the Large Magellanic Cloud (Bono et al., 1994), in the Boötes dwarf spheroidal galaxy (Siegel, 2006), in Andromeda (Contreras Ramos et al., 2013), in the Galaxy halo (Carney et al., 1991; Abbas, 2014), and most recently in the central bulge region using data from OGLE and Vista (Prudil et al., 2019a; Prudil et al., 2019b).

AROUND 20 YEARS AGO came prescient hints that the dichotomy may hold a key to understanding the formation history of the halo (Catelan, 2004). The argument runs as follows (Catelan, 2009): while the Galactic halo shows a sharp division between Oo I and Oo II types (with very few clusters with mean RR Lyrae ab pulsation periods in the range 0.58–0.62 days), the dwarf spheroidal satellite galaxies of the Milky Way, as well as their respective globular clusters, actually fall preferentially within the Oosterhoff gap (e.g. Siegel, 2006).

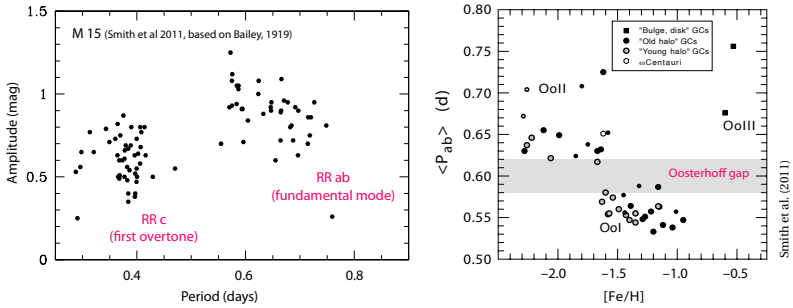

With growing evidence that the Galactic halo has been built up from the accretion of smaller protogalactic fragments, not unlike the present-day Milky Way dSph satellite galaxies, then the present-day halo should not, Catelan argued, display the Oosterhoff dichotomy. Therefore, he concluded, the Galactic halo cannot have been assembled by the accretion of dwarf galaxies resembling the present-day Milky Way satellites.

SUMMARISING THE status of the Oosterhoff dichotomy at the start of the Gaia era, Fabrizio et al. (2019) argued that further progress required accurate and homogeneous metal abundances across the full range of known RR Lyrae variables. Accordingly, they derived iron abundances for 2382 fundamental-mode pulsators from SDSS–SEGUE, and distances from Gaia DR2. Their resulting Bailey diagram shows a steady variation from the metal-poor, [Fe/H] = –3.0/–2.5, to the metal-rich, [Fe/H] = –0.5/0.0, regime. They argued that the smooth transition as a function of metallicity indicates that the Oosterhoff dichotomy among Galactic globular clusters is the consequence of the lack of intermediate metallicity clusters hosting RR Lyrae variables.

Further insights came from a study of 3653 RR Lyrae stars (2661 RRab, 992 RRc) by Zhang et al. (2023b), based on metallicities from SDSS and LAMOST, and full positions and space velocities from Gaia EDR3. From their locations in the Bailey diagram, they found that the Oo I RR Lyrae stars are more metal-rich, with radially dominated orbits and large eccentricities, while Oo II RRLs are more metal-poor, and have only mildly radially dominated orbits. They found that the Oosterhoff dichotomy of the Milky Way's halo is more apparent for the inner-halo region than for the outer parts.

Including the halos of the Milky Way's two largest satellites, the LMC/SMC, they found that the Oosterhoff dichotomy varies with Galactic location, and from galaxy to galaxy. They concluded that it results from a combination of stellar *and* Galactic evolution.

THE PICTURE was consolidated by Prudil & Arellano Ferro (2024), in work also based on Gaia EDR3. They found that the Oosterhoff gap, in the $< P_{ab} >$ versus [Fe/H] plane, is mostly populated by globular clusters associated with Milky Way dwarf galaxies, and those with only a small number of fundamental mode RR Lyrae pulsators. Indeed, their only globular clusters lying within the Oosterhoff gap are NGC 6402 (M14) associated with the Kraken/Heracles mergers (Kruijssen et al., 2020; Horta et al., 2021), and NGC 6715 (M54) associated with the Sagittarius merger.

From a catalogue of 2824 RR Lyrae stars in 115 Galactic globular clusters (including 1594 fundamental-mode, 824 first-overtone, and 28 double-mode pulsators), Cruz Reyes et al. (2024) also drew attention to the fact that their sample does not exhibit the Oosterhoff dichotomy.

CURRENT understanding is nicely brought together in the Gaia DR3 study by Luongo et al. (2024). They calculated orbits and integrals of motion for the Galactic globular clusters and field RR Lyrae stars previously attributed to halo streams. The likely origin of the field RR Lyrae (shown below) was matched to their globular cluster $E - L_z$ counterparts. The resulting Bailey diagrams for the inferred *in situ* stars show a wide and continuous range of metallicities, with no sign of the Oosterhoff dichotomy. The accreted halo RR Lyrae stars, in contrast, clearly show a much smaller metallicity dispersion, and a clear Oosterhoff gap.

Although they did not isolate the cause of the Oosterhoff dichotomy, they conclude that it was 'imported' into the Milky Way by these ancient mergers. It represents an important advance in our understanding of its origin. It is, I think, difficult to imagine this progress in the absence of Gaia's astrometry, and its deep insights into the phase-space structure of our Galaxy's halo.

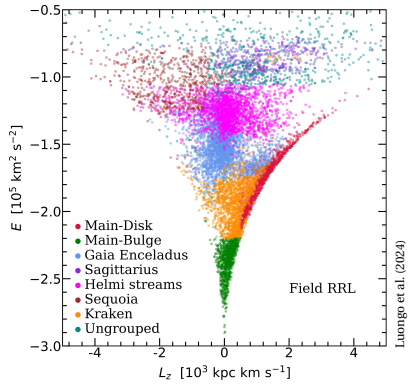

231. Dwarf spheroidals: an update

I DESCRIBED the early Gaia results on dwarf spheroidal galaxies, based on DR2, in essay 31 (Aug 2021), and the Sagittarius stream specifically in essay 198. Before outlining the new insights from EDR3/DR3, let me summarise what they are, and what we learned from DR2.

The 'classical' dwarf spheroidal galaxies, or dSph, are small, low-luminosity galaxies comprising an old stellar population with very little dust (the ultra-faint dwarfs are even fainter!). In contrast to dwarf *elliptical* galaxies, they are roughly spheroidal in shape. Some two dozen are known as companions to either the Milky Way or to the Andromeda Galaxy (M31), and they are named after the constellation in which they are found.

The first known, Sculptor and Fornax, were discovered by Harlow Shapley in 1938, who described them as *'unlike any known stellar organisation'*. But despite masses around $10^7 M_\odot$, further discoveries were challenged by their low luminosities and surface brightnesses. By the late 1990s, their rarity seemed in conflict with ΛCDM cosmology, which predicted that massive galaxies like the Milky Way should be surrounded by many dark-matter-dominated satellite halos.

CONFLICT eased with the discovery of a dozen faint dwarf spheroidals by SDSS around 2000, and a similar number by the Dark Energy Survey around 2015. The distinction between dwarf spheroidals and globular clusters is, incidentally, not always sharp: one discriminant may be the presence of a significant amount of dark matter in the former, and its absence in the latter.

All these dwarf galaxies are very distant, ranging from 26 kpc for Sagittarius, to around 250 kpc in the case of Leo I, well beyond the Magellanic Clouds. Their bulk proper motions are consequently very small, generally below 0.5 milli-arcsec per year. Some pre-Gaia determinations of these tiny motions were made using HST.

One main line of study is to use the Gaia data to reconstruct their orbits, structure, and internal dynamics. The goal is to characterise the gravitational forces of the galaxy that they are orbiting, either the Milky Way or M31, at larger distances than any other available dynamical tracer, and to probe their origin and past history.

THE MAIN INSIGHTS from Gaia DR2 came from an analysis by Gaia Collaboration et al. (2018b). They examined the motions of the nine 'classical' dwarf spheroidal galaxies (Fornax, Draco, Carina, Ursa Minor, Sextans, Leo I, Leo II, Sagittarius, Sculptor, and the 'ultra-faint dwarf' Boötes I), as well as 75 globular clusters. They identified a few hundred up to a few thousand members per dwarf system, and determined their distances with typical uncertainties of around 2–10 kpc. They noted suggestions of tidal streams in the case of Carina, and spatial asymmetries in the case of Fornax.

Most remarkable was the information on their derived orbits, which were reconstructed based on models of the Milky Way's mass distribution. They found that Draco and Ursa Minor have very similar orbits, orthogonal to that of Sagittarius. Most are on (slightly) prograde orbits, while Fornax is retrograde, qualitatively similar to what was found for globular clusters. But their eccentricities are very different: few have very eccentric orbits, with Carina even being somewhat circular. They concluded that there is only limited similarity between the orbits of globular clusters and dwarf spheroidals. And that their eccentricity distribution was inconsistent with recent cosmological simulations. Their orbits also contrast with those of the ultra-faint dwarf galaxies, for which Gaia-based proper-motions suggested largely eccentric and retrograde trajectories (e.g., Simon, 2018; Patel et al., 2020; Cerny et al., 2023a).

I gave more details on the planar distributions of the classical satellite galaxies of the Milky Way (the 'Vast Polar Structure') and of M31 (the 'Great Plane of Andromeda'), their appearance in cosmological simulations, and the 'plane of satellites' problem, in essay 118.

AT A BASIC LEVEL, Gaia DR3 is being used to filter out foreground objects in other studies, resulting in cleaner membership, and more accurate distances. This has been applied to HST studies of Sculptor (Tran et al., 2022) and Fornax (Oakes et al., 2022). Combining HST and Gaia data also gave significantly improved proper motions for the faintest Gaia sources, e.g. in the case of Fornax and Draco (McKinnon et al., 2024).

IMPROVED GAIA POSITIONS and proper motions have been used to derive better orbits and orbital histories of a number of these Local Group dwarf spheroidals. These have led to improved insights into their orbital alignments, infall trajectories, and perturbative effects.

Amongst these, Casetti-Dinescu et al. (2022) made a combined HST–Gaia analysis of 2300 Leo I stars, confirming that its orbital pole is well aligned with that of the Vast Polar Structure (defined by the majority of the Milky Way's brightest dSph satellites). Pace et al. (2022) used Gaia EDR3 to measure the bulk motion of 52 of the Milky Way's dwarf spheroidal galaxies. Of 46 with known line-of-sight velocities they identified six (Car II, Car III, Hor I, Hyi I, Phx II, and Ret II) as likely LMC satellites.

THE GAIA proper motions are also being used to probe their structure, internal kinematics, and bulk rotation. For Sagittarius, Ferguson & Strigari (2020) inferred a triaxial shape with axis ratios 1 : 0.76 : 0.43. From 120 000 members in its core, del Pino et al. (2021) identified a 2.5 kpc-long bar, tidal tails (the Sgr stream, essay 198), a main body strongly sheared by tidal forces, and an inner core, of dimension $500 \times 330 \times 300\,\mathrm{pc}^3$, rotating at $4.13 \pm 0.16\,\mathrm{km\,s^{-1}}$. Other models have been presented for Draco (Massari et al., 2020), Sextans (Tokiwa et al., 2023), and for Carina, Draco, Fornax, Sculptor, Sextans and Ursa Minor (Martínez-García et al., 2023). Significant bulk rotation has also been found in Carina, Fornax, and Sculptor (Martínez-García et al., 2021).

THE DERIVED orbits have remarkable consequences for understanding star formation and gas dissipation in these old stellar populations. The present assumption is that their gas-rich progenitors lost their gas during their infall into the Milky Way halo of order 10 Gyr ago. Star formation at the time is believed to have occurred as a result of ram pressure of their gas content, before its removal by the hot Galactic corona.

Observational verification requires accurate orbits and infall times, viz. when the galaxy first comes within the halo's growing virial radius (Yang et al., 2024b). From the orbits of eight of the classical dwarf spheroidals (Carina, Draco, Fornax, Leo I, Leo II, Sculptor, Sextans, and Ursa Minor), as well as eight ultra-faint dwarf galaxies, Miyoshi & Chiba (2020) showed that the satellite's infall time agrees with the epoch of maximum star-formation, specifically as derived from HST colour–magnitude diagrams (Weisz et al., 2014).

In contrast to their typical ages of around 8–10 Gyr, Yang et al. (2024b) reported a small population of young (~1 Gyr old) intermediate-mass ($1.8 - 3\,M_\odot$) stars in several of the Milky Way's dwarf spheroidals, including Sculptor, Ursa Minor and Sextans. They associate the birth of these young stars with the epoch when their gas-rich progenitors entered our Galaxy's halo and corona.

The detailed effects of tidal and ram-pressure stripping have been modelled in a number of systems: in Fornax (Borukhovetskaya et al., 2022; Yang et al., 2022; Di Cintio et al., 2024), in Leo I (Pacucci et al., 2023), in Draco (Grønnow et al., 2024), in Sculptor (Tolstoy et al., 2023), and in a number of others (Qi et al., 2022). Other modelling is leading to possible implications for their origin and dark matter content (Hammer et al., 2020; Pozo et al., 2022; Guerra et al., 2023; Andrade et al., 2024).

GLOBULAR CLUSTERS hold important clues about their history and tidal disruption (e.g. Rostami Shirazi et al., 2022). For Sagittarius, and in addition to its previously-known globular clusters (NGC 6715, Arp 2, Terzan 7, and Terzan 8 in the main body, and Pal 12, Whiting 1, NGC 2419, NGC 4147, and NGC 5634 in the extended tidal streams), Garro et al. (2021) used VISTA–VVV and Gaia EDR3 to identify 21 new clusters, 17 metal-rich and 4 metal-poor. With their own evolution controlled by the combined potential of both Sagittarius itself and the Milky Way, Kundu et al. (2022) used Gaia EDR3 to identify extra-tidal candidates, attributing their distribution to the dominant effect of Sagittarius itself. I said more on these globular clusters, and the relationship between Sagittarius and its nuclear star cluster, M54, in essay 198 on the Sagittarius stream.

The Fornax dwarf spheroidal has six associated globular clusters. The most recent, found in DECam imaging, and experiencing tidal destruction, is also seen as an overdensity in the Gaia data (Wang et al., 2019).

To identify the possible globular cluster progenitors, Boldrini & Bovy (2022) propagated the Gaia-based orbits of 170 Milky Way clusters, and its known satellite galaxies, backwards in time for 11 Gyr. None show clear association with any of the eight classical dwarf spheroidal galaxies, even though a large fraction of them are believed to have been accreted. They concluded that the globular clusters were either accreted as part of now-disrupted satellite galaxies, or that they may have had dark matter haloes in the past, affecting their orbits.

GAIA POSITIONS and space motions have assigned a number of high velocity and hypervelocity stars as originating from the Sagittarius dwarf. The first two were discovered with Gaia DR2, and originated 20–40 Myr ago (Montanari et al., 2019). The third, J1443+1453, at heliocentric distance $2.90^{+0.72}_{-0.48}$ kpc and space velocity $\sim 500\,\mathrm{km\,s^{-1}}$, was similarly found (from Gaia DR2) to intersect with its orbit $37.8^{+4.6}_{-6.0}$ Myr ago, close to its latest pericentric passage through the Milky Way (Huang et al., 2021a). With Gaia EDR3, a further 60 Galactic high-velocity stars, including two hypervelocity stars, were inferred to have been tidally stripped from it, also at pericentre (Li et al., 2022). These associations are further supported by their similar metallicities (Li et al., 2023d).

232. Delta Scuti stars

THE δ Sct class of variables are pulsating stars located at the intersection of the instability strip with the main sequence (shown schematically opposite), and excited mainly by the 'kappa opacity' mechanism. They are of spectral class A–F, masses $1.5-2.3\,M_{\odot}$ (depending on metallicity), luminosities $2-50\,L_{\odot}$, and they are moderate to rapid rotators. They are characterised by low-amplitude, short-period pulsations, primarily in p-modes in the range 20 min to 8 h, but usually also in g-modes (e.g. Breger, 2000b; Goupil et al., 2005; Gootkin et al., 2024). They mainly comprise Population I stars of the young Galactic disk, while Population II analogues in the halo and old disk are classified as SX Phe stars.

As detailed by Kurtz (2022, §2.1) who provides many more details on their classification and pulsation mechanisms, they actually display *'a rich variety of pulsation behaviour, ranging from rare singly periodic stars to stars with hundreds of frequencies spread across the 0–80 d^{-1} range, requiring g modes, r modes, p modes, mixed modes, rotationally split multiplets, nonlinear combination frequencies, and possibly more to understand'*.

They follow a period–luminosity relation in certain passbands (Cohen & Sarajedini, 2012), and have been used to estimate the distance to open clusters (Majaess et al., 2011), the Galactic centre (McNamara et al., 2000), and to the LMC (McNamara et al., 2000). But, perhaps most importantly, studies of their multi-periodic behaviour provide important tests of our understanding of stellar interiors and stellar evolution. Open questions include why they constitute only some 50–70% of stars in the instability strip (Balona & Dziembowski, 2011).

FOR THE PROTOTYPE, δ Sct, the (fundamental mode) 0.2 mag 4.65 hr periodicity was established by Campbell & Wright (1900). Sterne (1938) proposed a pulsation model, but also identified a second unexplained non-harmonic period. Nine periods were reported by Fitch (1976), and its considerable light-curve complexity was further illuminated by the 5-year asteroseismic analysis by Templeton et al. (1997), which identified six discrete non-beating pulsation modes. Recent studies include those of Daszyńska-Daszkiewicz et al. (2021).

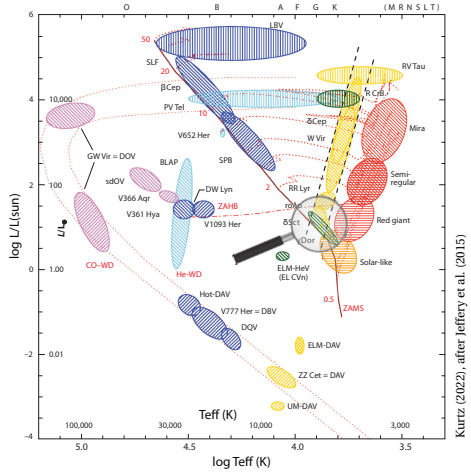

Other δ Sct stars show even greater complexity. As one example, Breger (2000a) reported 34 frequencies in the case of 4 CVn, with pulsations in low radial order and low degree. It is an example of variables showing strong amplitude variability on timescales of 10 years or more, with phase jumps suggesting the growth of new modes.

FROM JUST four known examples in 1956, Rodríguez et al. (2000) catalogued 636, and Chang et al. (2013) listed 1578. Many more have been found from microlensing and other all-sky surveys, starting in the 1990s.

Amongst these, Murphy et al. (2019) found 1988 δ Sct pulsators in the original 105 $\deg^2$ (2009–13) Kepler field. Jayasinghe et al. (2020) listed 8418 from the ASAS–SN survey. Pietrukowicz et al. (2020) reported 10 111 in the OGLE–IV Galactic bulge fields, and with a *'huge variety'* of light-curve shapes. Chen et al. (2020) listed 15 396 candidates from the Zwicky Transient Facility. And the OGLE and MACHO surveys have detected 2786 in the Large Magellanic Cloud (Poleski et al., 2010).

Many others are now being found from TESS and Gaia. Kepler's space-based observations have shown that numbers increase exponentially at low amplitudes, with 7% of their sample being below 100 ppm (Balona & Dziembowski, 2011).

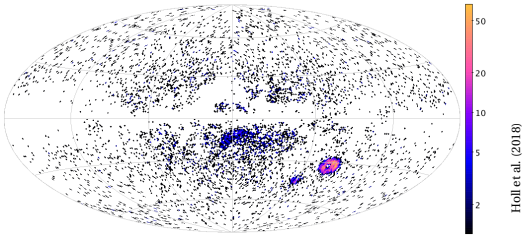

SIMPLY ADDING these previous numbers suggests that, pre-Gaia, some 40 000 δ Sct variables were known, of which around 3000 were in the LMC.

Within the DR2 variability analysis, and given that the δ Sct and SX Phe types cannot easily be distinguished without metallicity or other population-class indicator, Holl et al. (2018) assigned 8882 variables to a combination of the two. Their comparison with the Catalina catalogue of Drake et al. (2014) suggests completeness of 99%, with a contamination of 13%. They provide figures showing their sky distribution (Fig. 4, above), magnitude distribution (Fig. 5), and example light curves (Fig. 7).

With its extended 34-month temporal coverage, Gaia DR3 tabulates more than 10 million stars as variable (Eyer et al., 2023). As a result of period search and time-series modelling, they assigned 748 058 of these to a combination of δ Sct, γ Dor, and SX Phe variables. Of these (Rimoldini et al., 2023, Table 3), at least 12 000 (and probably many more) are likely to be δ Sct. As expected from the Kepler insights into their amplitude distribution, the sample is dominated by low-amplitude candidates (< 0.01 mag for 537 769 sources), which are therefore also expected to be significantly contaminated.

ONE OBJECTIVE of the new Gaia-enabled studies is to characterise the period–luminosity relation as a function of pulsation mode and metallicity, using the Gaia parallaxes and extinction corrections to determine absolute magnitudes.

Ziaali et al. (2019) examined 1500 stars from previous compilations including Kepler, based on DR2. Many fall on a period–luminosity sequence coinciding with the fundamental radial-mode pulsation. But others fall on a second ridge that is a factor two shorter in period. Seen more clearly in the TESS–DR3 sample of Barac et al. (2022, Fig. 2), and with several of them showing amplitude modulation on timescales of years, they suggest that this may signify a transfer of energy between modes, and hence a transient nature of the secondary ridge.

In a similar approach using 8400 δ Sct from ASAS–SN, Jayasinghe et al. (2020) found that the fundamental-mode pulsators have periods dependent on metallicity. They also identified a period-dependent Galactic scale height, and a median period increasing with Galactocentric radius, indicative of a radial metallicity gradient. From a larger sample of 15 000 TESS stars, Gootkin et al. (2024) found that the pulsator fraction within the instability strip peaks at 50–70%, of which 85% of the variables are probable δ Sct stars (the others being hybrid or γ Dor pulsators). They also identified a correlation between pulsator fraction and spectral line broadening as determined from the Gaia RVS instrument, confirming that rotation has a driving role the δ Sct pulsations.

Other details of the period–luminosity relation are revealing more complex dependencies on surface gravity and temperature, and confirming the power of combining TESS and Gaia for studies of pulsating stars (Poro et al., 2021; Read et al., 2024; Poro et al., 2024).

A RELATED GOAL of the Gaia δ Sct studies has been to accurately place them in the Hertzsprung–Russell diagram, and to characterise their complex variability as a function of location. A specific objective is to clarify the long-standing question of whether all stars in the instability strip pulsate or, alternatively, why many of the stars in the δ Sct instability strip do not.

The background to this interesting problem (Murphy et al., 2019) is that the δ Sct variables, of mass $1.5-2.3\,M_\odot$, occupy a region of the main sequence where the depth of the surface convection zone is a steep function of effective temperature, and consequently where time-dependent convection models are needed to accurately model the pulsations and compute instability strips (Dupret et al., 2004; Grigahcène et al., 2005).

From an original sample of 15 000 Kepler A and F stars, interpreted with the aid of Gaia DR2, Murphy et al. (2019) identified 1988 as genuine δ Sct variables (the others being mainly eclipsing binaries and γ Dor stars with harmonics or high-frequency modes). From this sample, they also found a peak pulsator fraction of 70% in the middle of the canonical instability strip, which they found to be underpopulated with pulsators at the red edge, and overpopulated beyond the blue edge.

This led them to define a new empirical luminosity-dependent instability strip, one that is systematically hotter than the theoretical boundaries currently in use. But inside even this revised instability strip, the pulsator fraction remains well below 100%, such that the 'problem', although alleviated, nonetheless persists.

SOME FURTHER PROGRESS was made with Gaia DR3. Murphy et al. (2024) isolated δ Sct pulsators within the Cep–Her complex, using light curves from TESS, and the colour–magnitude diagram from Gaia, to identify objects compatible with the zero-age main sequence. Here, their δ Sct pulsator fraction reached 100%, with a trend of higher pulsator fractions for younger stellar associations. They also found that rapid rotators are more likely to pulsate, specifically in low-order modes, but that they do so with less regular pulsation patterns.

233. Two more exoplanets: Gaia 4b & 5b

TODAY, NASA's Exoplanet Archive lists almost 6000 confirmed exoplanets. Amongst them are more than 600 transiting planets discovered with NASA's space mission TESS, on top of which are another 7000 TESS *candidates* awaiting confirmation.

I described astrometry's checkered historical contribution to exoplanet science in essay 78, with its series of claims and refutes dating back more than a century. Scientifically, astrometry holds the prospects of establishing the planet's orbital inclination to the line-of-sight, and hence its mass. But, because of the tiny angles involved, and numerous technical challenges, the astrometric detection of exoplanets remains very difficult.

Only five *astrometric* discoveries are in NASA's listing as of May 2025. DENIS–P J0823–49, discovered from ground-based measurements (with VLT–FORS2), is a $28 M_{\rm J}$ object orbiting an L dwarf of mass $0.07 M_{\odot}$ at a distance of 20 pc (Sahlmann et al., 2013). GJ 896 is a $2.3 M_{\rm J}$ planet orbiting a binary star system inferred from radio observations with VLBA (Curiel et al., 2022). HIP 66074 b is the first confirmed exoplanet detected by Gaia astrometry (Sozzetti et al., 2023, referred to there as Gaia–3 b). The latest confirmed candidates are Gaia–4 b and Gaia–5 b (Stefánsson et al., 2025), recent additions which I will say more about here.

I described the discovery of the first Gaia-named exoplanets (Gaia–1 b and Gaia–2 b from photometry, and HIP 66074 b from astrometry) in essay 78.[4] But this small number of Gaia discoveries today stands in contrast to the 20–50 000 astrometric detections that have been predicted from Gaia's full mission astrometry (Perryman et al., 2014). Let me recall why.

AS PART of the Gaia data processing, DPAC Coordination Unit 4 processes all non-single stars (Gaia Collaboration et al., 2023a). The latest Data Release 3 contains 800 000 solutions with either orbit elements or trend parameters (whether for astrometric, spectroscopic and eclipsing binaries, or some combination). Of these, 130 000 are full orbit solutions, while 300 000 show non-linear astrometric motion, i.e. indicative of partial orbit coverage (Holl et al., 2023). All will be substantially improved in future data releases as more data is included, and as the calibration models improve. Crucially, many of the non-linear solutions will progress to full orbit solutions as the temporal baseline improves.

Amongst sub-stellar companions, DR3 resulted in 1843 brown dwarf and 72 exoplanet *candidates* (Gaia Collaboration et al., 2023a). Of these, only 10 brown dwarfs and 9 exoplanets were previously known from radial velocity surveys, all with a reasonable agreement between their inferred orbital periods. Gaia Collaboration et al. (2023a) listed just two with *validated* orbits implying the presence of new planetary companions.[5]

Other candidates include NASA's astrometric listing DENIS–P J0823–49, and previous radial velocity discoveries including GJ 876, HD 114762, HD 162020, and HD 164604. Other candidates add to the rare class of giant planets orbiting white dwarfs, including WD 0141–675 which, at 9.8 pc, is one of the metal-enriched systems suggestive of the capture of planetary debris.

In independent tests, Winn (2022) found consistency between the Gaia orbits and precise Doppler measurements for BD–17 0063, HD 81040, and HD 132406. Of four inconsistencies, HD 111232 was attributed to additional planets not included in the astrometric model.

[4] The Exoplanet Archive lists five exoplanetary systems with an assigned 'Gaia' name: Gaia–1 b and Gaia–2 b, transiting systems identified from Gaia photometry (Panahi et al., 2022, essay 78); the microlensing system discovered from the Gaia science alerts pipeline, Gaia 22dkvL (Wu et al., 2024, essay 203); and Gaia–4 b and Gaia–5 b, these most recently confirmed Gaia astrometric candidates (Stefánsson et al., 2025). Although the name Gaia–3 b was assigned in the discovery paper (Sozzetti et al., 2023), the NASA Archive refers to it as HIP 66074 b.

[5] HIP 66074 with $P = 297 \pm 2.8$ d, $e = 0.46 \pm 0.17$, $a_0 = 0.21 \pm 0.03$ mas, and $M_{\rm p} = 7.3 \pm 1.1 M_{\rm J}$ (Sozzetti et al., 2023); and HIP 28193 with $P = 827 \pm 50$ d, $e = 0.07 \pm 0.10$, $a_0 = 0.25 \pm 0.02$ mas, and $M_{\rm p} = 5.3 \pm 0.6 M_{\rm J}$. Their sub-milli-arcsec semi-major axes are especially noteworthy, with their smallest candidate having $a_1 = 0.14 \pm 0.04$ milli-arcsec. I am not close enough to the work of CU4, nor the NASA Exoplanet Archive, to know why HIP 28193 is not listed in the NASA Archive.

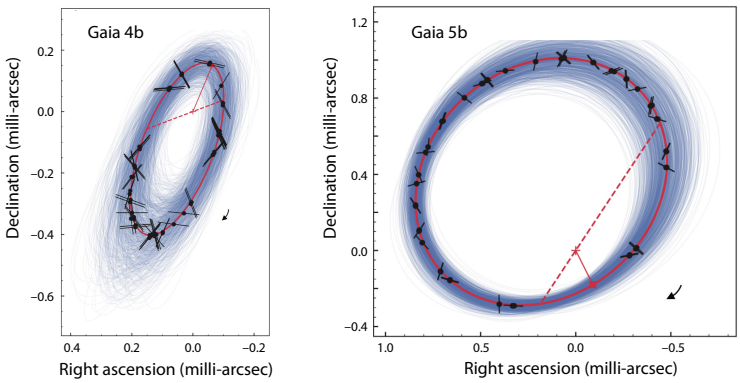

The Gaia astrometric exoplanet discoveries Gaia–4 b (left) and Gaia–5 b (right). The figures show the orbit of the photocentre, after subtraction of the parallax and proper motion. Black circles show the positions at each observation epoch, with their along-scan uncertainties. Blue curves show 1000 random draws of the Gaia orbit. Also shown are the system's barycentre (+), the position of periastron (red square), the line of nodes (dashed red line), and the direction of the motion along the orbit (arrow). From Stefánsson et al. (2025) Figures 9–10.

IN THE EARLY DAYS of exoplanet searches based on photometric transits, it became quickly evident that even a periodic transit-type signature cannot be taken as unambiguous evidence for a transiting planet without excluding many 'false-positive' signals that plague both ground and space searches. These include stellar binaries with grazing eclipses, background eclipsing binaries, eclipsing binaries in a hierarchical triple system, and eclipsing binaries with only secondary eclipses.

Similar uncertainties arise from the Gaia astrometric solutions alone. An unresolved source with a small observed photocentre amplitude might also be caused by a nearly equal-mass binary star, or by the blending of light from physically unrelated sources. More than one planetary companion could also bias the estimated parameters. For these reasons, radial velocity follow-up is required to validate each candidate. Early results have shown that a significant fraction of Gaia's current astrometric candidates may indeed be affected in these ways (Marcussen & Albrecht, 2023).

BUT THERE have also been successes. Radial velocity follow-up of the Gaia DR3 candidates, using the Hobby–Eberly Telescope's near-infrared Habitable-zone Planet Finder spectrograph (HPF), also found a number of stellar binaries. But it has confirmed two of the candidates as being of sub-stellar mass, designated Gaia–4 b and Gaia–5 b (Stefánsson et al., 2025).

Gaia–4 b is a massive planet ($M_p = 11.8 \pm 0.7 M_J$) in a $P = 571.3 \pm 1.4$ day orbit, with a semi-major axis $a_0 = 0.312 \pm 0.040$ milli-arcsec orbiting a $0.644 \pm 0.02 M_\odot$ star. Gaia–5 b is a brown dwarf ($M_p = 20.9 \pm 0.5 M_J$) in a $P = 358.58 \pm 0.19$ day eccentric orbit ($e = 0.6412 \pm 0.0027$), with angular semi-major axis $a_0 = 0.947 \pm 0.038$ milli-arcsec orbiting a $0.34 \pm 0.03 M_\odot$ star.

It is worth emphasising the tiny size of the angular orbits, of order 1 milli-arcsec or below. And to note how well Gaia's individual epoch measurements, with along-scan accuracies of a few tens of micro-arcsec, define the orbits (as seen in the figures above).

ALTHOUGH GAIA HAS so far nudged its way into only five of the 'Gaia named' exoplanets in the NASA Archive, it is directly enabling the discovery of others. Amongst these are the important class of directly imaged exoplanets. Here, Gaia's 'accelerating systems', mostly exploiting the 30-year time interval between the Hipparcos and Gaia proper motions, can be used as 'dynamical beacons' to pinpoint where a new planet must lie, and to determine masses for previous imaging discoveries.

I described this approach in essay 88 (September 2022), and summarised the systems that had been discovered or characterised in this way at that time. This included the imaging discoveries HD 33632 (Currie et al., 2020), π Mens (Damasso et al., 2020), and HIP 21152 in the Hyades cluster (Kuzuhara et al., 2022), and a dynamical mass for the companion to HD 984 (Franson et al., 2022). Other larger surveys are being made (Bonavita et al., 2022; Kervella et al., 2022).

Amongst Gaia-enabled imaging discoveries since then are HIP 99770 imaged by Subaru (Currie et al., 2023), and AF Lep, located within a debris disk, imaged by Keck–NIRC2 (Franson et al., 2023).

I HAVE EMPHASISED the enormous gulf between Gaia's three confirmed astrometric exoplanet discoveries to date, and the many thousands that are expected to be present in the final mission archive. As more Gaia data, a longer temporal baseline, improved calibrations, improved orbital coverage and improved orbit solutions, become available, Gaia's Coordination Unit 4 will be in a position to publish more discoveries.

In the absence of detailed insight into their activities, I will hazard a guess that DR4, at the end of 2026, will include of order 1000 astrometric discoveries. The numbers in DR5, around 2030, will depend on the achievable calibrations, and on the multiplicity and architecture of these systems, but upwards of 10 000 might be anticipated. And within the published epoch astrometry, and when combined with radial velocity observations or others, solutions should be enabled for many more.

234. Ultra-faint dwarf galaxies

THE FIRST TWO dwarf spheroidal galaxies (dSph) in the Local Group, Sculptor and Fornax, were identified by Harlow Shapley in 1938. But until around 2000, their rarity seemed in conflict with ΛCDM cosmology, which predicted that massive galaxies like the Milky Way should be surrounded by many dark-matter dominated satellite halos. Over the past 25 years, this conflict eased with the discovery of many more, by SDSS and others.

One of Gaia's earliest contributions (Gaia Collaboration et al., 2018b) involved determination of the orbits of the nine 'classical' dwarf spheroidal galaxies (Carina, Draco, Fornax, Leo I, Leo II, Sagittarius, Sculptor, Sextans, Ursa Minor), which I detailed in essay 31. Since then, and as I described in essay 231, Gaia's parallaxes and proper motions have been used to characterise their orbits, structure, internal kinematics, and bulk rotation; the correlation of their star formation episodes with their close orbital approaches to the Milky Way; and the nature of their accompanying globular clusters.

THE DISTINCT CLASS of *ultra-faint* dwarf galaxies was first mentioned (I believe) in 2005, with the discovery, from SDSS, of an unusually extended object (Willman I), at 45 kpc distance, with properties intermediate between those of globular clusters and dwarf galaxies (Willman et al., 2005a). The authors commented that: *'If it is a dwarf spheroidal, then it is the faintest yet known by two orders of magnitude, and is the first example of the ultra-faint dwarfs predicted by some theories.'*

A second, in Ursa Major at a distance of 100 kpc, also from SDSS, was reported by Willman et al. (2005b). This was followed by several others, including other companions to the Milky Way, in Canes Venatici at 220 kpc (Zucker et al., 2006), and in Boötes at 60 kpc (Belokurov et al., 2006b). Others have since been found in the vicinity of the Magellanic Clouds (Koposov et al., 2015).

These ultra-faint dwarfs contain from a few hundred to ~10^5 stars, and have luminosities $\lesssim 10^5 L_\odot$. While often resembling globular clusters in appearance, they are more extended, and with more dark matter (and more than in dwarf spheroidals), with typical $M/L \gtrsim 100$.

THE CURRENT PICTURE is that these ultra-faint dwarfs represent the faintest ($M_V \gtrsim -6$), most metal-poor ([Fe/H] ≤ -2), and most dark matter-dominated end of the dwarf galaxy spectrum (Willman & Strader, 2012). As the oldest and least chemically evolved systems known, they provide *'unique windows into the formation of the first galaxies, and the behaviour of dark matter on small scales'* (Simon, 2019). Formed only a few million years after the Big Bang, before reionisation, they provide important constraints on ΛCDM predictions (e.g., Bovill & Ricotti, 2009; Koposov et al., 2009; Li et al., 2010; Brooks et al., 2013; Sawala et al., 2016; Wetzel et al., 2016).

Galaxies close to the division between the classical dwarf spheroidals and these ultra-faint dwarfs include Antlia II and Crater II, which I discussed in essay 128. Their orbits, characterised by Gaia, are enabling studies of their mass loss, tidal evolution, and possible relationship to the Galaxy's disk warp (e.g. Vivas et al., 2020b).

OVER THE VARIOUS data releases, Gaia-based studies have been reported for a number of ultra-faint dwarf galaxies, amongst them Boötes I, Boötes III, Coma Ber, Eridanus II, Eridanus IV, Grus II, Hercules, Horologium I, Hydrus I, Leo V, Pegasus III, Pegasus IV, Pisces II, Reticulum II, Segue I, Segue II, Tucana II, Tucana III, Ursa Major I, and Ursa Major II.

These studies have targeted improved membership, as a first step in the most important goal of determining their improved orbits around the Galaxy. The orbits are of particular diagnostic value: they provide fundamental constraints on the mass and shape of the Milky Way halo, on their evolution and tidal disruption, on the connection between their orbits and their star formation histories, and ultimately how our Galaxy has assembled its population of dwarf galaxy satellites, and how this relates to the Galaxy's large-scale environment.

Gaia Collaboration et al. (2018b) considered Boötes I as the best for study with Gaia DR2, given its relatively well-populated red giant branch, and its relatively proximity, at 60 kpc. They determined a distance accurate to around 2 kpc, and a space velocity accurate to 20 km s^{-1}.

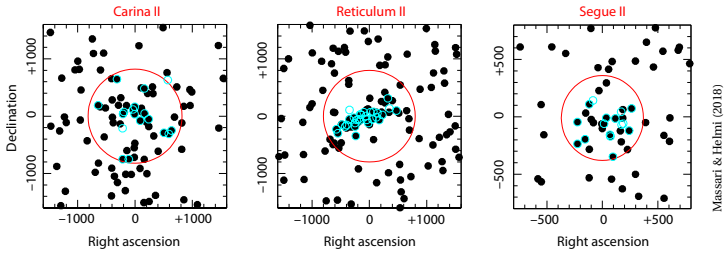

Final membership selection for three ultra-faint dwarf galaxies. Cyan circles indicate the initial candidate members from spectroscopy. The final distance cut has not been applied, but is shown by the red circles. From Massari & Helmi (2018), Figure 2.

ON THE DETERMINATION of bulk space motions of dwarf galaxies in general, Gaia DR2 *'has started a revolution'* (Fritz et al., 2018). Based on careful membership selection, starting with initial guesses but refined using Gaia DR2 astrometry and photometry (see figure above), Massari & Helmi (2018) derived absolute proper motions for seven ultra-faint dwarf galaxies within 70 kpc (Boötes III, Carina II, Grus II, Reticulum II, Sagittarius II, Segue II, and Tucana IV).

Gaia DR2 and DR3 proper motions have now been used to establish memberships and distances for many other systems, including Tucana II (Chiti et al., 2020), Hercules (Mutlu-Pakdil et al., 2020), and Ursa Major I, Coma Berenices, and Boötes I (Waller et al., 2023).

RIGOROUS MEMBERSHIP selection is essential for characterising the morphologies, and identifying possible extensions attributable to tidal disruption. Such extended morphologies have now been reported for Leo V (Mutlu-Pakdil et al., 2019), Hercules (Mutlu-Pakdil et al., 2020), Eridanus IV (Cerny et al., 2021), and Boötes I (Filion & Wyse, 2021).

Searching for RR Lyrae variables in the vicinity of these satellite galaxies provides a particularly powerful method for suppressing foreground contamination, and hence identifying potential extra-tidal members.

Searches in 27 nearby (< 100 kpc) ultra-faint dwarfs by Vivas et al. (2020a) associated 47 Gaia RR Lyrae stars with 14 different satellite galaxies, identifying extra-tidal RR Lyrae in six (three with extra-tidal stars in addition to members within their tidal radius: Boötes I, Boötes III and Sagittarius II; and three in which the galaxy itself does not contain any RR Lyrae: Tucana III, Eridanus III, and Reticulum III). They inferred that these galaxies may also be undergoing tidal disruption. Similarly, Tau et al. (2024) found seven new RR Lyrae stars in six ultra-faint dwarf galaxies (Hydrus I, Ursa Major I, Ursa Major II, Grus II, Eridanus II, and Tucana II).

ACCURATE BULK PROPER MOTIONS, and hence accurate orbits, provide the ingredients for computing their orbital histories.

Amongst these, Gaia EDR3 proper motions for Eridanus II suggest that it is on its first infall into the Milky Way (Fu et al., 2022b). In the case of the distant but closely separated (40 kpc) systems Pegasus III and Pisces II, the study by Richstein et al. (2022) found no morphological features indicating that a significant interaction between the two has occurred. Propagating their orbits in a combined Milky Way–LMC potential, they found a possible orbital history in which they experienced a close (10–20 kpc) mutual passage a little more than 1 Gyr ago, followed by a combined passage around the Large Magellanic Cloud (30–60 kpc) just under 1 Gyr ago. If confirmed, they would add to the rare occurrence of coherent satellite pairs within the Local Group.

For the newly discovered Pegasus IV, Cerny et al. (2023b) determined an elliptical retrograde orbit, currently near its orbital apocentre.

Foote et al. (2025) showed that the ultra-faint dwarf Segue II had a recent (77 ± 5 Myr ago) close flyby with the Cetus–Palca halo stream, within the stream's 2σ width. They show that this interaction potentially enables constraints on its mass and density profile at much larger, kpc-scale, radii than are probed by its stars.

THERE IS A CONNECTION between the orbits of satellite galaxies and their star-formation histories (Grebel, 2001; Tolstoy et al., 2009). This has been nicely demonstrated in the study of the orbits of the classical dwarf spheroidals by Miyoshi & Chiba (2020). These authors showed that their infall time, defined as when the satellite galaxy first crosses within the growing virial radius of the Milky Way's halo, coincides well with the peak star-formation rate, as a consequence of ram pressure on their gas content.

In contrast, the general consensus is that star-formation activity in ultra-faint dwarfs had already peaked prior to their infall times, possibly suppressed at the epoch of reionization of the Universe (Okamoto et al., 2008; Brown et al., 2012; Brown et al., 2014; Weisz et al., 2015; Simon, 2019).

ULTRA-FAINT GALAXIES provide specific challenges to the gravitational theory of Modified Newtonian Dynamics (MOND) as a (non-dark matter) explanation for the rotation curve of galaxies (e.g. Safarzadeh & Loeb, 2021; Sánchez Almeida, 2022). In this context, arguments against MOND relate to the observed velocity dispersion, infall history, and observed tidal features, established by Gaia, for Ursa Major I, Willman I, and Tucana III (Safarzadeh & Loeb, 2021).

235. Populations in globular clusters

I HAVE DEVOTED several essays to some of the Gaia-based studies of globular clusters: on their Galactic orbits (essay 30), on Palomar 5 and its tidal tails (essay 109), and on Omega Centauri (essays 40 and 157). In essay 230, I discussed the long-standing (and still open) question of the 'Oosterhoff dichotomy', related to the average period of their RR Lyrae stars, and which Gaia has shown is tied to the Milky Way's formation history.

Here I will look at Gaia's contributions to another globular cluster puzzle: their multiple stellar populations. In their review of this specific phenomenon, and which I will draw on for some of the background, Milone & Marino (2022) described this as *'…one of the most puzzling, open issues of stellar astrophysics'*.

And in their wider review of globular clusters, Gratton et al. (2019) commented that *'The increasing amount of observational data are revealing a complexity that has so far defied the attempts to interpret the whole data set in a simple scenario'*.

UNTIL THE 1990S, globular clusters were believed to have formed from a single burst of star formation. Their early formation epochs ($z \gtrsim 3$) would have preceded most of the Galaxy's assembly. Observations since then have revealed growing evidence for broad or distinct main sequences, red giant branches, and sub-giant branches (e.g. Anderson, 1997; Grundahl et al., 1998; Lee et al., 1999; Bedin et al., 2004; D'Antona et al., 2005; Piotto et al., 2007; Milone et al., 2008; and many others).

Starting with studies of M4 (Marino et al., 2008; 2011), these different populations are now known to be linked to their different abundances, in particular for the elements resulting from H fusion (C, N, O, Na, Al, and in some cases Mg, Si, and K).

Stars with lower N and Na, and higher C and O, resemble Galactic field stars with similar metallicity, and are referred to as 'first population' or 'first generation' (and denoted 1P or 1G). Conversely, stars enhanced in N and Na (also He and Al), and depleted in C and O, define one or more subsequent stellar populations, and are referred to collectively as second population (2P or 2G).

UNDERSTANDING THE ORIGIN of these multiple stellar populations has proven a challenge for models of stellar evolution, nucleosynthesis, and star-formation processes at high redshift. A simple scenario might attempt to attribute them to different generations of stars: the first burst of star formation would form stars out of pristine material, with subsequent events building stellar populations from their nucleosynthesis products, which then evolve faster. A challenge here that 2P stars represent the majority of stars in most clusters (Milone et al., 2017; Dondoglio et al., 2022). In such a model, this would imply that the progenitors of today's globular clusters were substantially more massive, having preferentially lost most of their initial 1P stars into the field.

Others have suggested that they form in a single burst of star formation, with a fraction then polluted by the ejecta of more massive stars of the same generation (Bastian et al., 2013; Gieles et al., 2018). Other explanations have been put forward (Milone & Marino, 2022, §4), attributing the chemical anomalies as arising from 'hot bottom burning' in asymptotic giant branch stars; massive stars rotating near break-up; massive interacting binaries; the loss of massive stars due to their sinking into black holes; the role of super-massive stars; or the results of stellar mergers. But their conclusion was that *'we do not properly understand the origin of multiple stellar populations in globular clusters'*.

As a comment on the field's nomenclature, 'chromosome maps' are 2-colour diagrams derived from colours which maximise the separation of these populations. And clusters are often described as Type I and Type II, based on the distribution of stars in the chromosome maps, or on star-to-star heavy-element variations.

CLUES AS TO how Gaia might assist come from scenarios which predict that these populations also differ in their initial structural and kinematic properties, specifically that 2P stars may form in a sub-system more spatially concentrated than the 1P system (e.g. D'Ercole et al., 2008; Bekki, 2011; Bekki et al., 2017; Calura et al., 2019; Lacchin et al., 2022; Livernois et al., 2024).

TWO MAIN aspects of the Gaia data are being used to throw further light on these multiple populations. The first is the use of the distances and proper motions to probe the morphology and kinematics of the cluster members. Important in this context, and in contrast to HST, is the quasi-inertial nature of Gaia's proper motion system. Another strength is that Gaia's kinematics extend to the outer cluster regions and beyond, compared with HST-based studies which tend to focus on the central regions where the star density is highest.

Studies are also leveraging Gaia's low-resolution XP (BP/RP) spectra, which were made available in Data Release 3 (June 2022) for the 220 million brightest stars. These allow construction of any desired 'synthetic photometry', subject to it lying within Gaia's optical spectral range (essay 187). This is allowing the definition of optimised colour indices (and chromosome maps) to separate the different populations.

THE CLUSTER NGC 1851 is the well-studied prototype of the less-common Type II systems. It shows large differences in both light- and heavy-element abundances, and has been hypothesised to be the remnant of accreted dwarf galaxies. Cordoni et al. (2023a) used the low-resolution XP spectra to construct synthetic photometry in the BVI bands, and thence the pseudo-colour index $C_{\rm BVI} = (B-V)-(V-I)$, which has been shown to be effective in separating the metal-rich 'anomalous' stars from the 'canonical' population.

They also constructed an optimised 'chromosome map', $m_{\rm F415}$ versus $m_{\rm F415}-I$, where their Gaia-based F415^{25} photometric filter (the notation indicating the filter's central wavelength and width, in nm) effectively separates bright red giant branch stars into canonical and anomalous groups (see figure opposite).

They demonstrated that both the canonical and anomalous populations are found both inside and outside the cluster's tidal radius, out to $3.5r_{\rm tidal}$, or about 45 arcmin. Nonetheless, the canonical population dominates outside the tidal radius, and it exhibits a more circular on-sky morphology, in contrast to the more elliptical shape of the anomalous population.

The Gaia proper motions also give access to the stellar kinematics. And while dynamical differences in the inner regions may be smoothed by relaxation processes, the outskirts of the cluster, characterised by much longer relaxation times, are more likely to retain evidence for any distinct dynamical evolution. And indeed they found hints of a tangentially anisotropic motion in the outer regions, indicating a preference for stars to escape on radial orbits.

They conclude that the Gaia DR3 low-resolution XP spectra, together with Gaia DR3 astrometry and proper motions, are indeed powerful tools for investigating the multiple populations in globular clusters.

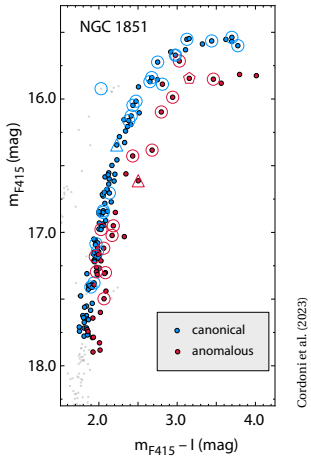

A SIMILAR APPROACH was followed by Mehta et al. (2025). They found that the most-efficient filters to distinguish the distinct stellar populations were F380^{200} and F430^{100}, which are sensitive to N and C variations respectively. They were able to identify, for the first time, 1P and 2P stars in the cluster's outermost regions and beyond its tidal radius, the 2P stars being more centrally concentrated. Similar chromosome maps effectively distinguished multiple populations in the outer regions of four other clusters with different metallicities: NGC 3201, NGC 6121, NGC 6752, and NGC 6397. Skipping over some detailed differences in these various clusters, the radial dependencies are consistent with cluster formation scenarios where the 2P stars originate in the central regions.

Jang et al. (2025) and Cordoni et al. (2025) extended this approach to examine the radial distributions for 29 globular clusters, using both Gaia and HST proper motions. They found that the 1P stars transition from isotropy to slight tangential anisotropy towards the outer regions, while the 2P stars become increasingly radially anisotropic beyond the half-light radius. Statistically significant differences in the anisotropy profiles were found for dynamically young and non-relaxed clusters. And clusters with orbits closer to the Galactic centre exhibit larger dynamical differences between 1P and 2P stars than those with larger peri-Galactic radii.

Together, their findings are again consistent with a scenario where 2P stars form in a more centrally concentrated environment, and where the interaction with the Milky Way's tidal field plays a crucial role in the dynamical evolution of both populations.

I HAVE BEEN LEFT with the impression that the combination of Gaia's astrometry, and its far-reaching capabilities in the area of synthetic photometry, has only just started its potential impact on this complex problem in the understanding of globular clusters.

236. More on interstellar extinction

In essay 191 (August 2024) I discussed the substantial progress being made, using Gaia data, in characterising interstellar extinction. But a further development recently reported by Zhang & Green (2025), in the journal *Science*, merits specific mention. Their work brings a further improvement to the description of extinction along many lines-of-sight throughout the Galaxy. But it also provides some rather remarkable conclusions about the underlying physical processes involved.

As the authors state in their introduction, interstellar dust plays a major role in many areas of astronomy… *'either as a nuisance, or as an object of study in its own right.* Their work brings a new perspective on the latter.

Let me first summarise some key points from essay 191 by way of background. Interstellar extinction is important in the determination of stellar parameters (e.g. $T_{\rm eff}$, $\log g$, and [M/H], through spectral modelling), and in describing the distribution of gas and dust in the solar neighbourhood. Light is absorbed and scattered by any gas and dust between star and observer, and most stellar spectra are affected to a greater or lesser extent. The details and spatial variation of the extinction depend on the properties of dust grains along the line-of-sight, and measurements also convey information about their composition and size distribution.

Interstellar extinction is a rather smooth function of wavelength, albeit with superimposed absorption features due to particular chemical species. These include the ultraviolet (217 nm) bump, diffuse interstellar bands, and other features beyond Gaia's response in the infrared. Extinction in a given direction can be inferred by comparing an observed spectrum with its closest atmosphere model. In the solar neighbourhood, extinction in the V-band averages some 0.7–1.0 mag kpc^{-1}, but it is much higher in specific regions, notably in the Galactic plane, and especially towards the Galactic centre.

Since blue light is more strongly attenuated than red, extinction also causes objects to appear redder as well as dimmer. This 'reddening' is often simply characterised by an object's *colour excess* in some specified photometric system, e.g. $E_{B-V} = (B-V)_{\rm obs} - (B-V)_0$.

The parameter $R \equiv A_V/E(B-V)$ characterises the ratio of total-to-selective extinction. Ranging between 2.2–5.8 for sight lines where ultraviolet extinction has been measured, a mean relation $A_V = 3.1\,E(B-V)$ is frequently used (e.g. Cardelli et al., 1989; Fitzpatrick, 1999; Fitzpatrick & Massa, 2007).

There is a huge literature on extinction, and advances have benefitted from ultraviolet and infrared observations. Even so, around the time of the Gaia launch, Lallement et al. (2014) noted that *'3d maps of the Galactic interstellar matter are a potential tool of wide use, but accurate and detailed maps are still lacking'*.

Gaia is changing this. Parallaxes provide the fundamental means of quantifying the dependence of extinction on distance for millions of sight lines in the Galaxy. And crucially, reddening and extinction *for each star* can be determined from Gaia's low-resolution BP/RP (aka XP) spectra, and from its RVS spectra.

Early Gaia DR2-based work to characterise extinction only had access to the *integrated* photometry, and most studies also included infrared photometry, e.g. using 2MASS and WISE (Andrae et al., 2018; Leike & Enßlin, 2019; Chen et al., 2019; Lallement et al., 2019; Green et al., 2019; Anders et al., 2019; Sun et al., 2022). Improved maps followed from EDR3 (Anders et al., 2022; Lallement et al., 2022; Vergely et al., 2022).

As I detailed in essay 191, major improvements came with DR3, partly from the improved parallaxes, but also with the availability of the mean BP/RP spectra for 220 million stars (Andrae et al., 2023a; Kordopatis et al., 2023; O'Callaghan et al., 2024). Revisions also used improved reductions of the XP spectra for some 100 million stars (Zhang et al., 2023c; Andrae et al., 2023b; Hattori, 2025; An et al., 2024; Gontcharov et al., 2023).

The XP spectra also allow determination of extinction at their intrinsic spectral resolution, $R \sim 20-100$. X. Zhang et al. (2023c) constructed a 'universal extinction' versus wavelength curve, with each wavelength interval modelled separately. The resulting smooth extinction dependence (their Fig. 15) agrees reasonably well with the $A_V = 3.1\,E(B-V)$ model of Cardelli et al. (1989).

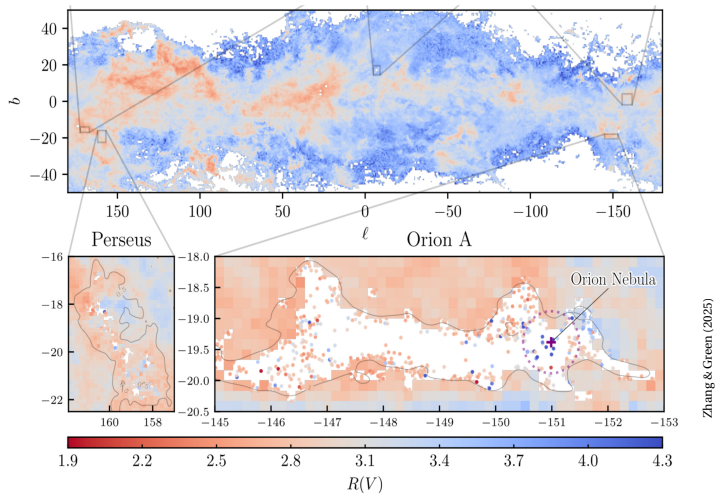

VARIATIONS OF the total-to-selective extinction, $R(V)$, actually provide valuable information on the dust grain properties. Compared to its average of around 3.1, values up to 6 occur along sight lines passing through dense molecular clouds. This has been attributed to the growth of dust grains through accretion and coagulation (e.g. Vrba & Rydgren, 1984; Fitzpatrick, 1999; Draine, 2003; Köhler et al., 2012; Foster et al., 2013). In low-density regions, more exposed to stellar radiation, values as low as 2 have been attributed to grain destruction through sputtering by impinging atoms or ions, and photolysis by ultraviolet photons (e.g. Draine, 2003).

WITH THESE GOALS, Schlafly et al. (2016) examined $R(V)$ for 37 000 stars using spectroscopy from APOGEE combined with photometry from Pan-STARRS1, 2MASS, and WISE. But significantly increased sample sizes are now becoming available. R. Zhang et al. (2023a) selected 3 million stars from LAMOST, supplemented by Gaia photometry, to investigate the relationship between $R(V)$ and parameters such as gas-to-dust ratio, dust temperature, dust emissivity, column densities, and the ratio of atomic to molecular hydrogen.

Their $R(V)$ distribution is well-described by a Gaussian distribution with a mean of 3.25 and a dispersion of 0.25. Within the Galactic disk, $R(V)$ exhibits a wide range on various scale sizes, from small structures within individual molecular clouds to larger scales spanning kpc.

BASED ONLY ON Gaia data, X. Zhang & Green (2025) used the low-resolution BP/RP spectra to measure extinctions, and $R(V)$, for 130 million stars. Rich spatial structure is seen on many length scales (see figure). In the Galactic plane ($|z| < 400$ pc), within 2.6 kpc of the Sun (their Fig. 1), they found spatial correlations between $R(V)$ and several large-scale structures, including the Radcliffe Wave (Alves et al., 2020), the 'Split' (Lallement et al., 2019), and the Carina–Sagittarius arm.

There is some interesting physics encoded in these diagrams. Rather than increasing continuously with density (as a simple consequence of growing grain size), they found that $R(V)$ is above average in very diffuse regions, but then *decreases* as the dust density *increases*. But in very dense regions, such as the Orion Nebula and dense cores in Taurus, $R(V)$ increases sharply.

Their explanation involves the two dominant mechanisms of dust grain growth in the interstellar medium: *accretion* of elements from the gas phase onto the grain surfaces, and *coagulation* of grains that collide and stick together, the latter occurring preferentially at higher densities. While both processes increase the average grain size, their effects on the grain-size *distribution*, and thus $R(V)$, are very different (Hirashita, 2012).

In a simplified picture, accretion deposits a layer of equal thickness onto each grain, such that the fractional increase in surface area is larger for smaller grains. The increasing contribution of the small grains causes a steepening of the extinction curve, and hence a decreasing $R(V)$. Coagulation, in contrast, transforms pairs of small grains into larger grains, decreasing the relative abundance of small grains. The extinction curve becomes flatter, thus increasing $R(V)$.

Their results, they argue, are consistent with a picture in which accretion is the dominant mechanism of grain growth in the less dense regions of interstellar clouds, leading to the observed decrease in $R(V)$ with increasing dust density. In the densest regions, coagulation takes over, causing $R(V)$ to increase rapidly.

THE WORK has already had some wider consequences. The extinction curves now require additional dependencies than $R(V)$ alone (Green et al., 2025). It offers the prospects of characterising magnetic field dependencies (Hensley, 2025). And it offers insights into the growth of polycyclic aromatic hydrocarbons as a consequence of gas-phase accretion (X. Zhang et al., 2025).

237. Beta Cephei variables

THE β Cephei (BCEP) variables are the most massive pulsating stars on the main sequence, and are named after the class's $V = 3.2$ mag prototype β Cephei. They are core H-burning stars, spectral type B0–3 IV–V, with $T_{\rm eff} = 20$–$30\,000$ K, and mass $7 - 20 M_{\odot}$. They are characterised by pulsations of small amplitude (typically 0.01–0.3 mag) and short period (typically 0.1–0.3 d). They are also known as Beta Canis Majoris stars – and should not be confused with Cepheid variables.

Discovered from radial velocity variations of β Cephei (Frost, 1902), and later by photometry (Guthnick, 1913), the variations were originally ascribed to a spectroscopic binary, since such rapid stellar variations were unprecedented at the time. But from monitoring of other similar objects, Struve (1955) identified long-term changes in the pulsation amplitude. These were interpreted as a beat effect, and duly explained as the simultaneous presence of radial and non-radial modes with closely separated periods.

THE PHYSICAL MECHANISM responsible for their pulsations remained uncertain for several decades: the κ mechanism, specifically when attributed to the changing ionisation and hence opacity of He (as inferred for Cepheids), would not operate due to their much higher temperatures and ionisation states. Cox (1976) listed nine different possible pulsation mechanisms.

Only in the 1990s, with newly calculated opacities, were the pulsations explained by the κ mechanism, but in this case due to the changing opacity of the iron-peak elements (Kiriakidis et al., 1992; Moskalik & Dziembowski, 1992; Gautschy & Saio, 1993; Dziembowski & Pamiatnykh, 1993). For example, Moskalik & Dziembowski (1992) demonstrated that the fundamental radial mode is unstable, and that the instability persists in non-radial modes of similar and lower frequencies.

Fritzewski et al. (2025) summarises the progressive chronology in identifying their oscillation modes, and in understanding the mode excitation and mode selection (viz. why certain modes are excited to observable amplitudes, and some evolve with time).

DETAILED ASTEROSEISMOLOGY studies started with the 21-year ground-based photometric time series of HD 129929 by Aerts et al. (2004b), which provided evidence for at least six periods. Similar long-term ground-based photometry extended such detailed modelling to ν Eri (Aerts et al., 2004a; Pamyatnykh et al., 2004), θ Oph (Handler et al., 2005; Briquet et al., 2007), 12 Lac (Handler et al., 2006; Desmet et al., 2009), and V2052 Oph (Handler et al., 2012; Briquet et al., 2012). Space-based asteroseismology with MOST, CoRot and Kepler added a handful of other well-studied examples.

THE NUMBER of known β Cep stars has grown steadily in the past decades. Sterken & Jerzykiewicz (1993) listed 59 secure examples (and 79 candidates), while Stankov & Handler (2005) quoted 93 confirmed (and 77 candidates). Pigulski & Pojmański (2008) found 103 new objects with ASAS–3. Labadie-Bartz et al. (2020) detected 113 (86 new) from KELT. Balona & Ozuyar (2020) identified 327 from TESS, while Eze & Handler (2024) added a further 78 in eclipsing binary systems. Shi et al. (2024) concluded that, allowing for duplicates, the number of known Galactic β Cep stars is about 400.

Various of their properties remain poorly understood. Questions include whether changes in the dominant pulsation period can be explained as evolutionary effects over their short (~10 Myr) main-sequence lifetimes as the H fuel is depleted, e.g. in the case of BW Vul (Cowall & Odell, 2018), or σ Sco (Struve et al., 1955; Sterken, 1975; Jerzykiewicz & Sterken, 1984; Pigulski, 1992; Tkachenko et al., 2014). Another is the discrepancy between the dynamical masses in binaries, and model predictions, e.g. for σ Sco (Tkachenko et al., 2014).

OF 1.8 million variable stars in Gaia DR3 (Eyer et al., 2023; Rimoldini et al., 2023), the time-series photometry allowed detection of the dominant mode in around 100 000 intermediate- and high-mass dwarfs (Gaia Collaboration et al., 2023d). Of these, 222 were classified as β Cep variables, with dominant frequency in the range $\nu_1 = 3 - 8\,{\rm d}^{-1}$ (Fritzewski et al., 2025).

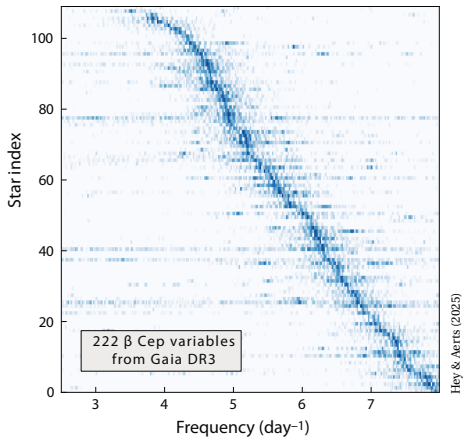

THE GAIA light curves are only sparsely sampled, albeit of high (milli-mag) accuracy, and it is not immediately evident that Gaia could contribute to the identification of such asteroseismic pulsation modes.

But as part of a wider study based on a TESS–Gaia cross-matched (g-mode pulsator) sample comprising 85 313 δ Scuti, 11 636 γ Dor, 3426 slowly pulsating B (SPB) stars, and these 222 β Cep variables, Hey & Aerts (2024) used the first 2 years of the more densely-sampled TESS photometry to independently classify the Gaia DR3 list of non-radial pulsators, including their dominant and secondary pulsation frequencies.

They found that the majority of Gaia classifications are indeed consistent with those from TESS, concluding that *'the Gaia photometry is exceptionally accurate for detecting the dominant and secondary frequencies, reaching approximately 80% accuracy in frequency for p- and g-mode pulsators'*. Indeed, for the higher frequency p-modes, they concluded that it is, as yet, unclear whether the Gaia or TESS data is more accurate for measuring the 'true' dominant frequency.

Their analysis showed that the g-mode pulsators form a continuous group of variable stars along the main sequence across B, A, and F spectral types, implying that the mode excitation mechanisms for all these pulsators *'need to be updated with improved physics'*.

Their Figure 7, shown above, is 'stacked' according to the dominant pulsation frequency. In contrast to the multiple ridge-like features for the δ Sct variables (the ridges corresponding to various overtone frequencies), the β Cep sample shows no obvious secondary structures… precisely as expected for these low-order pulsators (Stankov & Handler, 2005).

A parallel study by Shi et al. (2024) identified 155 β Cep candidates using data from TESS and Gaia, of which 83 were confirmed as β Cep pulsators. With magnitudes in the range 8–12 mag, amplitudes of 0.1–55.8 mmag, and pulsation periods 0.06–0.31 d, the Gaia DR3 parallaxes are mostly between 0.2–0.6 milli-arcsec.

ASTEROSEISMIC MODELLING, I should emphasise, targets the measurement of fundamental stellar properties such as internal rotation, age (in terms of core hydrogen mass fraction), core boundary mixing, and even tidal effects in multiple systems (e.g. Bowman, 2020).

Further insights into the physics of these pulsators can be expected from future Gaia data releases, on the basis of an increased sample size, and improved light curves. For example, current theoretical models do not precisely match the observed location of these pulsators in the Hertzsprung–Russell diagram (e.g. Burssens et al., 2020), while numerical computations predict fewer excited modes than those detected from the latest space-based photometry (e.g. Rehm et al., 2024).

More detailed physics in computing excited modes changes the predicted instability regions. This will further constrain phenomena such as the Coriolis effect due to rapid rotation (Szewczuk & Daszyńska-Daszkiewicz, 2017), and radiative levitation due to atomic diffusion, in which the segregation of different elemental isotopes leads to different modes being excited by the opacity mechanism (Rehm et al., 2024).

Another of Gaia's strengths for asteroseismology is that, compared with the single 600–1000 nm TESS passband, Gaia's multi-colour time series (in G, BP, and RP) assists identification of the spherical harmonic wavenumbers (l, m) which characterise the mode's geometry (via the inclination of the pulsation symmetry axis). More specifically, mode-dependent perturbations of the stellar flux, and limb darkening, can be derived from the amplitude ratios at the different wavelengths (e.g. Heynderickx et al., 1994; Dupret et al., 2003).

FURTHER analysis of the Gaia sample, interpreted with more extended TESS-based photometry, is given by Fritzewski et al. (2025). They identified the mode degrees for 148 stars and, based on grid modelling, derived mass, convective core mass, and ages for 119. Their location in the HR diagram, constructed from Gaia DR3, is shown below, with the solid black line delineating the instability region for p-modes from Bowman (2020).

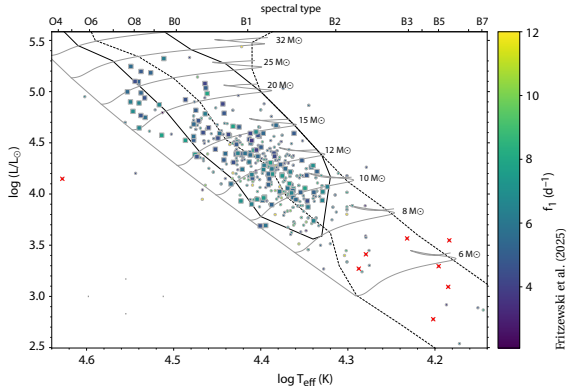

238. Ophion: a most curious cluster

THE recent study entitled *'Gaia Net: Toward Robust Spectroscopic Parameters of Stars of all Evolutionary Stages'*, by Huson et al. (2025), reports a new processing of the 220 million XP spectra contained in Gaia Data Release 3 (June 2022). In this essay, my main interest is in one of the scientific findings that followed from this data set: the discovery of a new cluster, which they named Ophion, which has some particularly interesting kinematic properties.

Let me first summarise their revised processing, and provide some background to the wider insights being gained by Gaia for young clusters and associations.

GAIA DR3 includes the mean low-resolution BP/RP spectra (frequently together referred to as the XP spectra) for the brightest 220 million stars (essay 76). Accompanying the spectra were the Gaia Data Processing and Analysis Consortium's project-level estimates (determined by its Coordination Unit 8) of the astrophysical data for each star, derived from the XP spectra.

I outlined the approach used for these estimates in essay 89. Briefly, the GSP–Phot module within the 'astrophysical parameters inference system' (Apsis) provides *model-dependent* estimates of $T_{\rm eff}$, $\log g$, [M/H], absolute magnitude, radius, distance, line-of-sight extinctions (A_0, A_G, A_{BP} and A_{RP}) and reddening $E(G_{BP}–G_{RP})$, by forward-modelling the BP/RP spectra, apparent G magnitude, and parallax using a Markov Chain Monte Carlo method. Details are given by Creevey et al. (2023).

THESE ASTROPHYSICAL data made available with DR3 were never considered to be the final word in classification or parameter estimation. Additional mission data, alongside improvements in calibration, and in training sets and algorithms, were always anticipated.

And indeed, since the release of Gaia DR3, several revised community-generated catalogues of $T_{\rm eff}$, $\log g$, and [M/H] have been made available, which I described in essay 189. Amongst these are the catalogues of Andrae et al. (2023b), Zhang et al. (2023c), Khalatyan et al. (2024), Yao et al. (2024), and Hattori (2025).

THE CONTRIBUTION by Huson et al. (2025) uses a new data model, Gaia NET. As detailed in their Section 3, they describe it as a 'one-dimensional residual convolutional neural network' based on (SDSS) BOSS Net (Sizemore et al., 2024). But the key point they make is that previous parameter determinations from the Gaia XP spectra have been mostly trained on OBAFGK *main-sequence* stars, poorly representing low-mass stars, pre-main sequence stars, and objects below the main sequence (such as hot subdwarfs and white dwarfs).

In contrast, their training set employed a wider spectral range, from SDSS–APOGEE, SDSS–BOSS, and LAMOST. Their goal was to provide a more comprehensive catalogue, covering a wide range of masses and evolutionary stages ($T_{\rm eff} \sim 2000$–$50\,000$ K, $\log g \sim 0$–10), with particular attention to pre-main sequence stars. These were, they argue, the first (and only) spectroscopic catalogues providing sufficiently robust estimates of $\log g$ for young stars to enable their use as a proxy for age.

They stress that methods to identify young stars and their ages based on photometry (e.g. using Gaia DR2; McBride et al., 2021) are complicated by the effects of extinction, as well as the contribution from binary systems. From spectroscopy, they argue, estimates of $T_{\rm eff}$ allow the characterisation of sources independently of extinction, while $\log g$ measurements are less biased by binary stars (equal mass binaries producing the same spectroscopic template). And, importantly in this context, given that young stars contract over time, their ages are strongly correlated with $\log g$.

With these results, they then examined the distribution of young low-mass stars with ages $\lesssim$20 Myr in the solar neighbourhood. The sky projection of their selected pre-main sequence candidates is shown over. It correctly traces the known distribution of the nearby star-forming regions, with populations associated with Sco–Cen, Vela, Orion, Perseus, and Cepheus, and many others. In the case of Cepheus, for example, instead of being a monolithic star-forming region, it is seen as several small clouds that are distinct both spatially and kinematically (Szilágyi et al., 2023).

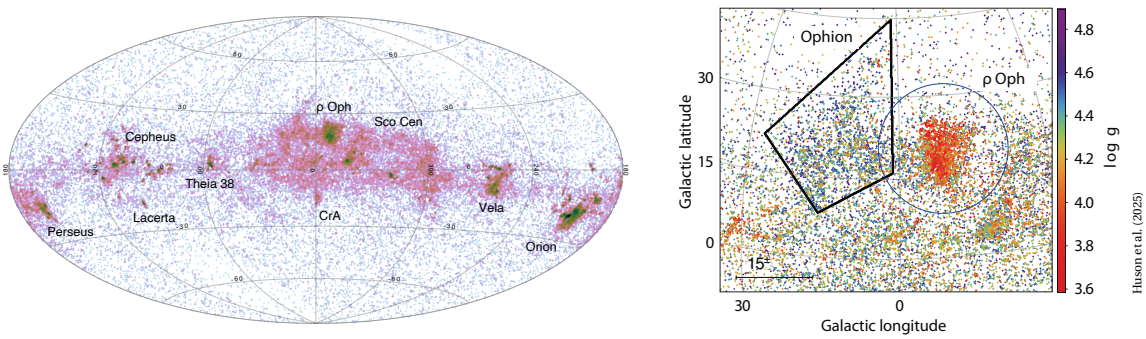

Left: sky projection of pre-main sequence stars, colour-coded by density. Right: zoom-in of the Ophion region. The overdensity is highlighted by the black polygon, and the circle delineates a 'bubble' around ρ Oph. From Huson et al. (2025), Figures 6 and 8.

BEFORE SAYING more on their newly discovered cluster, Ophion, let me underline a few key points about the progress in characterising young stellar associations and open clusters with Gaia so far.

To summarise the advances being made in the study of open clusters, Gaia's distances and proper motions are allowing the identification of vastly more clusters than previously known (essay 219), along with rigorous membership and age estimation (essay 220). The motions of *individual* stars allows measurement of their Galactic orbits, as well as details of their dissolution, bulk rotation, and internal dynamics (essay 221).

Concerning young associations (which I reviewed in essay 223), a recurring theme that emerges from the Gaia studies is their spatial complexity. For example, the massive star-forming regions within 600–700 pc (such as Orion, Sco–Cen, and Vela) trace a complex three-dimensional pattern. And cluster analyses often point to structural connections between spatially-separated populations, such as between the Orion Complex and Perseus OB2, and between the sub-regions of Vela.

THE NEAREST and most well-studied association is Scorpius–Centaurus (Sco–Cen, aka Sco OB2), and subgroups including Lower Centaurus Crux and Upper Scorpius. At 130 pc, and extending over 2000 sq. deg., Hipparcos identified over 400 members, while several independent Gaia-based studies have brought the current census to ~15 000 (essay 223). And whether associations are expanding or not is linked to the underlying star-formation processes. During their early phases, radiation from hot stars and supernovae can rapidly strip residual gas, although not necessarily resulting in the association's rapid dispersal. Gaia studies find that many associations are expanding, although others are not.

In their wide-ranging review, Krumholz et al. (2019) concluded that while we now have a broadly satisfying picture, star clusters, which cover a huge range of mass, size, and density scales, *'remain mysterious'*.

ADDING TO this mystery, and amongst their identified structures of pre-main sequence stars selected through the use of $\log g$, Huson et al. (2025) drew attention to a population of more than 1000 stars, east of Sco–Cen, and which they named Ophion. This overdensity had been noted in the Gaia DR3 study of the Sco–Cen OB association by Ratzenböck et al. (2023b), who found some 13 000 young co-moving objects organised into 37 co-moving groups (essay 223).

What makes this particular overdensity unusual is that, despite a coherent age of ~20 Myr, and at a common distance of ~200 pc, it has negligible kinematic coherence. It has a large velocity dispersion $> 20\,\mathrm{km\,s^{-1}}$, without any obvious pattern of expansion. It therefore appears to be fully 'disrupted', but at the same time still persisting as a spatial overdensity. Seeing such a massive young population without a coherent core velocity structure is, they argue, somewhat unexpected.

Given the fragmented morphology in this region of Sco–Cen, and the presence of several apparent 'bubbles' in the distribution of young stars, they infer that these features were likely driven by one or more supernovae. Their conclusion is that this Ophion star-forming region lost mass rapidly during the gas-expulsion phase, possibly through a combination of both supernovae and tidal interactions, and resulting in the acceleration of the bulk of the stars to very high velocities.

That the region remains spatially coherent would simply be because it has been caught in the earliest stages of its rapid and complete disruption. Cluster search algorithms relying on both spatial and kinematic coherence would not have found Ophion!

I FOUND IT interesting that the first three of the five authors of this study are computer scientists, with only one (Logan Sizemore) having another presence on ADS. This nice development perhaps underlines the importance of cross-disciplinary approaches in optimally exploiting the vast Gaia data base.

239. Actinide-boost stars

THE ELEMENTS found in stars reflect the composition of the interstellar medium from which they formed. But an understanding of their origin, especially in the case of the heavier elements, remains highly incomplete (e.g. Cowan et al., 2021). My short introduction can only touch on the complexities of this subject.

Elements heavier than iron (found in halo stars, the interstellar medium, dust grains, meteorites, and Earth), are mainly formed by the process of neutron-capture.

At low neutron densities, heavy element production occurs via *slow* neutron-capture (termed the s-process). The process is 'slow' in the sense that there is sufficient time for possible radioactive decay to occur before another neutron is captured. Extending over thousands of years, it occurs in the He-burning layers of asymptotic giant branch stars and during the He- and C-burning phases of massive stars, seeded by iron nuclei from earlier supernovae (Busso et al., 1999; Käppeler et al., 2011).

High neutron densities enable heavy-element nucleosynthesis by *rapid* neutron-capture (the r-process). This involves a succession of neutron captures by heavy seed nuclei. The process is rapid in the sense that the nuclei cannot have time to undergo decay before another neutron is captured. It is inferred to occur over timescales of seconds, and is therefore presumably restricted to explosive environments. Possible sites include core-collapse supernovae, and neutron star–neutron star or neutron star–black hole mergers (e.g. Martínez-Pinedo et al., 2014; Côté et al., 2019; Cowan et al., 2021; Vieira et al., 2023; Wanajo et al., 2024).

This NASA Astronomy Picture of the Day provides a visual synopsis of the likely origin of the elements.

CONSTRAINTS ON these processes can be gained from the overall atomic mass distribution in specific objects. High-resolution optical spectroscopy provides access to some 20–30 elements heavier than the iron-group in late-type (FGK) stars. A dozen others (including Ge, As, Se, Cd, Te, Lu, Os, Ir, Pt, Ag, and Pb) are accessible to near-ultraviolet spectroscopy, for example using HST–STIS (e.g. Sneden et al., 1998; Cowan et al., 2005; Roederer & Lawler, 2012).

WITHIN THIS bigger panorama, the actinides are a series of 15 radioactive metallic elements with atomic numbers 89 to 103: actinium (hence their name) to nobelium. Naturally occurring (and long-lived) uranium (U) and thorium (Th), and synthetically produced plutonium (Pu), are the most abundant. Like the lanthanides (of which I looked at cerium in essay 91), they form a family with similar if wide-ranging properties.

ACTINIDES PLAY a role in several areas of astrophysics. Nucleo-cosmochronology, which started with the work of Fowler & Hoyle (1960), exploits the very long half-lives of ^{232}Th, ^{235}U and ^{238}U to derive ages within the solar system and beyond (e.g. Cowan et al., 1991; Meyer & Truran, 2000; Goriely & Arnould, 2001).

Determining nuclear-based *stellar* ages developed from the first detections of Th and U in a number of very metal-poor stars, amongst them the 'neutron-capture-rich' giant CS 22892–052 (McWilliam et al., 1995; Sneden et al., 1996; 2003), and the r-process rich CS 31082–001 (Cayrel et al., 2001; Hill et al., 2002). Incidentally, Hill et al. (2002) gave abundances for 44 elements, while Sneden et al. (2003) gave abundances or upper limits for 57.

Shorter-lived actinides have also been detected in Galactic cosmic rays, providing potential constraints on their acceleration sites (e.g. Westphal et al., 1998; O'Sullivan et al., 2001; Lingenfelter et al., 2003).

AS DETAILED by Holmbeck et al. (2020), the relative level of (lanthanide) Eu to Fe abundance in a star is a proxy for how much r-process enhancement preceded the star's formation, compared to the chemical evolution of that gas from supernova events. Stars over-enhanced with Eu relative to Fe compared to the Sun are called 'r-process enhanced', and are divided into two categories: r-I, with $0.3 < [\mathrm{Eu/Fe}] \leq 1.0$ (i.e., a factor 2–10 greater than solar), and r-II, with $[\mathrm{Eu/Fe}] > 1.0$ (i.e., more than a factor 10 greater than solar).

As underlined by Holmbeck et al. (2020), these stars are relics of prolific r-process event(s) that occurred before the gas was enriched by supernovae, and are therefore considered tracers of nearly pure r-process events.

OF THE VARIATIONS in elemental abundances of stars enhanced with r-process elements, the variation in the actinide-to-lanthanide ratio is one of the most significant. Stars with an over-abundance of [Th/Eu] relative to the solar system are widely referred to as 'actinide-boost' stars, occurring in 30% of r-process enhanced stars (e.g. Holmbeck et al., 2020).

By 2014, just six actinide-boost stars were known: CS 31082–001 (as above; with CS designating the Curtis Schmidt survey), CS 30306–132 (Honda et al., 2004), CS 31078–018 (Lai et al., 2008), HE 1219–0312 (Hayek et al., 2009), CS 30315–029 (Siqueira Mello et al., 2014), and HE 2252–4225 (Mashonkina et al., 2014). Other discoveries since include 2MASS J09544277+5246414, identified from LAMOST (Holmbeck et al., 2018), and SPLUS J142445.34-254247.1, identified from the 12-filter S–PLUS Survey (Placco et al., 2023).

A KEY QUESTION is then whether such high actinide abundances result from conditions different to those in other r-process enhanced metal-poor stars. For example, does it depend on how neutron-rich the ejecta from an r-process event may be?

While still considering that *'the astrophysical production site of the heaviest elements in the Universe remains a mystery'*, Holmbeck et al. (2019) concluded that all observed levels of actinide enhancements, including those of the 'actinide-boost stars', do not necessarily demand distinct r-process progenitors if such a process (such as a neutron star merger) can generate the requisite variations in the neutron flux of its ejecta (Holmbeck et al., 2020).

GAIA ENTERS the discussions, providing distances and proper motions for the first time, with the discovery of three of the latest r-process enhanced stars.

For the $G = 13.8$ mag SPLUS J1424–2542, with an estimated age of 10.1 Gyr, (Placco et al., 2023) identified 36 elements, from C to Th. With [Fe/H] = –3.39, it has the highest known Th/Eu ratio. The Gaia DR3 parallax, $\varpi = 0.0796 \pm 0.0182$ mas, places it at $1/\varpi = 8.13^{+1.41}_{-1.05}$ kpc, with a (Bayesian) photo-geometric distance 7.82 kpc.

From the Gaia proper motions and line-of-sight velocity, they inferred that it belongs to the Galaxy halo, although not to any of the known halo streams. From a comparison of its abundances with Pop III supernova nucleosynthesis yields, the r- and s-process fractions, and simulations of neutron star mergers, they concluded that its heavy elements resulted from r-process event(s) only, with no contributions from the s-process.

Remarkably, their models imply that its nascent gas cloud was enriched by at least two progenitor populations: a supernova explosion from a metal-free star of mass $11.3 - 13.4 M_\odot$, and the aftermath of a binary neutron star merger with masses $1.66 M_\odot$ and $1.27 M_\odot$.

LAMOST J1124+4535 is r-process-enhanced, although not an actinide-boost star. Xing et al. (2024) derived an age of ~11.3 Gyr through radioactive-decay dating, on the assumption that the r-process material was produced by a single event immediately preceding the star's formation. The abundances suggest that it was accreted from a disrupted dwarf galaxy similar to the surviving Ursa Minor (UMi) dwarf galaxy.

From the Gaia DR3 parallax ($\varpi = 0.09 \pm 0.02$ mas) and proper motion, they infer a distance 7.6 kpc, and a radial orbit with eccentricity $e = 0.53$. The star is associated with an r-II cluster, itself dynamically associated with the LMS–1/Wukong stream (Hattori et al., 2023). This suggests that LAMOST J1124+4535 is the remnant of a disrupted dwarf galaxy with mass similar to that of UMi.

SUBARU–HDS spectroscopy of the $V = 11.5$ mag, very metal-poor ([Fe/H] = –2.38), r-process-enhanced ([Eu/Fe] = 0.80), actinide-boost LAMOST J0804+5740, gave abundances for 48 species (Lin et al., 2025). They evaluated three r-process models: a neutron star merger (Just et al., 2015), a collapsar model (He et al., 2024), and the magnetorotationally-driven jet supernova model (Nishimura et al., 2017). They found that the latter successfully reproduced the actinide-boost signatures.

At a Gaia DR3 distance of 3.05 ± 0.18 kpc (Anders et al., 2022), and based on the DR3 proper motion and radial velocity, Zhang et al. (2024a) had already shown that LAMOST J0804+5740 is a member of the Gaia Sausage–Enceladus (GSE) stream. This first such GSE actinide-boost star provides new insights into r-process nucleosynthesis in accreted dwarf galaxies.

FROM 27 million Gaia DR3 stars, Li et al. (2024b) used their kinematics (and actions) to identify more than 160 000 *ex situ* stars, with 0.1%, 1.6%, and 63.2% members of the thin disk, thick disk, and halo respectively. From the same sample, Lin et al. (2025) found that 2/3 of the known actinide-boost stars are *ex situ*, and thus more likely to originate from accreted dwarf galaxies.

This scenario in which the r-II stars formed in an extremely neutron-rich environment in which a rare astrophysical event occurred, is supported by the ultra-faint dwarf galaxy, Reticulum II, where most members are highly enhanced in r-process elements (Ji et al., 2016; Roederer et al., 2016). Other r-enhanced dwarf galaxies accreted by the Milky Way will have deposited many r-II stars in the Galactic halo with similar orbital actions.

Hattori et al. (2023) used Gaia DR3 to construct the orbital actions of 161 r-II stars in the solar neighbourhood. They found 6 clusters of r-II stars that have similar orbits and chemistry (one was a new discovery). These clusters are therefore inferred to be good candidates for remnants of completely disrupted r-enhanced dwarf galaxies that merged with the ancient Milky Way.

240. Extreme nuclear transients

THE EXISTENCE of supermassive black holes (SMBH) is implicit in various scientific areas being impacted by Gaia: most notably in its survey of active galactic nuclei (AGN, essay 82), and the subset of compact dual AGN providing quantitative evidence for galaxy mergers (essay 163), in the detection of hypervelocity stars, which result from the disruption of a binary star system passing close to a black hole (essays 22 and 166), and in the detection of tidal disruption events (TDE), which result from the tidal disruption of a star as it passes close to a supermassive black hole (essay 206).

With the development of powerful optical transient surveys, a number of particularly luminous short-period transients have recently been discovered. They display a range of properties (such as variability timescale, light-curve trends, spectral index, and infrared flux), making it difficult to attribute them to a single physical mechanism. As well as tidal disruption events (TDE), there are sources classified as 'ambiguous nuclear transients' (ANT) and, most recently, the class of very high-luminosity 'extreme nuclear transients' (ENT).

In the latter category are ZTF20abrbeie/AT2021lwx (Subrayan et al., 2023, Wiseman et al., 2023), and two recent Gaia science alerts discoveries: Gaia16aaw (AT2016dbs) and Gaia18cdj (AT2018fbb), reported by Hinkle et al. (2025). Indeed, Gaia18cdj is notable as *'the most energetic single transient yet found'*. IFL Science described it as *'twenty-five times more powerful than the most energetic supernova ever observed…, and the biggest explosion event since the Big Bang'*. These extreme nuclear transients are the subject of this essay.

ACCRETION ONTO a galaxy's central supermassive black hole powers many of the most luminous events known. At redshifts $z \sim 1$, roughly 10% are actively accreting mass, and observed as AGN (e.g. Zou et al., 2024). AGN light curves commonly show stochastic variability on a range of timescales from minutes to years (e.g. Ulrich et al., 1997, MacLeod et al., 2012), with some showing long-term photometric trends often accompanied by dramatic spectral changes. Rarely, some also exhibit large coherent flares (Graham et al., 2017).

Optical transient surveys, including ASAS-SN and ZTF, have also revealed several classes of flares coincident with the nuclei of their host galaxies. These include tidal disruption events (TDE); rapid turn-on AGN (Wyrzykowski et al., 2017, Trakhtenbrot et al., 2019), and 'ambiguous nuclear transients' (ANT). The latter cannot easily be classified as either AGN flares or TDEs, with examples including ASASSN-18el (Trakhtenbrot et al., 2019), ASASSN-18jd (Neustadt et al., 2020), and ASASSN-20hx (Hinkle et al., 2022).

These various accretion-powered transients nevertheless share several key observational properties, including bright ultraviolet emission, strong emission lines, and often X-ray emission. And the smooth flares of nuclear transients over timescales of several months are distinct from the stochastic variability typical of AGN (Frederick et al., 2021, van Velzen et al., 2021).

TIDAL DISRUPTION EVENTS result from the disruption of a star as it passes close to a supermassive black hole (e.g. Rees, 1988, Evans & Kochanek, 1989, van Velzen et al., 2011, Gezari, 2021). Typically, the host galaxies of TDEs do not coincide with a strong AGN, although this is considered to be largely due to selection effects. More recently, an increasing number of TDE candidates have been discovered in host galaxies exhibiting weak AGN-type activity (Onori et al., 2022, Wevers et al., 2022, Hoogendam et al., 2024).

Most are considered to be consistent with the disruption of main-sequence stars of mass $0.5-2\,M_{\odot}$ (Ryu et al., 2020). Nevertheless, enhanced N/C ratios suggest a population resulting from more massive stars (Kochanek, 2016, Mockler et al., 2022, Miller et al., 2023).

AS OF SEPTEMBER 2024, the Gaia Science Alerts data base listed 25 919 alerts (Hodgkin et al., 2021). Of these, 7 141 were assigned to 23 classes, with 25 inferred to be tidal disruption events.

I say more about the phenomenon, their discovery history, the insights that are being gained from them, and details of Gaia's two brightest (15–18 mag) TDE discoveries, Gaia19bvo and Gaia19eks, in essay 206.

FROM THE Gaia alerts transient stream, Hinkle et al. (2025) leveraged its 10-year all-sky survey to select a sample of flare events with three major characteristics: large amplitudes (>1 mag), smooth light curves (less than 10% excess variability about the long-term flare evolution), and long timescales (>1 yr). Their search yielded two transients, Gaia16aaw (AT2016dbs) and Gaia18cdj (AT2018fbb) which, combined with the 'extraordinary accretion event' ZTF20abrbeie/AT2021lwx (Subrayan et al., 2023, Wiseman et al., 2023), resulted in a sample of three events which they referred to as 'extreme nuclear transients' (ENT). Their detailed properties, derived by Hinkle et al. (2025), are worth outlining.

FIRSTLY, BOTH Gaia events are located within 0.8 kpc of their host-galaxy centres, confirming their nuclear transient nature (AT2021lwx has no detected host galaxy prior to the flare, so its offset is unknown). All three flares are smooth, luminous, and long-lived, with a rise of order 100 d to peak luminosity, and a slow decline of order 150 d to half their peak luminosity.

Pre- and post-flare: Somewhat reminiscent of extreme versions of ANTs, the ENTs detected prior to the flare show tentative signs of pre-flare variability, suggesting weak AGN activity within their host galaxies. After the ultraviolet/optical emission peaks, they show an infrared excess, suggesting transient heating of circumnuclear dust and re-emission at longer wavelengths.

Host galaxies: Optical and near-infrared follow-up spectra indicate that the events are at relatively high redshift, $z \approx 1$. From stellar population synthesis models, Hinkle et al. (2025) estimated that the host galaxies of Gaia16aaw and Gaia18cdj have masses $\sim 9 \times 10^{10} M_\odot$, and high star-formation rates $75 - 110 M_\odot\ \mathrm{yr}^{-1}$.

Black hole mass: Typical galaxy–SMBH scaling relations (McConnell & Ma, 2013) imply SMBH masses of $10^{8.4} M_\odot$ for Gaia16aaw and Gaia18cdj, and a similar upper limit for AT2021lwx. These are more massive than the majority of known nuclear transient hosts, and the host-galaxy masses are within the top few percent of stellar masses at $z = 1$ (when the Universe was half its current age), suggesting that the inferred SMBH masses are similarly extreme at such redshifts. In contrast, the high star-formation rates underlying Gaia16aaw and Gaia18cdj are only moderately exceptional at $z = 1$ when the star formation rate in the Universe was a factor 6 higher than today (Madau & Dickinson, 2014).

Luminosity and spectra: Their extremely high peak luminosities ($2-7\times10^{38}\ \mathrm{J\,s^{-1}}$) are 1000 times higher than core-collapse supernovae (SNe), 100 times higher than typical Type Ia supernovae, and 30 times higher than the extreme H-poor superluminous supernovae (SLSNe-I). The spectral energy distributions are well-fit by a blackbody model, consistent with super-Eddington accretion expected for TDEs (Evans & Kochanek, 1989).

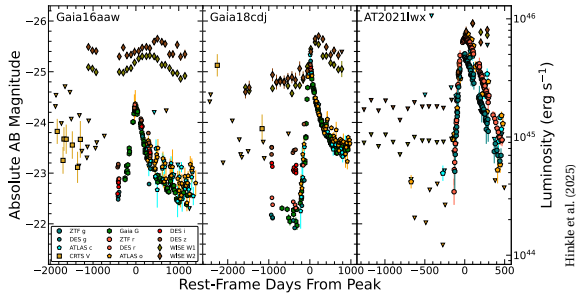

Light-curve duration: Their light-curve decay timescales are significantly longer than most transients. The rest-frame durations for the flares to fade by half are around 171 d for Gaia16aaw, 155 d for Gaia18cdj, and 210 d for AT2021lwx. They stand out in the parameter space of peak absolute magnitude versus characteristic timescale as being particularly luminous and long-lived.

Radiated energy: Their total radiated energies are particularly high, ranging between $2 - 5 \times 10^{45}$ J, and corresponding to accreted masses $0.3 - 1.4 M_\odot$ (assuming a typical 10% accretion efficiency). These are much higher than typical TDEs and ANTs, being more than twice as energetic as the next most energetic known flares, PS1-10adi (Kankare et al., 2017) and ASASSN-15lh (Dong et al., 2016, Leloudas et al., 2016), and up to an order of magnitude higher in the cases of Gaia18cdj and AT2021lwx. Indeed, Gaia18cdj is *'the most energetic single transient discovered to date'*.

Space density: Compared to other known transient classes, such extreme nuclear transients are extremely rare, with a space density $\sim 10^{-3}\ \mathrm{Gpc^{-3}\,yr^{-1}}$.

Physical origin: Hinkle et al. (2025) argue that their high peak luminosities, long flare timescales, immense radiated energies, and implied accreted masses are consistent with the tidal disruption of an *intermediate-mass* ($\sim 3 - 10 M_\odot$) star by a massive ($> 10^8 M_\odot$) supermassive black hole. With the flare timescale scaling as $M_{BH}^{0.5}$, the high implied masses of the SMBHs naturally provide long-duration flares consistent with the ENT timescales. As roughly half the stellar mass in a tidal disruption event leaves the system (rather than falling back onto the black hole), the total radiated energies provide a lower limit on the stellar masses of around $3 M_\odot$.

More detailed models of the accretion processes, fallback rates, and energetics of these highly luminous flares are given by Fancher et al. (2025).

FOR THE FUTURE, these Gaia discoveries point to the probable detection of extreme nuclear transients at even higher redshifts, $z \sim 4 - 6$, for example with the Vera Rubin–LSST and Roman Space Telescope surveys. These even more extreme populations would provide further insights into the high-mass end of the supermassive black hole mass distribution.

241. Asteroid masses

In my recent review of scientific results from Gaia (Perryman, 2026), I mentioned that *'Asteroid masses are known for a dozen or so main belt asteroids, determined from their orbit evolution as a result of gravitational perturbations during close approaches with other minor bodies. While no such results are yet available from the Gaia astrometry, it is expected that masses for more than a hundred will be obtained by this method.'*

I had missed a number of relevant papers, an omission kindly pointed out by Dr Fan Li of the Purple Mountain Observatory, and which this essay aims to rectify!

The determination of asteroid masses from mutual orbit perturbations can exploit asteroid–asteroid and asteroid–planet perturbations, as well as the motion of asteroid satellites (e.g. Siltala & Granvik, 2017; Fienga et al., 2020) and, in specific circumstances, asteroid–spacecraft perturbations (e.g. Park et al., 2020). A distinct approach for low-mass objects is from the Yarkovsky effect (essay 181), in which solar radiation and re-radiated thermal emission contribute a force tangential to the orbital motion (Chesley et al., 2003).

Masses combined with sizes yield the body's bulk density, an important constraint on its internal structure and composition (e.g. Podlewska-Gaca et al., 2020).

Orbit perturbations from close asteroid–asteroid encounters was applied to the data from Hipparcos, which observed 48 minor planets between 1989–93 with single epoch accuracies 10–100 mas. Estimates were derived for (20) Massalia ($2.42 \pm 0.41 \times 10^{-12} M_\odot$), from its close encounters with (44) Nysa and (4) Vesta (Bange, 1998); and (1) Ceres ($4.759 \pm 0.023 \times 10^{-10} M_\odot$), from its perturbations on 9 other asteroids (Viateau & Rapaport, 1998).

The present status of Gaia's solar system astrometry is given by David et al. (2023). For the 157 000 asteroids in the 34-month Gaia DR3 solution, their 'Focused Product Release' study used the 66-month time interval being used for DR4 (essay 159). The 100 00 objects best observed have an average of around 30 ± 10 visibility periods or epochs, with along-scan accuracies better than 1 mas for $G < 18$ mag, degrading to ~10 mas at $G \simeq 20$.

An essential starting point for all of these dynamical studies are the solar system (DE) ephemeris models developed at JPL (e.g. Folkner et al., 2014; Park et al., 2021), or the INPOP models developed at IMCCE, Paris. INPOP19a, for example, considers the Earth–Moon barycentre with the seven other planets, the dwarf planet Pluto, 343 asteroids, and the ten most massive trans–Neptunian objects. Its construction also led to the mass determination for 103 asteroids, deduced from their perturbations on the orbits of the inner planets, in particular Mars and Earth (Fienga et al., 2019).

Estimates of the improvements expected with Gaia were made in the early pre-launch study phases. The goal is to obtain the mass of (smaller) target asteroids using all (massive) perturbers simultaneously, based on an analysis of the observed minus calculated positions through a reconstruction of the six orbital elements, or state vector, for each object (Mouret et al., 2007; Mouret et al., 2008). They showed that it should be possible to derive more than 100 asteroid masses, 42 with better than 10% precision. They also considered the possible contribution of ground-based observations for specific close approaches. Further studies using Gaia DR2, including a list of the most promising encounters, were given by Murray (2023).

In most of these mutual encounters, the smaller target asteroids are not massive enough to significantly affect the orbit of the more massive perturber. For an encounter between two massive asteroids, the masses must be estimated simultaneously (e.g. Baer & Chesley, 2017). Indeed, these authors concluded that future Gaia studies should search for such possible gravitational 'couplings', and account for their effects.

Detailed numerical methods, not restricted to Gaia data, for example using Markov-chain Monte Carlo (MCMC) algorithms, have been variously described (e.g. Siltala & Granvik, 2017). These include application to (1) Ceres and (4) Vesta observed by the Dawn mission (launched in 2007), and to (16) Psyche, the target of NASA's Psyche mission, launched in 2023 (e.g. Siltala & Granvik, 2020; Siltala & Granvik, 2021).

WITH THE AVAILABILITY of Gaia DR2, various studies have considered asteroid masses and have targeted mass determinations. In the initial analysis and orbit fitting using the DR2 data alone, Spoto et al. (2018) used the JPL DE431 planetary ephemeris for the orbits and masses of the planets (Folkner et al., 2014). They included 16 massive perturbers in their dynamical model.

SUBSEQUENT STUDIES using Gaia DR2 included a detailed consideration of the sensitivity of the orbital adjustment of 14 099 asteroids on the chosen planetary ephemeris (Deram et al., 2022).

Kuznetsov & Chernetenko (2022) included Gaia DR2 data in their mass estimate for (7348) $1993FJ_{22}$, based on its observed perturbation of asteroid (7562) Kagiroino–Oka during their close approach (1060 km) on 26 March 1993. Their result, $(0.867 \pm 0.243) \times 10^{-14} M_\odot$, was the smallest mass determined by this method at the time.

Siltala & Granvik (2022) also used the mas-level accuracies for the 14 099 asteroids included in Gaia DR2, selecting various combinations of Gaia and/or Earth-based astrometry to determine the impact of Gaia on the mass estimates. For example, using only Gaia data, their value for (367) Amicitia improves on the solution previously published by Spoto et al. (2018), while no solution using Gaia DR2 data alone could be found for (445) Edna, based on its close mutual encounter with (1764) Cogshall. In contrast, a combination of Gaia DR2 and Earth-based astrometry results in significantly reduced uncertainties compared with the less accurate Earth-based astrometry alone.

The few objects for which mass determinations could be derived should, they estimated, be advanced significantly with DR3, allowing for *'a wave of numerous accurate mass estimates for a wide range of asteroids'*.

Simulations of the capabilities of asteroid mass determination using Gaia DR2, in combination with positions expected from planned observations with the Chinese Space Station Telescope (CSST), are detailed by Li et al. (2023c).

THE 22-MONTH SOLUTION for the 14 099 asteroids in Gaia DR2 was duly superseded by the 34-month solution of DR3. This gave astrometry for 158 000 solar system objects, orbits for 154 787, and BP/RP reflectance spectra for 60 518 (Tanga et al., 2023).

Li et al. (2023b) combined the DR3 astrometry with the available ground-based observations to determine the masses of 20 asteroids by means of these asteroid–asteroid encounters, with Gaia DR3 providing *'substantial benefits in terms of improving mass precision'*. For 10 asteroids, a mass precision better than 5% was achieved, with 15 asteroids better than 10%. Combined with diameters from the literature, they derived bulk densities for 20 asteroids.

THE 'Focused Product Release' data set provides a major improvement with respect to Gaia DR3 by making use of the 66-month time interval adopted for DR4.

Farnocchia et al. (2024) used the FPR data to estimate the mass of (16) Psyche from the astrometric solutions for asteroids that came within 0.05 au, yielding $GM = 1.601 \pm 0.017\,\mathrm{km^3\,s^{-2}}$, and a bulk density $4.172 \pm 0.145\,\mathrm{Mg\,m^{-3}}$, compatible with its M-type taxonomic classification. The specific interest in (16) Psyche is that its mass is a critical parameter for determining the altitude to be used for the different Psyche mission phases (Elkins-Tanton et al., 2022). Mass estimates for 38 other asteroids were derived in the process (their Figure 3).

Fuentes-Muñoz et al. (2025) used the FPR data to search for close encounters between all known asteroids and a list of the largest asteroids, finding some 975 000 that may have been perturbed in a measurable way, and 86 000 with an astrometric signal for one or more asteroid masses. They derived 77 asteroid masses with signal-to-noise ratio >10, and 232 asteroid masses with SNR >3, all in the main belt or outer main belt.

GAIA'S FINAL DATA RELEASE, DR5 in around 2030, will yield a much larger number of mass detections as well as a better mass accuracy per event. Also of considerable importance for the future, Gaia's accurate stellar reference frame allows ground-based observatories to place asteroid positions on an inertial coordinate system with systematic errors well below 1 mas.

In particular, the LSST survey, to be conducted with the Vera Rubin Observatory from 2025–2035, will detect and track millions of main belt asteroids. The individual astrometric uncertainties are smaller than for Gaia at Gaia's faint magnitude limit, and the LSST observations will extend some 3 mag deeper, increasing the number of potential tracers by a factor of 100. This will allow mass estimates of several hundred main belt asteroids with uncertainties below 30% (Bernstein et al., 2025).

MUTUAL ENCOUNTERS amongst the main belt asteroids that cannot be predicted from the ephemeredes of larger bodies is a source of stochastic astrometric noise. Bernstein (2025) estimated that the rms azimuthal shift of this noise contribution accumulates to 2–9 km, or 1–5 mas over $t = 10$ yr, increasing as $t^{3/2}$, and affecting inferences from the Gaia astrometry. The LSST survey data is expected to improve the knowledge of the main belt asteroid masses, lowering this uncertainty to 260–400 m, or 140–210 μas.

For full exploitation of Gaia and LSST main belt asteroid data, Bernstein (2025) shows that ephemeris models should include the 10 000 or so largest asteroids as active bodies with free masses. The rms value of deflections from the less massive main belt asteroids would then be reduced to some 17–60 m, or 9–40 μas.